SCUOLA DI DOTTORATO

UNIVERSITÀ DEGLI STUDI DI MILANO-BICOCCA

School of Medicine and Surgery

PhD program in Neuroscience

Cycle XXXV

International Curriculum in Neuroscience

ASSESSMENT OF METABOLOMIC CHANGES IN CHEMOTHERAPY-INDUCED PERIPHERAL NEUROPATHY

BONOMO ROBERTA

Registration number: 862932

Tutor: PROF. GUIDO CAVALETTI

Co-tutor: PROF. DEBRA J. SKENE

Supervisor: DR. DAAN VAN DER VEEN

Coordinator: PROF. ROSA MARIA MORESCO

ACADEMIC YEAR 2021/2022

CONTENTS

List of abbreviations

Abbreviation	Definition
ARE	antioxidant response element
AT1R	angiotensin II type 1 receptor
BDNF	brain-derived neurotrophic factor
CB2	cannabinoid type 2 receptor
CIPN	chemotherapy-induced peripheral neuropathy
CIPN20	CIPN twenty-item scale
CMAP	compound muscle action potential
CV	coefficient of variation
DRG	dorsal root ganglion
EORTC	European Organization for Research and Treatment of Cancer
ESI	electrospray ionization
FDR	False Discovery Rate
FIA	flow injection analysis
GWAS	genome-wide association studies
IENF	intraepidermal nerve fiber
IFN-γ	interferon-γ
IL	interleukin
IQR	interquartile range
LLOQ	lower limit of quantification
LOD	limit of detection
LOQ	limit of quantification
NCI-CTC	National Cancer Institute-Common Toxicity Criteria
NCS	nerve conduction studies
NCV	nerve conduction velocity
NfL	neurofilament light chain
NF-κB	nuclear factor-kappa light chain enhancer of B cells
NGF	nerve growth factor
NMDA	N-methyl-D-aspartate
Nrf2	nuclear factor erythroid 2-related factor 2
OPLS-DA	Orthogonal Partial Least Squares-Discriminant Analysis
ORA	Over Representation Analysis
PCA	Principal Component Analysis
PGP 9.5	protein gene product 9.5
PIPN	paclitaxel-induced peripheral neuropathy
PITC	phenylisothiocyanate
PLS-DA	Partial Least Squares-Discriminant Analysis
QC	quality control
QLQ-C30	Quality of Life Questionnaire-Core 30
QST	quantitative sensory testing
ROS	reactive oxygen species
S1P	sphingosine-1-phosphate

S1PR	S1P receptor
SEM	Standard Error of the Mean
SNAP	sensory nerve action potential
SNP	single nucleotide polymorphism
TCA	tricarboxylic acid
TNF-α	tumor necrosis factor-α
TNS	Total Neuropathy Score
TRP	Transient receptor potential
TRPA	TRP ankyrin
TRPV	TRP vanilloid
UPLC-MS	Ultra-Performance Liquid Chromatography-Mass Spectrometry
VIP	variable influence on prediction

Summary

Chemotherapy-induced peripheral neuropathy (CIPN) has long represented one of the most relevant neurological side effects of oncological therapies. Nevertheless, despite the progress in drug regimens, the occurrence of troublesome adverse events still affects the efficacy of antineoplastic therapy, leading to the reduction or discontinuation of the treatment. Paclitaxel is an anti-tubulin drug which has emerged as an efficacious antitumor agent in the treatment of different cancers. However, its clinical use is often limited by the onset of paclitaxel-induced peripheral neuropathy (PIPN). Numerous alterations related to aging have been hypothesized to underlie age-related susceptibility to nerve damage. Nevertheless, the results of these studies are inconclusive and other targets, which might be used as potential biomarkers of nerve impairment, deserve to be considered.

On these bases, the aim of our study was to investigate the age-related effects of paclitaxel treatment on the peripheral nervous system, and the metabolic changes that might be induced by paclitaxel administration at different ages. Our project included neurotoxicity experiments based on neurophysiological, behavioral and histopathological evaluations to assess age-related chemotherapy-induced phenotypic alterations in a neuropathic model of PIPN. We additionally investigated through a targeted Ultra-Performance Liquid Chromatography-Mass Spectrometry (UPLC-MS) based metabolomics approach differences in the plasma and liver metabolite profiles in order to identify potential biomarkers of PIPN development and progression, according to age. Our results suggest that age might be a potential risk factor for more severe CIPN, and should be considered in future studies in order to tailor the chemotherapy regimen and dosage on individual susceptibility of older cancer patients. Our study also identifies for the first time multiple related metabolic axes involved in PIPN,

establishing a mechanistic insight into the biomolecular signaling pathways underlying this neurological complication, and also spurs development of effective therapies by providing sensitive metabolic measures of neurotoxicity development and progression.

1. Introduction

1.1 Epidemiology and predisposing factors of PIPN

Taxanes are a class of antimitotic agents used for the treatment of a wide array of malignancies, including breast, ovarian and lung cancers, as well as Kaposi's sarcoma (*Velasco and Bruna, 2015*). Paclitaxel and docetaxel are the most commonly used taxanes and are currently considered among the most effective oncological treatments in both early-stage and metastatic breast cancer, improving the overall and disease-free survival (*Willson et al., 2019*).

Taxane-based therapies are associated with a predominantly sensory neuropathy, with an overall incidence of chemotherapy-induced peripheral neuropathy (CIPN) ranging from 57% to 83% in paclitaxel-treated patients, and from 11% to 64% in docetaxel-treated cases (*Velasco and Bruna, 2015*). Severe sensory symptoms have been observed in 64% of cases at one year and in 41% of patients at three years after initiating paclitaxel (*Tanabe et al., 2013*). In addition, clinically meaningful symptomatology of CIPN can persist for up to two years in 30% of breast cancer patients treated with adjuvant taxane-based therapy (*Hershman et al., 2018*).

The cumulative dose represents the most important risk factor for paclitaxel-induced peripheral neuropathy (PIPN) development, with a neurotoxic threshold of 1000 mg/m^2 for paclitaxel, and 400 mg/m^2 for docetaxel (*Grisold et al., 2012*). The treatment regimen is also critical for the development of neurotoxicity. Patients receiving higher doses of paclitaxel (≥250 mg/m^2) can develop PIPN even after the first cycle *(Freilich et al., 1996*). In particular, PIPN occurs in a higher percentage of cases (20% to 35%) in which patients are treated with 250 mg/m^2 every three weeks, in contrast to the percentage (5% to 12%) of those treated with less than 200 mg/m^2 every three weeks

(*Lee and Swain, 2006*). Concerning frequency of administration, studies have yielded mixed results. Two clinical trials reported more frequent neurotoxicity with weekly (80 mg/m^2) therapy compared to every three-week (175 mg/m^2) schedule (*Seidman et al., 2008; Sparano et al., 2008*). Conversely, others documented a lower incidence of peripheral neuropathy with a weekly paclitaxel or docetaxel schedule (*Mauri et al. 2010*). Short infusion duration apparently is related to a higher incidence of paclitaxel-associated acute pain syndrome (*Moulder et al., 2010*); whereas the impact of infusion duration on the incidence of severe neurotoxicity is unclear (*Lee and Swain, 2006*).

A novel nanoparticle albumin-bound formulation of paclitaxel (nab-paclitaxel, Abraxane®) showed a better toxicity profile and shorter recovery duration than conventional paclitaxel, despite a higher incidence of transient sensory neurotoxicity (*Gradishar et al., 2005; He et al., 2022*).

The role of cancer itself in the pathogenesis of peripheral neuropathy has recently been suggested in other CIPN models (*Housley et al., 2020*). In particular, it has been observed that pathobiological interactions between cancer and chemotherapy may contribute to CIPN development (*Housley et al., 2020*). The importance of the duration of chemotherapy has also been emphasized (*Mielke et al., 2005; Molassiotis et al., 2019*).

Specific characteristics related to the patient profile also contribute to the development of peripheral neuropathy. Important comorbidities, such as diabetes, kidney and thyroid diseases, vitamin deficiencies, and systemic infections (i.e., hepatitis B, C, HIV, polio) may predispose to neurotoxicity (*Kaley and Deangelis, 2009; Hershman et al., 2016*). Environmental and behavioral factors, such as cigarette smoking, may also be conducive to peripheral neuropathy (*Zajączkowska et al., 2019*). Certainly, previous administration of chemotherapeutic drugs further increases the risk of neurotoxicity, as

does the development of paraneoplastic antibodies (*Zajączkowska et al., 2019*). It has also been observed that the co-administration of platinum agents is associated with greater nerve damage in cancer patients undergoing taxane-therapy (*Hershman et al., 2016*).

Concerning the association between aging and PIPN, current literature reports mixed results. Some studies have suggested that aging can be a risk factor for CIPN in taxane-treated patients, with increased odds of neuropathy of 4% per year of age (*Hershman et al., 2016*), and up to 13% per decade of life (*Schneider et al., 2015*). Other studies indicated that older patients are more likely to present neuropathy progression and persistence (*Chase et al., 2015; Hershman et al., 2018*). However, when the hypothesis that advanced age would increase incidence and severity of CIPN was tested, neurophysiological and clinical data did not significantly differ between elderly and younger cancer patients (*Argyriou et al., 2006*). A recent study described a discrepancy between the objective assessment of worse light touch, cold and vibration sensations in older cancer survivors, despite subjectively reported lower pain severity scores and less interference with common activities (*Wong et al., 2019*). Another recent study indicated a similar escalation in CIPN symptomatology in older and younger patients during the active treatment phase, but a higher risk for chronic neuropathy in older cancer patients after treatment completion (*Bulls et al., 2019*).

As a multifactorial disease, the combination of individual predisposing factors with genetic susceptibility may increase the risk of developing PIPN. Numerous single nucleotide polymorphisms (SNPs) have been identified through genome-wide association studies (GWAS), revealing that polymorphisms in genes related to neuronal function, drug transport and microtubule function (EPHA5, ABCB1, SLCO1B1, TUBB2A) are significantly associated with taxane-induced CIPN (*Leandro-García et*

al., 2013; Abraham et al., 2014; Boora et al., 2016). Some authors reported a significant association between SNPs in genes involved in inherited neuropathies (FGD4, FZD3) and onset or severity of taxane-related CIPN (*Baldwin et al., 2012*). Other studies provided evidence for the significant association between SNPs in genes involved in drug metabolism (NR1I3, UGT2B7, CYP2C8*4, CYP1B1*3) and increased risk of CIPN in taxane-treated cancer patients (*Abraham et al., 2014; Arbitrio et al., 2019*).

1.2 Pathophysiology of PIPN

It has been demonstrated that taxane administration determines the alteration of numerous subcellular and systemic pathways which contribute to the development of CIPN. Paclitaxel and its semi-synthetic derivative docetaxel exert their mechanism of action through targeted inhibition of microtubule dynamics, determining a cell cycle arrest in G2 and M phase, and cell death (*Carozzi et al., 2015a*). Another scenario of cell fate assumes an exit from mitosis without appropriate chromosome segregation determining the generation of a tetraploid G1 cell, which may die, persist growth arrested, or progress to more divisions (*Mikuła-Pietrasik et al., 2019*). It has been observed that taxanes may also cause DNA single-strand breaks, leading to the activation of different forms of DNA repair mechanisms (*Branham et al., 2004*). Depending on the efficiency of the DNA repair process, the cancer cells can arrest and repair the damage, enter into apoptosis, or proceed with the program of cell proliferation without repairing the damage. Paclitaxel also produces alterations in signaling related to apoptosis, so that cell death can occur independently of microtubule stabilization and mitotic inhibition (*Falah et al., 2019*).

Disruption of microtubule function results in length-dependent nerve degeneration starting from the most distal segments, known as “Wallerian degeneration”, due to altered anterograde and retrograde axonal flow. Besides axonal damage, taxanes may also affect the myelin sheath through indirect mechanisms related to mitochondrial dysfunction (*Flatters and Bennett, 2006*). In fact, paclitaxel induces a vacuolization of mitochondria in myelinated and unmyelinated sensory nerve fibers (*Flatters and Bennett, 2006*), and a release of calcium from mitochondria, leading to rapid mitochondrial membrane depolarization (*Zajączkowska et al., 2019*). Mitochondrial impairment certainly plays a key role in the induction and maintenance of a state of oxidative stress, with local and generalized consequences (*Doyle et al., 2012; Areti et al., 2014; Duggett et al., 2016*). Indeed, the increased production of reactive oxygen species (ROS) causes damage to lipid and protein components (*Doyle et al., 2012; Areti et al., 2014; Duggett et al., 2016*), as well as the activation of cell death processes (*Cashman and Höke, 2015*). It has also been observed that taxanes would be able to affect the expression of potassium ion channels (K2P and Kv7), resulting in increased dorsal root ganglion (DRG) nociceptor activation (*Li et al., 2019*). Paclitaxel also regulates the expression of other ion channels, including increased expression of the calcium channels Cav2.2, Cav2.3, Cav3.2, and the upregulation of sodium channel Nav1.7 (*Okubo et al., 2011; Li et al., 2017, 2018; Shan et al., 2019*). Other receptors involved in altered sensitivity to thermal and mechanical stimulation can be affected, like the Transient receptor potential (TRP) channels present in DRGs, specifically TRP ankyrin-1 (TRPA1), TRP vanilloid-1 (TRPV1) and TRPV4 (*Materazzi et al., 2012; Hara et al., 2013*). *In vivo* models also demonstrated a role of glutamatergic receptors in paclitaxel-induced neuropathic pain. Specifically, paclitaxel stimulates presynaptic N-methyl-D-aspartate (NMDA) receptors, and increases the expression of the α2δ-

1voltage-gated calcium channel subunit as well as GluN1, GluN2A, and GluN2B NMDA receptor subunits (*Chen et al., 2019*). Impaired functions of nuclear factor erythroid 2-related factor 2 (Nrf2)-antioxidant response element (Nrf2-ARE) and Nrf2-responsive gene (HO-1, γ-GCLC, and NQO1) expression have been also associated with neuropathic pain (*Zhao et al., 2019*).

Taxanes additionally determine the activation of satellite glial cells surrounding DRGs, leading to increased expression of angiotensin II type 1 receptor (AT1R) and a subsequent increase of inflammatory cytokines contributing to neuropathic pain (*Kim et al., 2019*). Paclitaxel also stimulates microglial cells in the dorsal horn of the spinal cord with increased expression of cannabinoid type 2 receptor (CB2), and of chemokines (CCL2) and pro-inflammatory interleukins (*Pevida et al., 2013; Ha et al., 2019; Wu et al., 2019*). The activation of spinal astrocytes stimulates the secretion of the tumor necrosis factor-α (TNF-α), interleukin-1β (IL-1β) and IL-6, contributing to neuropathic pain development (*Burgos et al., 2012; Ba et al., 2018*). The increased stimulation of pro-inflammatory cytokines eventually leads to a state of neuroinflammation (*Zaks-Zilberman et al., 2001; Doyle et al., 2012; Makker et al., 2017*). A recent association between the innate immune system involving the complement and PIPN has also been described (*Xu et al., 2018*).

1.3 Clinical manifestations of PIPN

Patients undergoing paclitaxel administration usually present with a length-dependent "dying-back" sensory axonal polyneuropathy, manifesting with a progressive development of burning paresthesias in a distal-proximal fashion, and loss of reflexes (*De Iuliis et al., 2015*). Neurophysiological investigations reveal a decrease in sensory

nerve action potentials (SNAPs) in the nerve conduction studies (NCS), consistent with axonal damage of the sensory nerve fibers (*Pace et al., 1997; Openshaw et al., 2004*). In particular, sural nerve involvement is a reliable index of PIPN occurrence in the clinical setting (*Argyriou et al., 2005*). Symptoms can develop in a median time of 21 days [range 11–101] with a tri-weekly schedule, and 35 days [range 14–77] with weekly administration (*Tanabe et al., 2013*). The sensory symptomatology can be less frequently accompanied by motor and autonomic manifestations (*De Iuliis et al., 2015*). In fact, paclitaxel can cause motor neuropathy, mainly involving proximal muscles in up to 14% of cases (*Freilich et al., 1996; Lee and Swain, 2006*), resulting in altered compound muscle action potential (CMAP) in motor nerve conduction tests. Taxanes may also be responsible for an acute pain syndrome, occurring after one or two days of treatment with severe arthralgias and myalgias associated with numbness and tingling, lasting a median of four-five days (*Fernandes et al., 2016a*). The incidence (0.9% to 86%) is higher in patients treated every three weeks, and in the metastatic setting (*Fernandes et al., 2016b*). Further progression of neuropathy can be observed after 1–2 months from chemotherapy completion, due to the so-called "coasting effect" (*Velasco and Bruna, 2015*).

In the clinical setting, the combination of clinician-based and patient-reported outcomes could provide the specialist with substantial information for suspecting PIPN (*Bonomo and Cavaletti, 2021*). As part of neuropathic pain investigation, quantitative sensory testing (QST) is suggested for the early diagnosis of PIPN (*Cruccu et al., 2010; Haanpää et al., 2011*). In particular, QST investigates alterations in touch detection to monofilaments, and bumps test (A-beta fibers), sharpness (A-delta fibers), and pin-prick (C-fibers) stimulation (*Flatters et al., 2017*). Changes in QST correlate with altered intraepidermal nerve fiber (IENF) density (*Boyette-Davis et al., 2013*).

Treatment-related toxicity is conventionally measured with toxicity criteria grading scales, including The National Cancer Institute-Common Toxicity Criteria (NCI-CTC) and the Total Neuropathy Score (TNS) clinical version (*Cornblath et al., 1999; Trotti et al., 2003*). The European Organization for Research and Treatment of Cancer Quality of Life Questionnaire-Core 30 (EORTC QLQ-C30) is another, not specific, but reliable tool for neuropathy assessment in cancer patients (*Aaronson et al., 1993*). Sensory, autonomic and motor symptoms can also be examined with CIPN twenty-item scale (CIPN20) quality-of-life measures (*Wolf et al., 2012*). In the last years, time-consuming procedures requiring specialized equipment have been revised and reduced to be more practical and easily accessible to non-specialists, such as the TNS scoring system (*Park et al., 2019*).

A recent systematic literature review on the recommended prevention and treatment approaches in the management of adult cancer survivors revealed that duloxetine, a serotonin–noradrenaline reuptake inhibitor antidepressant, represents the only agent with sufficient data to encourage its use for painful CIPN patients (*Loprinzi et al., 2020*). However, the beneficial effect of duloxetine administration is still limited.

1.4 Rodent models of PIPN

A number of rodent studies have investigated the mechanisms underlying PIPN using *in vivo* models (*Carozzi et al., 2015b; Alberti, 2017*). The advantage of the *in vivo* approach lies in the development of pathophysiological methods similar to the clinical scenario, using reliable neurophysiological, behavioral, and neuropathological instruments for the investigation of nerve damage, without the potential confounders of

the clinical setting, i.e., diabetes, vitamin deficiencies, HCV-related neuropathies (*Radaelli et al., 2018*).

A few studies have demonstrated the impact of age in rodent models of peripheral neuropathy due to specific changes in functional and pathophysiological mechanisms in older animals (*Verdú et al., 1996; Ceballos et al., 1999; Canta et al., 2016*). For instance, diabetes animal models showed more severe and early manifestation of neuropathy in relation to age (*Garcia-Perez et al., 2018; Wang-Fischer and Garyantes, 2018*), including a marked reduction of axonal size (*Thomas et al., 1990*). Aging determines a delay in recovery and compensatory responses to axonal damage due to decreased expression and axonal transport of cytoskeletal proteins in the peripheral nerve, altered endoneurial blood flow, and reduction in trophic and tropic factors secreted by reactive Schwann cells (*Verdú et al., 2000*). In this regard, the inclusion of older animals in CIPN models has been suggested to provide further results on age-related responses to chemotherapy administration (*Bruna et al., 2020*), giving insights into the aging effect on peripheral neuropathy, as a model for the therapeutic and clinical management of older cancer patients.

Concerning the impact of sex, it has been observed that paclitaxel-treated female rodents might be more sensitive to cold stimulation than males, but not to mechanical stimulation (*Ward et al., 2011; Hwang et al., 2012; Naji-Esfahani et al., 2016; Brewer et al., 2020*). Nevertheless, due to the heterogeneity of current studies in terms of protocols and included animals, it remains difficult to state a clear sex effect on CIPN models.

Paclitaxel is usually administered to mice and rats via intravenous or intraperitoneal injection. The intraperitoneal drug delivery is an easy and practical method (*Hirota and Shimizu, 2012*), despite not being as accurate in the site of injection as intravenously

(*Lewis et al., 1966*). In addition, intraperitoneally, the drug may be metabolized by the liver before reaching systemic circulation. In the majority of cases, dosing regimens involve intermittent systemic administration in order to mimic cycles of chemotherapy, in animals without tumor load (*Authier et al., 2009; Hopkins et al., 2016*). Nonetheless, rat models that carry an implanted subcutaneous tumor have been used (*Boyle et al., 1999, 2001*). Indeed, rodent models of PIPN with a tumor might be clinically more reliable, despite the fact that the tumor is often removed before chemotherapy administration, to avoid the spreading of micro-metastases. Moreover, the ethical concern of such an approach should be considered. In fact, ill animals are less responsive to CIPN behavioral investigations. Accordingly, studies involving chemotherapy administration alone have been adopted as a valid model (*Flatters et al., 2017*). Recently, established protocols using intermittent dosing schedules to reproduce CIPN models have been suggested across different laboratories to improve the reproducibility of study results. Indeed, dose estimation always requires careful consideration about the difference in pharmacokinetics and pharmacodynamics among species, for a safe and effective drug administration (*Nair and Jacob, 2016*). Intravenous doses of paclitaxel ranging from 5 to 12.5 mg/kg administered weekly for four weeks are usually effective in inducing evident neurophysiological changes in a dose-dependent fashion (*Persohn et al., 2005*).

The assessment of nerve damage in animals with paclitaxel-induced neuropathy can be tested through the NCS of sensory and motor nerve fibers. The neurophysiological evaluation can be accurately performed in anesthetized animals with needle electrodes placed in the digital or caudal nerves to follow the progression of the neuropathy over time (*Bruna et al., 2020*). Two NCS parameters, amplitude and velocity of the potentials, reflect axonal or myelin involvement, respectively. In PIPN, axonal damage

is usually observed, which in severe cases can be associated with the impairment of the myelin sheath and a decrease in the nerve conduction velocity. These findings usually correlate with morphological examination of peripheral nerves. Histological evaluations of nerve fibers, both axonal and myelin sheath components, contribute to further understanding of the pathological processes underlying PIPN (*Marmiroli et al., 2012*). Large and long axons are affected early, and fibers of the caudal nerve are especially vulnerable to the "dying back" axon degeneration (*Schaumburg and Spencer, 1979*; *Boehmerle et al., 2014*). Of note, SNAP amplitudes mainly reflect the involvement of large myelinated fibers, and thus are not suitable for investigating small myelinated and unmyelinated fibers (*Boehmerle et al., 2014*). In this regard, skin biopsy in CIPN models has emerged as a minimally invasive technique for the examination of epidermal small-diameter nerve fibers (*Lauria et al., 2005, 2010*). In particular, IENF density can be measured by immunohistochemistry and image analysis tools to assess small fiber neuropathy in CIPN animal models (*Meregalli et al., 2018*). Small myelinated A-delta and unmyelinated C fibers contribute to nociception by conveying punctate pressure and laser heat, and blunt pressure stimuli, respectively (*Beissner et al., 2010*). The involvement of small fibers can be additionally investigated through the von Frey test (*Chaplan et al., 1994; Casals-Diaz et al., 2009*). A brief vertical stimulation of the skin with a thin von Frey filament usually causes a short deformation of the skin surface with an "on-off" activation of A-beta mechanoreceptors (*Landerholm and Hansson, 2011*). In case of peripheral neuropathic pain development, a sustained stimulation of about 10 seconds of the skin with a von Frey filament would result in activation of epidermal C- and A-delta nociceptors (*Garell et al., 1996; Treede et al., 2002*). The thermal algesimeter assessment instead uses a radiant heat source for stimulating animal plantar surface (*Hargreaves et al., 1988*). The nociceptive threshold

is expressed as the heat intensity that triggers hind paw withdrawal in response to the stimulus (*Bruna et al., 2020)*. A reduced withdrawal threshold in mice or rats undergoing chemotherapy is indicative of hyperalgesia development (*Hama and Takamatsu, 2016*). Conversely, a progressive decreased response to the same stimulus can be ascribed to sensitization of nociceptors to repeated mechanical or thermal stimulation (*Bruna et al., 2020)*. Moreover, in longer drug exposure experiments, skin denervation can cause increased withdrawal thresholds suggestive of hypoalgesia development (*Bruna et al., 2020)*.

1.5 Current biomarkers of PIPN

Numerous studies have investigated the alterations in molecular biomarkers of PIPN for identifying and risk-stratifying cancer patients with peripheral neuropathy, focusing on neurotrophic factors and neuro-inflammatory mediators.

Preclinical studies on rodent models suggested the involvement of the nerve growth factor (NGF) in the rescue from neurotoxic damage caused by paclitaxel administration (*Nakahashi et al., 2014*). Some authors observed a highly significant correlation between the decrease in circulating levels of NGF and the severity of CIPN in taxane-treated patients according to the chemotherapy cycle and severity of CIPN, despite not being informative of the final neurological outcome of each patient (*De Santis et al., 2000; Cavaletti et al., 2004*). Others described an increase in NGF in cancer patients treated with taxane or platinum with painful CIPN, proposing the association between NGF levels and presence of neuropathic pain (*Velasco et al., 2017*). Azoulay and colleagues instead reported the possible role of dysfunctional neuronal brain-derived neurotrophic factor (BDNF)-induced repair mechanism due to polymorphisms as a predisposing factor for paclitaxel-induced neurotoxicity (*Azoulay et al., 2015*).

Further studies analyzed cytokines involved in inflammatory signaling in taxane-treated breast cancer patients, concluding that increased levels of interferon-γ (IFN-γ), IL-1β, and IL-8 and decreased IL-6 and IL-10 levels can be related to CIPN symptoms (*Kleckner et al., 2021*). Other studies reported the association between lower baseline levels of osteopontin, a protein involved in cell recruitment to inflammatory sites, and moderate to severe CIPN (*Pizzamiglio et al., 2020*). Moreover, baseline osteopontin levels were inversely correlated to the extent of alterations found in nerve conduction studies over time (*Pizzamiglio et al., 2020*).

Animal models have also identified some associations between microRNA-124, which increases in extracellular fluid when cellular membrane integrity is compromised, and PIPN development (*Peng et al., 2019*). Another recent clinical study investigated the association between serum microRNA and the risk of peripheral neuropathy in paclitaxel-treated breast cancer patients (*Noda-Narita et al., 2020*). The authors reported that the microRNA-451a, which is involved in the metabolism of paclitaxel through the regulation of the drug-transporter protein P-glycoprotein, was an accurate discriminatory marker of patients with peripheral neuropathy (*Penson et al., 2004; Kovalchuk et al., 2008*).

Meregalli and colleagues have recently examined the feasibility of using serum neurofilament light chain (NfL) as a reliable biomarker of CIPN in rats chronically treated with cisplatin and paclitaxel (*Meregalli et al., 2020*). The neurofilament proteins represent the major constituent of the neuronal cytoskeleton, and their increase in concentration can reflect axonal injury (*Kuhle et al., 2015*). In particular, the authors found that increased NfL values were significantly associated with the severity of axonal damage, especially in paclitaxel-treated rats (*Meregalli et al., 2020*). Moreover, significantly higher NfL levels were observed in the very early treatment stage in

animals undergoing paclitaxel administration, with a progressive increase in line with the severity of the axonal impairment.

Recent advances in “omics" technologies have supported the discovery of a number of biomarkers that may predict response to chemotherapy (*Bonomo et al., 2020*; *Meregalli et al., 2021*). Metabolomics provides the opportunity of recognizing, classifying and measuring alterations in endogenous metabolites echoing the functioning of specific metabolic pathways, and biological variations in the microenvironment (*Nicholson and Lindon, 2008*). Preclinical models investigated the metabolic changes induced in female Sprague-Dawley rats undergoing paclitaxel administration (8 mg/kg, cumulative dose of 24 mg/kg on 3 alternate days) by an ultra-performance liquid chromatography-electrospray ionization-mass spectrometry (UPLC-ESI-MS) method (*Wu et al., 2018*). The authors found 19 significant altered metabolites associated with the neurotoxic effect of paclitaxel, most of which were lipids, organic acids, and ketones. In addition, results of pathway analysis indicated that paclitaxel-induced peripheral neuropathy mainly interferes with linoleic acid and glycerophospholipid metabolic pathways, determining alterations of the stability, permeability and fluidity in neural membranes and their lipid compounds. Other studies investigated the metabolic alterations which might reveal the onset and progression of CIPN in the clinical setting. One study examined the involvement of 1-deoxysphingolipid plasma levels in peripheral neuropathy symptomatology, as measured by the EORTC and CIPN20 clinical scales, in 27 paclitaxel-treated patients with breast cancer (*Kramer et al., 2015*). The authors found a dose-dependent association between the incidence and severity of CIPN and the concentrations of very-long-chain 1-deoxyceramides, especially with motor neuropathy, denoting a role for these compounds as molecular intermediates of paclitaxel-induced peripheral neuropathy. Sun and colleagues instead conducted a

whole blood metabolomics analysis to test the association between a pre-treatment metabolic profile, early treatment-induced metabolic alterations, and the occurrence of PIPN in 60 breast cancer patients receiving 80 mg/m^2 weekly treatment (*Sun et al., 2018*). The analysis revealed an inverse association between pre-treatment histidine, phenylalanine, and threonine concentrations with the maximum change in clinical scale scores. In addition, paclitaxel caused a significant change in 2-hydroxybutyrate, 3-hydroxybutyrate, pyruvate, o-acetylcarnitine, and several amino acids concentrations from baseline to the end of the first paclitaxel infusion, and 24 hours after the first infusion, despite these associations not correlating with the clinical scales. Accordingly, the authors concluded that pre-treatment histidine, phenylalanine, and threonine levels may be predictive of the severity of future PIPN symptomatology. In a very recent study, Chen and colleagues investigated whether sensory and motor CIPN presented different predictive biomarkers in 60 patients with breast cancer receiving up to 12 weekly infusions of 80 mg/m^2 paclitaxel (*Chen et al., 2022*). Their analysis revealed that lower levels of histidine, phenylalanine, threonine, and vitamin D were associated with more severe sensory CIPN, and lower histidine was specifically related to more severe motor neuropathy.

1.6 Role of liver in paclitaxel-induced metabolic stress

Paclitaxel administration affects numerous systemic pathways, inducing a series of metabolic responses, with the liver playing a key role. In particular, the liver reacts to systemic altered metabolism, leading the body to deal with the stress states by carbohydrate and lipid mobilization. The liver directs glucose and lipid metabolism by orchestrating hepatic glucose production and glycogen storage. During stress or the

fasting state, the liver stimulates hepatic glucose production and glycogen breakdown via transcriptional and non-transcriptional mechanisms (*Rui, 2014*), thus providing peripheral tissues (i.e., brain, adipose tissue, skeletal muscle) with glucose. The liver also has an important function in lipid metabolism in response to nutrient availability, as well as in response to insulin. Specifically, insulin facilitates hepatic fatty acid uptake, the synthesis and storage of triglycerides via the utilization of dietary fatty acids, and promotes *de novo* lipogenesis in the liver, favoring long-term lipid storage (*Rui, 2014*).

Of note, the liver is responsible for the selective uptake, metabolism, and excretion in the bile of taxanes (*Cresteil et al., 1994; Hirth et al., 2000*). In particular, paclitaxel is primarily oxidized by the cytochrome P450 system, mostly CYP2C8 and to a lesser extent CYP3A4 (*Cresteil et al., 1994).* Some reports have documented the association of paclitaxel administration with relatively mild and anicteric hepatic impairment, and temporary increased levels of alkaline phosphatase, aspartate aminotransferase, and bilirubin have been described in about 5% to 20% of patients (*Huizing et al., 1995*). Genetic predisposition may contribute to paclitaxel-induced hepatotoxicity. Recently, the nucleotide excision repair gene ERCC1 c.118C>T polymorphism has been associated with an increased risk for moderate to severe hepatotoxicity (*da Costa Junior et al., 2020*). In this regard, the study of the liver in animals developing PIPN would provide a more comprehensive understanding of the altered metabolic responses induced by paclitaxel administration.

2. Objectives

The aims of our project were:

a) to investigate the neurophysiological, behavioral and histopathological effects of paclitaxel treatment according to age;

b) to assess through a metabolomics approach which metabolic changes might be induced by paclitaxel administration at the different ages compared to controls.

3. Materials and methods

3.1 Study design and experimental protocol

Our experiments were designed to optimize the number of animals according to pre-study power analysis. In particular, sample size was calculated on the basis of nerve conduction velocity reference values of our laboratory (*Monza et al., 2021*), assuming that the relevant difference between controls and paclitaxel-treated groups is 5 m/s (standard deviation = 7); thus, if setting power = 80% and $\alpha = 5\%$, the sample size is 7 animals/group. In our study the sample size was increased above the defined number (12 animals/group) in order to have enough animals to be tested at each time point, and to prevent underpowered statistical analysis in case of animal loss due to chemotherapy (*Ballarini et al., 2022*).

We investigated 24 young (2 months of age) and 24 adult (9 months of age) Wistar male rats (Envigo, Bresso, Italy), which were randomized according to their baseline values of behavioral and neurophysiological parameters into 4 experimental subgroups (n=12) undergoing either paclitaxel treatment (10 mg/kg i.v. once a week for 4 weeks) or vehicle administration (controls). The care and husbandry of animals conformed to

the Institutional guidelines in compliance with national (D.L. n. 26/2014, Gazzetta Ufficiale della Repubblica Italiana, Serie Generale n.61 del 14-3-2014) and international laws (European Union Directive 2010/63/EU: Guide for the Care and Use of Laboratory Animals, US National Research Council, 1996). Animals were housed 2 per cage (2 months of age rats) and 1 per cage (9 months of age rats) in a certified and limited access animal facility under constant temperature (20 ± 2 °C) and humidity (55 ± 10%). Artificial lighting provided a 24-hour cycle of 12 hours of light/12 hours of dark (7.00 h – 19.00 h). Light intensity during the light-phase was 400 lux (measured in direction of gaze, lux meter held in vertical plane). Animals had access to food (pellets 12 mm, Global Diet 2018 certificate, Mucedola srl, Settimo Milanese, Italy) and *ad libitum* access to water. Animal health status was examined daily, and body weight recorded twice a week in order to supervise general conditions and to adjust treatment dose accordingly.

Dosage of paclitaxel (10 mg/kg LC laboratories, Woburn, MA, USA; intravenous injections via the tail vein once a week for 4 weeks) and route of administration were based on previous experience and literature data (*Persohn et al., 2005; Meregalli et al., 2020*). All drug administrations were performed from 09.00 h to 11.00 h.

Neurophysiological and behavioral tests were performed in order to investigate nerve damage at baseline, after 4 weeks of treatment and 2 weeks of follow-up. Blood samples for metabolomics analysis were collected at baseline, after 4 weeks of treatment and 2 weeks of follow-up. At the end of treatment period and after 2 weeks of follow-up, 4 animals per experimental group were sacrificed under terminal CO_2 anesthesia for tissue samples' collection. All procedures were conducted in accordance with protocols approved by the Ethics Committee of the University of Milano-Bicocca and approved by the Italian Ministry of Health. The experimental protocol is presented in **Figure 1**.

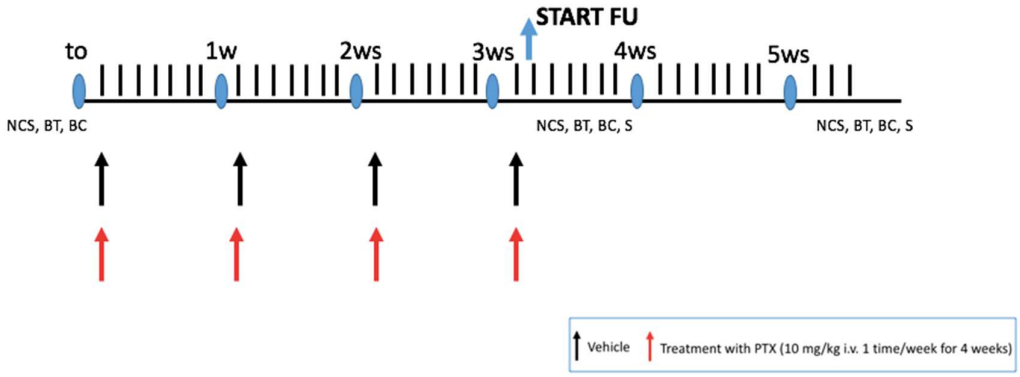

Figure 1. Experimental protocol.

The image shows the experimental protocol of our study. The rows indicate the administration of either paclitaxel (red rows) or the vehicle (black rows). BC: blood collection; BT: behavioral tests; FU: follow-up period; NCS: nerve conduction studies; PTX: paclitaxel; S: sacrifice; W: week.

3.2 Neurophysiological assessments

Caudal and digital nerve conduction velocity and amplitude were investigated in order to assess paclitaxel-induced nerve damage (*Meregalli et al., 2020*). Electrophysiological recordings were performed in the morning (9.00 h – 13.00 h), under deep isoflurane anesthesia and constant body temperature at 37 ± 0.5 °C with an electromyography apparatus (Matrix Light, Micromed, Mogliano Veneto, Italy) involving the application of subdermal needles (Ambu Neuroline, Ambu, Ballerup, Denmark). Specifically, caudal nerve studies were performed orthodromically by placing recording cathode and anode at 6 and 5 cm from the tip of the tail, and the ground electrode at 2.5 cm from it, and stimulating anode and cathode at 2 and 1 cm, respectively (*Meregalli et al., 2018*). Equally, the digital nerve was investigated orthodromically by placing recording cathode at the base and anode at the tip of the fourth toe of the hind limb, while the ground electrode was located subcutaneously in the sole. Stimulating anode and cathode were placed at the ankle and subcutaneously near the patellar bone, respectively (*Meregalli et al., 2018*). Intensity, duration and

frequency of stimulation were established in order to achieve supramaximal results. Filters were set between 20 Hz and 3 KHz (*Meregalli et al., 2018*).

3.3 Behavioral tests

Behavioral assessments were performed in the morning from 9.00 h to 13.00 h. To evaluate chemotherapy-induced alterations in response to mechanical stimuli, we used the dynamic test (model 37450; Ugo Basile Biological Instruments, Comerio, Italy). Mechanical allodynia was defined as a significant decrease in the mechanical threshold response to a metal filament determining the hind paw withdrawal (*Meregalli et al., 2018*). Specifically, rats were individually located on an elevated wire mesh floor in a plexiglas chamber, then animals were allowed to acclimatize to the testing environment for at least 15 minutes. The mechanical hind paw withdrawal threshold (expressed in grams) was calculated by the mean value of six repeated applications of a 0.5 mm diameter metal filament to the plantar surface, determining a gradually increasing tactile pressure to the central region of the plantar surface, up to 50 g within 20 seconds. A cut-off time of 30 seconds was set to prevent tissue damage in the absence of response.

The response to noxious thermal stimuli was determined using the plantar test (model 37370; Ugo Basile Biological Instruments, Comerio, Italy). The reaction time for hind paw withdrawal was recorded to evaluate the nociceptive threshold response to a heat source applied to the plantar surface of the hind paw. In particular, rats were placed in a plexiglas chamber for a 15-minute acclimatization period. The plantar surface of the hind paw was then stimulated by a movable infrared radiant heat source (IR 40 W) determining hind paw withdrawal. The nociceptive threshold response to thermal

stimulus (withdrawal latency expressed in seconds) was calculated by the mean value of four repeated measures (*Meregalli et al., 2018*). A cut-off time of 30 seconds was set to avoid any tissue damage.

3.4 Blood sample collection

Animals were fasted overnight prior to blood collection according to previous protocols (*Skene et al., 2017*). Blood samples for metabolomics analysis were collected from the tail vein during the morning (9.00 h – 15.00 h) into lithium heparin tubes, inverted 8-10 times and transported to the laboratory in a refrigerated cool box. Within 10 minutes of the sample being obtained the tubes were centrifuged (1620 g at 4°C for 10 minutes), then stored (15 µl aliquots x 3) at -80°C. Food was provided with *ad libitum* access on completion of the blood sampling. Samples were subsequently shipped on dry ice to the United Kingdom (University of Surrey) for targeted metabolomics analysis by UPLC-MS/MS.

3.5 Neuropathological analysis

After the fourth and sixth weeks from the beginning of the study, 4 animals/group were sacrificed and tissue samples collected (9.00 h – 13.00 h). In particular, sciatic and caudal nerves, L4-L5 DRGs, and skin were dissected and fixed for histological examination. Livers were stored at -80°C, then shipped on dry ice to the United Kingdom (University of Surrey) for targeted metabolomics analysis by UPLC-MS/MS. After sacrifice, the skin of the hind paw footpad was collected to define small-fiber peripheral nerve damage by quantifying the IENF density (*Meregalli et al., 2018*). Five-mm round samples of epidermis and dermis were collected by biopsy from the plantar

glabrous skin, then fixed in 2% paraformaldehyde-lysine-sodium periodate for 24 hours at 4°C. Samples were cut in 20-µm sections with a cryostat, then immunostained with rabbit polyclonal anti-protein gene product 9.5 antibodies (PGP 9.5; Proteintech Group, Rosemont, Illinois, USA) using a free-floating section protocol. Two raters blind to the condition quantified the total number of PGP 9.5–positive IENFs in each section under a light microscope at 40x magnification (Nexcope NE 920 light microscope, TIEsseLab S.r.L., Milan, Italy). Individual fibers were identified in the dermal-epidermal junction or in the epidermal layer, excluding secondary branching within the epidermis. The IENF density was defined according to the number of PGP 9.5-positive fibers per epidermal length.

Sciatic and caudal nerves, L4-L5 DRGs were collected from sacrificed rats without stretching, then analyzed according to previously validated protocols (*Ballarini et al., 2022*). Specimens were fixed by immersion in 3% glutaraldehyde (nerves) or 2% glutaraldehyde/4% paraformaldehyde (DRGs) in 0.12 M phosphate buffer solution (pH 7.4), post-fixed in osmium tetroxide, epoxy resin embedded, and used for light microscopy and morphometric analysis. For morphological and morphometric evaluation, semi-thin 1.5-µm sections of sciatic and caudal nerves and DRGs were prepared, stained with toluidine blue, and examined with a Nikon Eclipse E200 light microscope (Leica Microsystems GmbH, Wetzlar, Germany). Nerve morphometric analysis was performed using a Nexcope NE 920 light microscope (TIEsseLab S.r.l., Milan, Italy). The images were acquired in stitching mode (60x) using Capture V2.0 Software (Revolutionary Computational Imaging Software, TIEsseLab S.r.l., Milan, Italy) and processed by Image-Pro Plus Software (Immagini e Computer SNC, Milan, Italy). The fiber diameter and the frequency distribution of myelinated fibers were

determined and analyzed with GraphPad Prism Software (GraphPad Software, San Diego, CA).

3.6 Targeted metabolomics analysis

Plasma and liver samples were analyzed using the MxP® Quant 500 targeted metabolomics kit (Biocrates Life Sciences AG, Innsbruck, Austria), and a Waters Xevo TQ-S mass spectrometer combined with an Acquity UPLC system (Waters Corporation, Milford, MA, USA). Liver samples were prepared according to previously validated protocols (*Römisch-Margl et al., 2012*). Specifically, liver tissue samples were placed into pre-cooled (dry ice) 2 ml homogenization tubes containing ceramic beads (Fisherbrand™ Pre-Filled Bead Mill Tubes, Thermo Fisher Scientific, Waltham, MA, USA). Thereafter, 6 µl/mg of pre-cooled extraction solvent (methanol) was added to each tube. Tissue samples were subsequently homogenized (TissueLyser, QIAGEN, Hilden, Germany) three times for 20 seconds at 30 Hz, with 30 second intervals, to ensure freezing temperatures in sample vials between the homogenization steps. The tubes were subsequently centrifuged for 5 minutes at 10,000 x g_{av} at room temperature. Plasma samples (10 µl) were processed according to the Biocrates MxP Quant 500 kit user manual. In particular, 10 µL of sample (plasma, liver) were randomized, then each added with blank and zero samples, kit calibrators (n=7), and 3 levels of quality controls (QCs) directly onto the 96-well plate provided with the kit according to the pipetting plan predefined in Biocrates MetIDQ software. After drying for 30 minutes using nitrogen, a derivatization step for one hour using a 5% phenylisothiocyanate (PITC) solution was performed. After another drying step of one hour, 300 µL of 5 mM methanolic ammonium acetate were added as extraction solvent and, after shaking of

the kit plate for 30 min, the contents were filtered into a lower sandwich plate by centrifugation at 500 g for 2 minutes. The sample extracts were diluted for successive flow injection analysis-MS/MS (FIA-MS/MS) and UPLC-MS/MS as indicated in the kit user manual.

3.7 Statistical analysis

Statistical analyses of body weight, nerve conduction studies, behavioral tests, and neuropathological data were performed using GraphPad Prism software version 4.0 (GraphPad Software, San Diego, CA, USA). Normally distributed data were analyzed with parametric tests (t-test, ANOVA methods) and described as mean ± Standard Error of the Mean (SEM); while non-normally distributed data were analyzed with non-parametric tests (Mann-Whitney U test, Kruskal-Wallis test followed by Dunn's multiple comparison test) and described by the median and interquartile range (IQR) in square brackets (*Ballarini et al., 2022*). A p value < 0.05 was considered statistically significant.

For metabolomics analysis, the levels of metabolites present in each QC were compared to the expected values and the percent coefficient of variation (CV%) calculated. Data were scaled between plate batches using the results of quality control level 2 (QC2) repeated across each plate (n=5/plate) and between plates (n=2) using Biocrates MetIDQ software (QC2 correction).

For inter-study consistency, metabolites were excluded where >25% concentrations were below the limit of detection (<LOD) or below lower limit of quantification ($\ll$LLOQ) or above limit of quantification (>LOQ) or blank out of range, or the QC2 coefficient of variance was >30% (*Skene et al., 2017*).

Significant differences in individual metabolite levels between experimental groups and time periods and their interaction were analyzed in R version 4.2.1 using the linear models and ANOVA methods in the statistical package. P-values were corrected for multiple comparisons according to the Benjamini-Hochberg False Discovery Rate (FDR) method. Comparisons were considered as significant at the FDR cut-off <0.05. Correlation analysis was performed to investigate the associations between neurophysiological, behavioral and neuropathological data, and the relationships between these parameters and metabolite concentrations. Pearson's and Spearman's correlation tests were used to assess linear and monotonic relationships, respectively. Statistically significant correlations were identified (p values <0.05). For data visualization, we used a heat map combined with hierarchical clustering (Euclidean distance and Ward linkage). Potential outlier measures were identified by Random Forest algorithm.

Multivariate analysis was performed on log-transformed and pareto-scaled metabolomics data by unsupervised, Principal Component Analysis (PCA), and supervised methods, Partial Least Squares-Discriminant Analysis (PLS-DA) and Orthogonal Partial Least Squares-Discriminant Analysis (OPLS-DA), using MetaboAnalyst 5.0 (*Pang et al., 2022*). We considered a model robust if the R^2 and Q^2 values >0.5, with Q^2 value close to the R^2 value (*Blasco et al., 2014*). Models were rejected if there was complete overlap of Q^2 distributions, Q^2(cum)<0, or low classification rates, Q^2(cum)<0.05 (*Blasco et al., 2014*). The contribution of variables to the separation of classes was evaluated by the loading variable influence on prediction (VIP) plot. Variables with VIP values >1 were considered relevant (*Dauvilliers et al., 2022*). Enrichment analysis and Over Representation Analysis (ORA) were implemented by the hypergeometric test to evaluate whether a particular

VIP metabolite set was represented more than expected by chance within the identified compound list using MetaboAnalyst 5.0 (*Pang et al., 2022*).

Quantitative Pathway analysis was performed using MetaboAnalyst 5.0 (*Pang et al., 2022*). Specifically, a metabolite concentration (μM) table was inputted, with metabolite names standardized by a built-in tool so that these could be compared with the metabolite set library. Pathway analysis investigates the complex relationships among molecules within a cell or a living organism, estimating which pathways are significantly changed under conditions of study. The most significant pathways affected by paclitaxel administration, in relation to age, were defined according to the FDR (cut-off <0.05), impact > 0.05 and number of hits ≥ 2.

4. Results

4.1 Safety and tolerability of paclitaxel

Paclitaxel administration was well tolerated by treated animals during the experiment, inducing a moderate difference in body weight in young-treated animals compared to control rats, without reaching the statistical significance ($p > 0.05$). By contrast, adult-treated animals presented a lower body weight all over the study compared to controls, with a statistically significant loss of weight after the last two paclitaxel administrations (486.5 ± 7.1 vs 515.9 ± 9.0 g, $p<0.05$, in the third week of treatment; 475.2 ± 8.3 vs 518.9 ± 11.4 g, $p<0.01$, in the fourth week of treatment). No lethal complications were recorded. Body weight measures over the study are presented in **Figure 2**.

A)

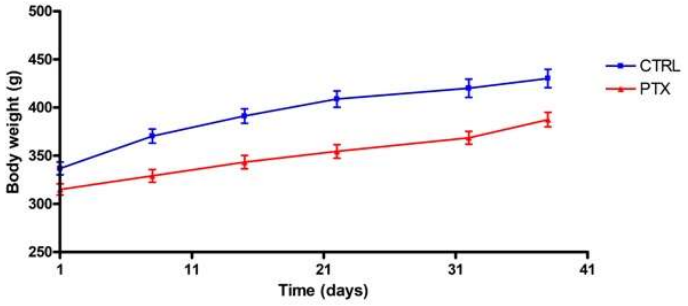

B)

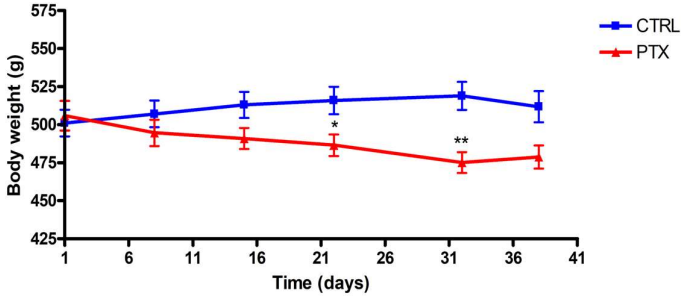

Figure 2. Body weight measures over the study.

Data are described as mean ± Standard Error of the Mean (SEM). The graphs show the body weight measures over the study in young (A) and adult (B) animals. CTRL: control group; PTX: paclitaxel-treated group. *$p<0.05$ vs CTRL, **$p<0.01$ vs CTRL (t-test).

4.2 Nerve conduction studies

Neurophysiological data and statistical analysis are reported in **Table 1** and **2**.

At the end of treatment, the neurophysiological studies revealed a significant reduction in SNAP amplitude ($p<0.05$) of the caudal nerve of young-treated animals, and in both the caudal nerve ($p<0.05$) and the digital nerve ($p<0.05$) of adult-treated animals compared to age-matched controls. Conversely, the nerve conduction velocity of caudal and digital nerves did not significantly differ ($p >0.05$) between treated animals and controls in both young and adult rats after the last paclitaxel-administration.

After the follow-up period, young-treated animals presented a significantly decreased SNAP amplitude ($p<0.01$) and velocity ($p<0.05$) in the caudal nerve compared to controls. Conversely, NCS of the digital nerve did not show any significant difference between young-treated animals and controls. Concerning adult animals, treated rats developed a significantly reduced SNAP amplitude ($p<0.01$) and velocity ($p<0.01$) in the caudal nerve compared to controls, with no alterations in NCS of the digital nerve. Neurophysiological results are presented in **Figure 3** and **4**.

A. End of treatment			
	CTRL	PTX	
	N = 12	N = 12	p value
Caudal nerve amplitude (μV)	98.2 [93.1-101.7]	68.6 [32.1-86.0]	< 0.05 *
Caudal nerve velocity (m/s)	44.7 [41.0-44.7]	41.0 [39.3-44.7]	> 0.05
Digital nerve amplitude (μV)	62.9 [57.2-70.8]	60.7 [55.5-67.4]	> 0.05
Digital nerve velocity (m/s)	45.1 [44.9-46.2]	45.2 [42.3- 45.9]	> 0.05
Mechanical threshold (g)	39.7 [37.8- 40.5]	32.4 [29.6- 34.4]	< 0.001 *
Thermal threshold (s)	10.3 [9.1-12.1]	12.0 [10.7-14.7]	> 0.05
B. End of the follow-up period			
	CTRL	PTX	
	N = 8	N = 8	p value
Caudal nerve amplitude (μV)	129.7 [114.5- 137.8]	69.0 [35.7-90.6]	< 0.01 *
Caudal nerve velocity (m/s)	44.7 [43.7- 45.8]	37.8 [35.8- 41.9]	< 0.05 *
Digital nerve amplitude (μV)	103.7 [96.7-110.1]	91.4 [82.3-95.0]	> 0.05
Digital nerve velocity (m/s)	46.2 [44.8-47.3]	45.8 [43.5-46.9]	> 0.05
Mechanical threshold (g)	39.3 [38.4-39.9]	35.5 [33.4-37.2]	< 0.05 *
Thermal threshold (s)	7.9 [7.4-8.7]	9.9 [8.2-11.4]	> 0.05

Table 1. Summary of neurophysiological and behavioral results of the young group.

Data are median and interquartile range (IQR) in square brackets; Mann–Whitney U test p value. * significant p value (<0.05). CTRL: control group; PTX: paclitaxel-treated group.

A. End of treatment			
	CTRL	PTX	
	N = 12	N = 12	p value
Caudal nerve amplitude (μV)	170.7 [152.7-208.2]	122.2 [102.8-172.1]	< 0.05 *
Caudal nerve velocity (m/s)	56.2 [53.2-57.8]	53.2 [45.8-56.2]	> 0.05
Digital nerve amplitude (μV)	61.34 [49.2-77.8]	45.71 [42.0-51.8]	< 0.05 *
Digital nerve velocity (m/s)	47.6 [44.1- 49.2]	47.7 [45.4- 49.6]	> 0.05
Mechanical threshold (g)	37.2 [35.7-39.4]	35.9 [34.3- 36.4]	> 0.05
Thermal threshold (s)	9.5 [7.1-11.1]	8.3 [7.8-9.9]	> 0.05
B. End of the follow-up period			
	CTRL	PTX	
	N = 8	N = 8	p value
Caudal nerve amplitude (μV)	213.0 [195.1-240.9]	122.1 [91.8-164.2]	< 0.01 *
Caudal nerve velocity (m/s)	45.8 [44.7-46.8]	41.0 [41.0-43.72]	< 0.01 *
Digital nerve amplitude (μV)	86.5 [73.5-95.4]	64.0 [60.6-80.3]	> 0.05
Digital nerve velocity (m/s)	46.9 [45.3-48.0]	46.9 [44.8-48.4]	> 0.05
Mechanical threshold (g)	38.0 [37.4-39.2]	36.2 [34.9-38.5]	> 0.05
Thermal threshold (s)	11.0 [9.5-12.2]	11.9 [10.8-12.7]	> 0.05

Table 2. Summary of neurophysiological and behavioral results of the adult group.

Data are median and interquartile range (IQR) in square brackets; Mann–Whitney U test p value. * significant p value (<0.05). CTRL: control group; PTX: paclitaxel-treated group.

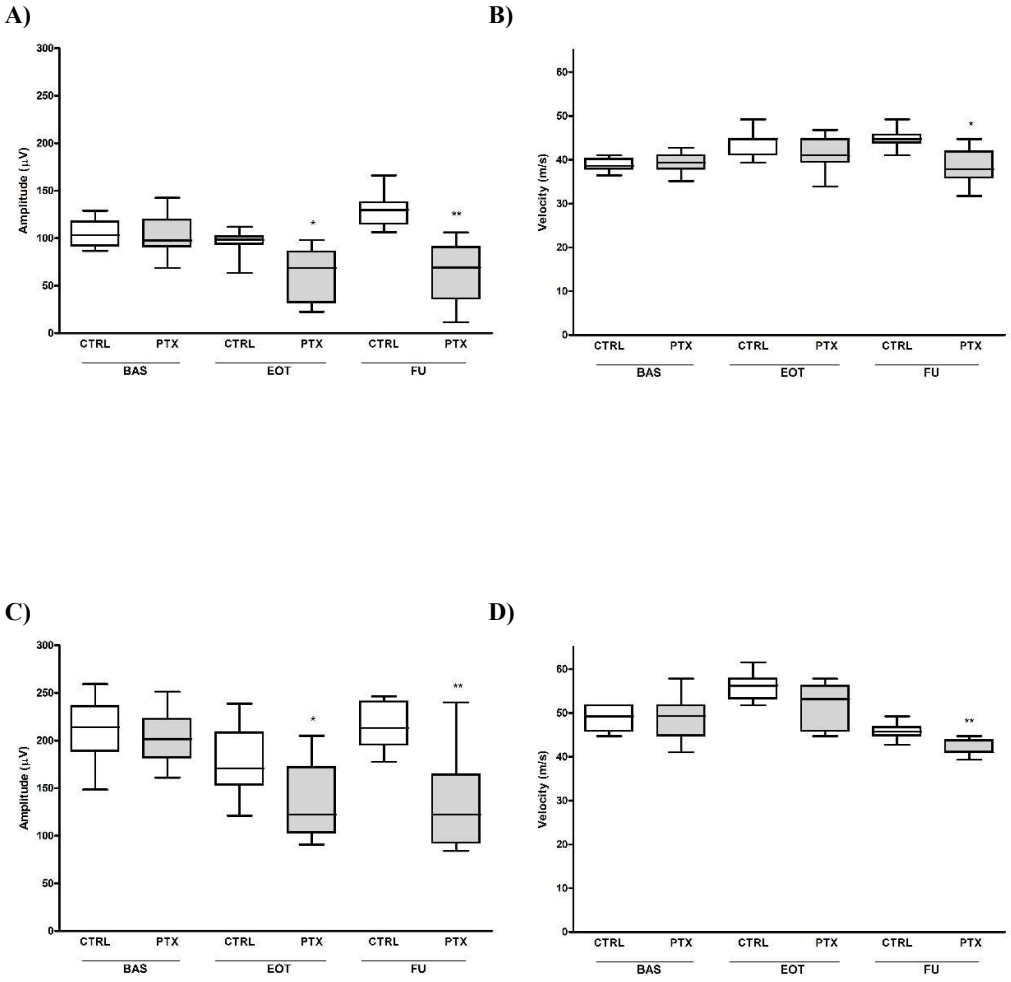

Figure 3. Nerve conduction studies of the caudal nerve.

The graphs show the nerve conduction amplitude (A) and velocity (B) of the caudal nerve in young animals, and the nerve conduction amplitude (C) and velocity (D) of the caudal nerve in adult animals. Variables are described by the median and quartile values, as well as maximum and minimum values. BAS: baseline; CTRL: control group; EOT: end of treatment; FU: end of the follow-up period; PTX: paclitaxel-treated group. *p<0.05 vs CTRL, **p<0.01 vs CTRL (Mann-Whitney U test).

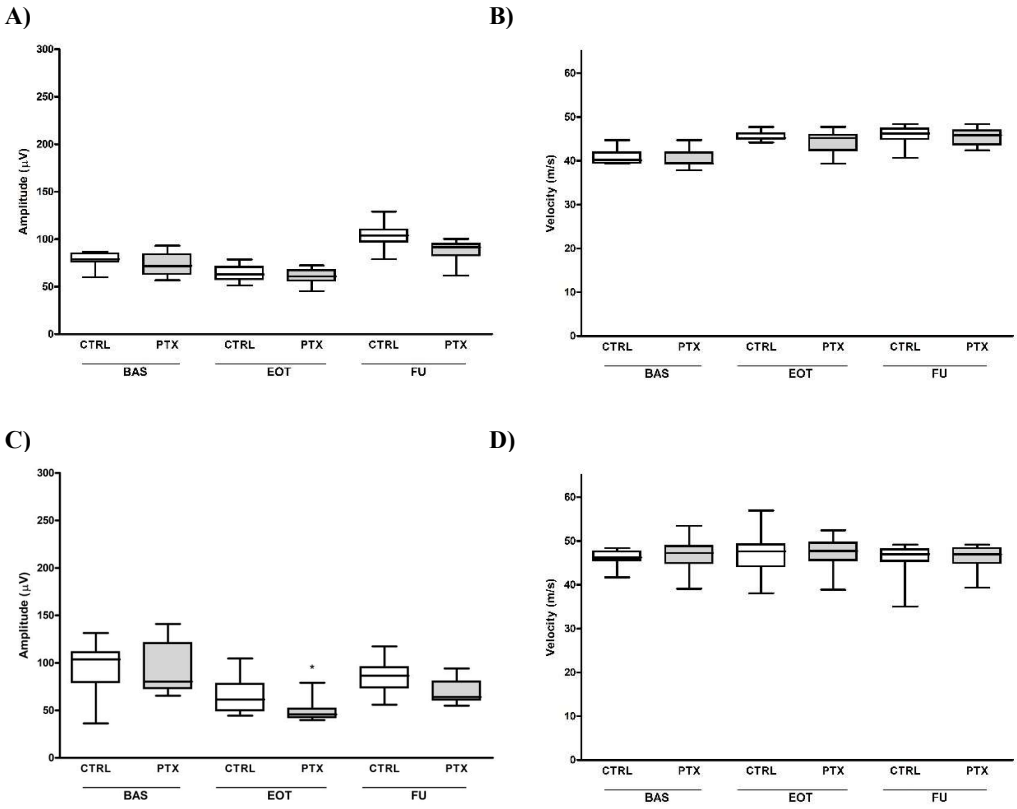

Figure 4. Nerve conduction studies of the digital nerve.

The graphs show the nerve conduction amplitude (A) and velocity (B) of the digital nerve in young animals, and the nerve conduction amplitude (C) and velocity (D) of the digital nerve in adult animals. Variables are described by the median and quartile values, as well as maximum and minimum values. BAS: baseline; CTRL: control group; EOT: end of treatment; FU: end of the follow-up period; PTX: paclitaxel-treated group. *p<0.05 vs CTRL (Mann-Whitney U test).

4.3 Behavioral tests

Behavioral data and statistical analysis are reported in **Table 1** and **2**.

Analyzing behavioral tests, at the end of treatment the dynamic assessment revealed the development of mechanical allodynia with a significant decrease ($p<0.001$) in the mechanical threshold in young-treated animals compared to controls, which persisted at the end of the follow-up period ($p<0.05$); while adult-treated rats did not present a statistically significant difference for the mechanical threshold compared to controls ($p>0.05$). The plantar test for thermal threshold was not statistically significant in both

young- and adult-treated animals compared to controls (p >0.05). Behavioral tests' results are presented in **Figure 5**.

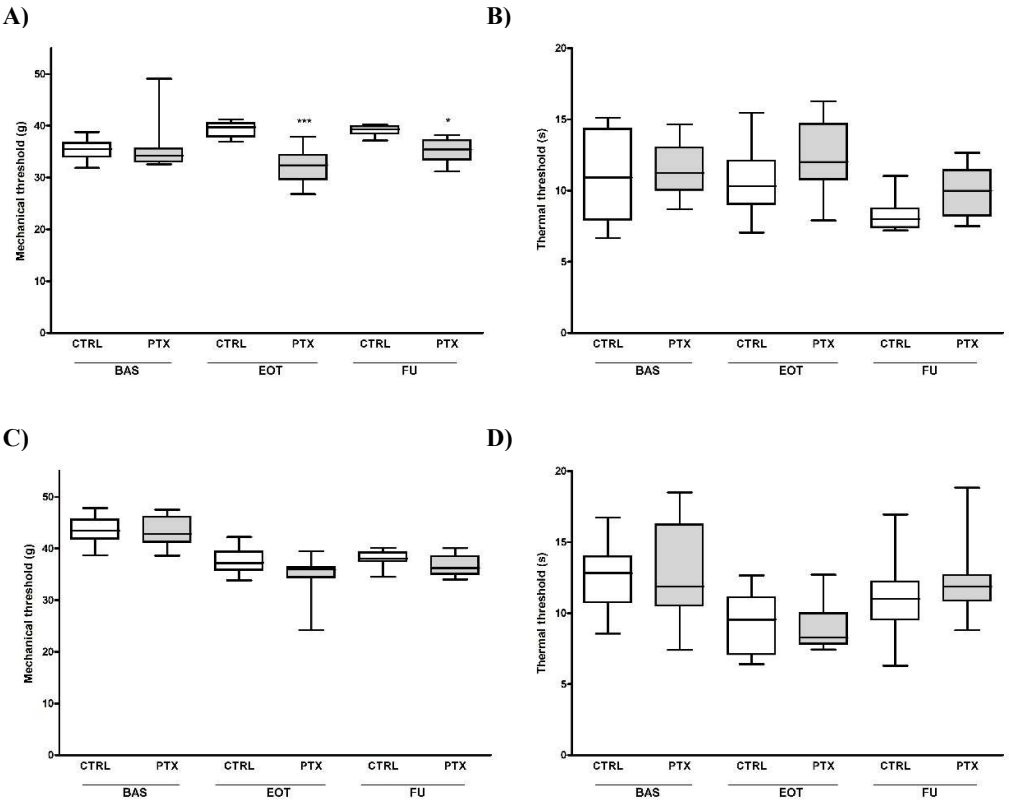

Figure 5. Behavioral tests' results.

The graphs show the dynamic (A) and plantar (B) test results in young animals, and the dynamic (C) and plantar (D) test results in adult animals. Variables are described by the median and quartile values, as well as maximum and minimum values. BAS: baseline; CTRL: control group; EOT: end of treatment; FU: end of the follow-up period; PTX: paclitaxel-treated group. *p<0.05 vs CTRL, ***p<0.001 vs CTRL (Mann-Whitney U test).

4.4 IENF density assessment

Concerning IENF density assessment, young-treated rats presented a significantly reduced IENF density after paclitaxel administration compared to controls: 16 [IQR 14.5-17.0] vs 24.3 [20.5-25.9] fibers/mm, p<0.0001. Similarly, IENF density was significantly lower in adult-treated rats after treatment completion compared to controls: 13.4 [11.8-14.3] vs 20.1 [19.0-23.3] fibers/mm, p<0.0001. Of note, IENF density was significantly more affected in adult-treated rats compared to young-treated animals after the end of treatment: 13.4 [11.8-14.3] vs 16 [14.5-17.01] fibers/mm, p<0.01. Significantly reduced IENF density persisted in treated animals at the end of the follow-up period: 13.8 [12.3-15.9] vs 20.9 [20.2-22.8] fibers/mm, p<0.0001, in the young group; 12.6 [11-15.6] vs 21.0 [20.3-21.8] fibers/mm, p<0.0001, in the adult group. Results of IENF density assessment are shown in **Figure 6**.

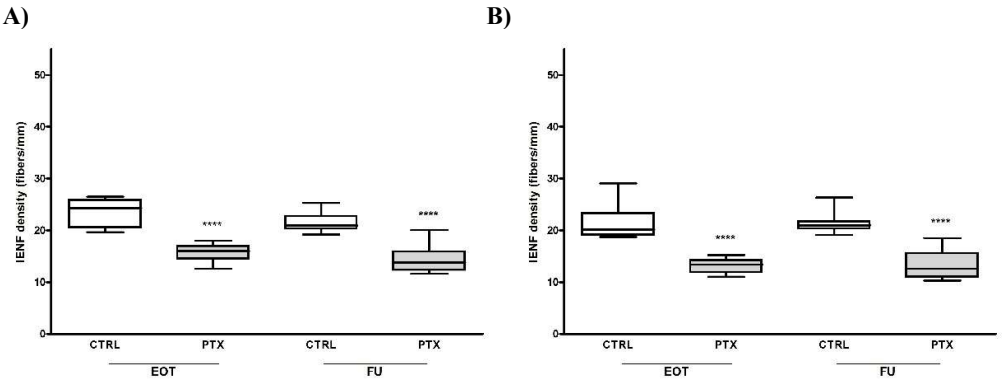

Figure 6. IENF density assessment.

The graphs show the IENF density of young (A) and adult (B) animals. Variables are described by the median and quartile values, as well as maximum and minimum values. CTRL: control group; EOT: end of treatment; FU: end of the follow-up period; IENF: intraepidermal nerve fiber; PTX: paclitaxel-treated group. **** p<0.0001vs CTRL (Mann-Whitney U test).

4.5 Morphological and morphometric evaluations

Morphological and morphometric investigations performed on distal and proximal caudal nerve segments showed the typical distal-to-proximal degeneration pattern of PIPN (*Cavaletti et al., 2007*). In particular, both young and adult paclitaxel-treated rats presented numerous degenerated fibers in the distal caudal nerve at the end of treatment, which was associated with a statistically significant reduction in large myelinated fiber density in treated-animals compared to controls (5591 ± 4547.8 vs 19735 ± 608.6 fibers/mm^2, $p<0.05$, in 2-month group; 4329 ± 2166.8 vs 12807 ± 465.3 fibers/mm^2, $p<0.05$, in 9-month group), until the end of the observational period (1111 ± 315.2 vs 15135 ± 2856.1 fibers/mm^2, $p<0.05$, in 2-month group; 2824 ± 1546.9 vs 10091 ± 1543.6 fibers/mm^2, $p<0.05$, in 9-month group).

The morphological aspects described in the distal caudal nerve were also detected in the proximal caudal nerve, with numerous degenerated fibers and myelin irregularities. However, treated-animals did not present a statistically significant difference in large myelinated fiber density of the proximal caudal nerve compared to controls at the end of treatment (13147 ± 984.8 vs 15546 ± 1139.6 fibers/mm^2, $p >0.05$, in 2-month group; 8191 ± 2920.9 vs 9790 ± 423.6 fibers/mm^2, $p >0.05$, in 9-month group), and at the end of the follow-up period (10788 ± 3269.6 vs 14097 ± 868.6 fibers/mm^2, $p >0.05$, in 2-month group; 7747 ± 3089.2 vs 8921 ± 4960 fibers/mm^2, $p >0.05$, in 9-month group). Representative images of caudal nerve sections obtained from animals at different time points are presented in **Figure 7**.

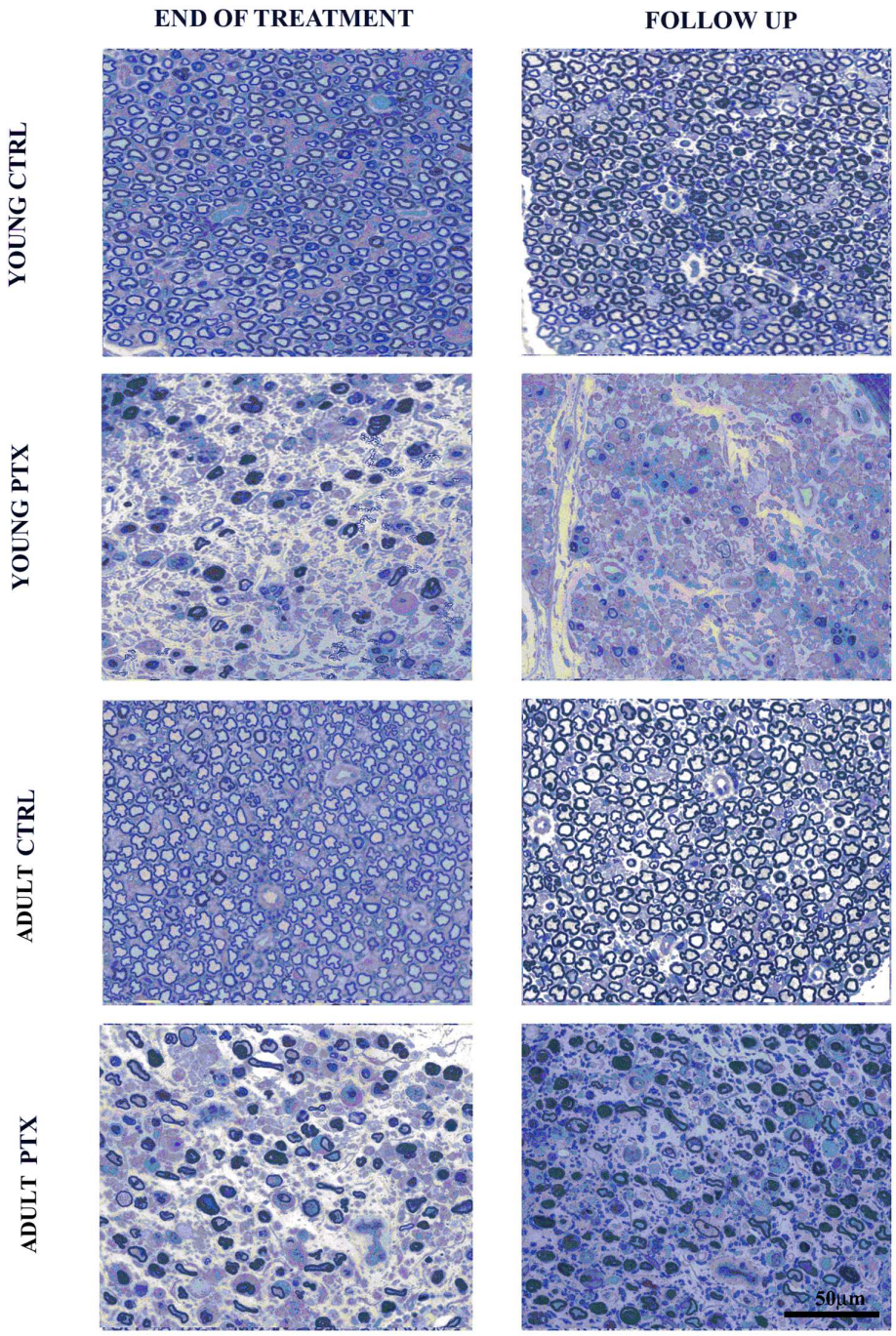

Fig. 7. Effects of paclitaxel administration on the caudal nerve.

Morphological examination of resin-embedded caudal nerve sections, stained with toluidine blue, revealed the development of paclitaxel-induced severe axonopathy in treated-animals compared to controls (60x magnification). CTRL: control group; PTX: paclitaxel-treated group.

At the end of treatment, the sciatic nerve analysis showed mild axonal changes in all treated rats, despite the overall extent of these alterations being fairly limited in both the end of treatment (13234 ± 1482.9 vs 14468 ± 6665.5 fibers/mm^2, p >0.05, in 2-month group; 7632 ± 540.6 vs 9441 ± 3124.5 fibers/mm^2, p >0.05, in 9-month group), and the end of the follow-up period (7760 ± 5479.4 vs 8257 ± 3541.2 fibers/mm^2, p > 0.05, in 2-month group; 5294 ± 2214 vs 5908 ± 2515 fibers/mm^2, p >0.05, in 9-month group).

The frequencies of large myelinated fibers according to their external diameter are shown in **Figure 8** and **9**. The analysis of the fiber size distribution at the end of treatment and of the follow-up period mainly showed unimodal distributions, and a lower caudal and sciatic nerve large myelinated fiber density in treated-animals compared to controls. We observed a bimodal distribution only in the proximal caudal nerve of adult-treated animals at treatment completion (**Figure 8C**). In addition, adult animals presented a lower large myelinated fiber density compared to young rats in both the caudal nerve and the sciatic nerve, with a mild shift to larger fiber diameter with aging in the caudal nerve.

A)

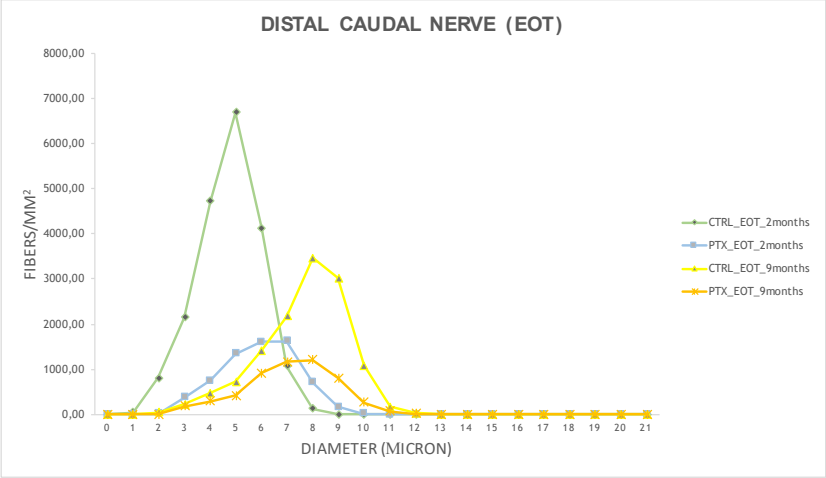
DISTAL CAUDAL NERVE (EOT)
FIBERS/MM²
8000,00
7000,00
6000,00
5000,00
4000,00
3000,00
2000,00
1000,00
0,00
0 1 2 3 4 5 6 7 8 9 10 11 12 13 14 15 16 17 18 19 20 21
DIAMETER (MICRON)
CTRL_EOT_2months
PTX_EOT_2months
CTRL_EOT_9months
PTX_EOT_9months

B)

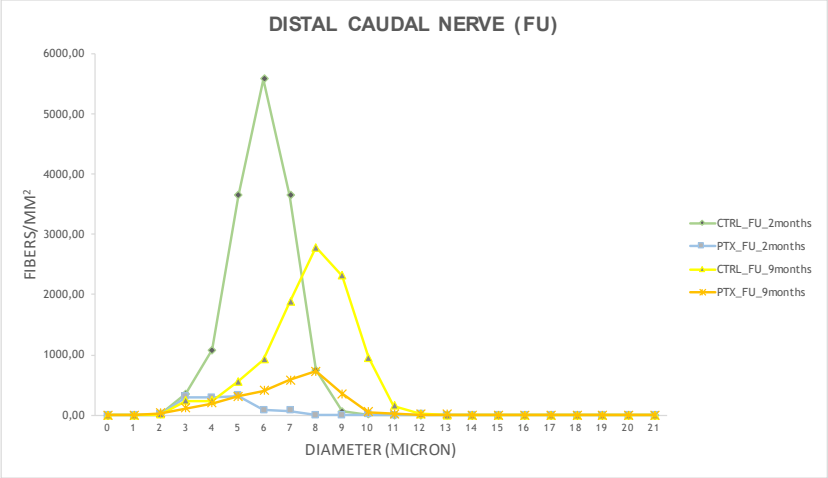
DISTAL CAUDAL NERVE (FU)
FIBERS/MM²
6000,00
5000,00
4000,00
3000,00
2000,00
1000,00
0,00
0 1 2 3 4 5 6 7 8 9 10 11 12 13 14 15 16 17 18 19 20 21
DIAMETER (MICRON)
CTRL_FU_2months
PTX_FU_2months
CTRL_FU_9months
PTX_FU_9months

C)

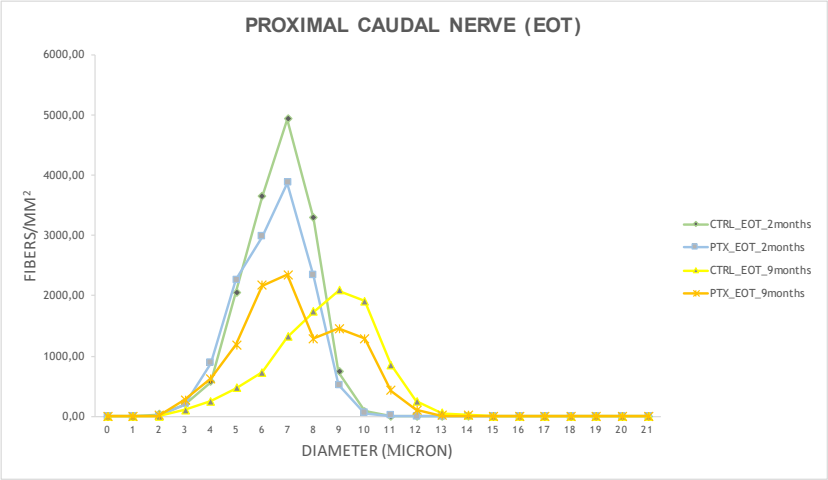

D)

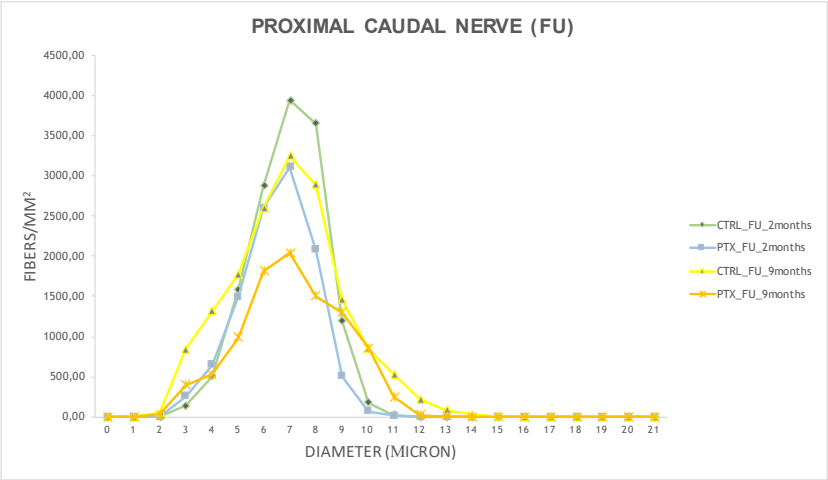

Figure 8. Frequencies of myelinated fibers according to their external diameter in the caudal nerve.

Comparison between the morphometric results obtained at different time-points of treated animals versus controls from the distal caudal nerve at the end of treatment (A) and at the end of the follow-up period (B), and from the proximal caudal nerve at the end of treatment (C) and at the end of the follow-up period (D). CTRL: control group; EOT: end of treatment; FU: end of the follow-up period; PTX: paclitaxel-treated group.

A)

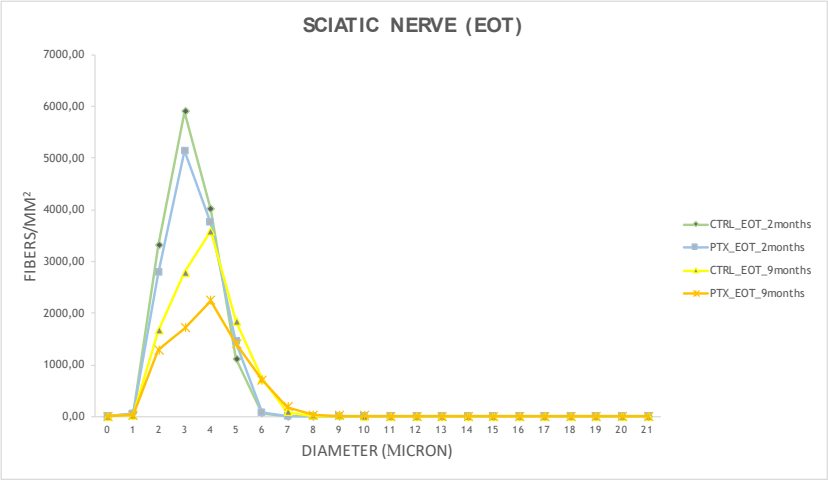

B)

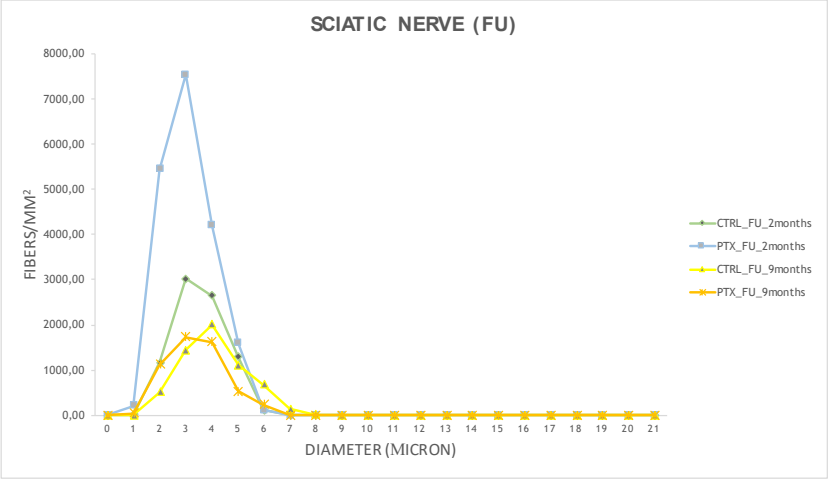

Figure 9. Frequencies of myelinated fibers according to their external diameter in the sciatic nerve.

Comparison between the morphometric results obtained at different time-points of treated animals versus controls from the sciatic nerve at the end of treatment (A) and at the end of the follow-up period (B). CTRL: control group; EOT: end of treatment; FU: end of the follow-up period; PTX: paclitaxel-treated group.

When the nerve morphometric findings were plotted against the neurophysiological results to assess their correlation, we found that the caudal SNAP amplitude and nerve conduction velocity (NCV) data represented a linear function of myelinated fibers' density. Correlation analysis results are shown in **Figure 10** and **11**.

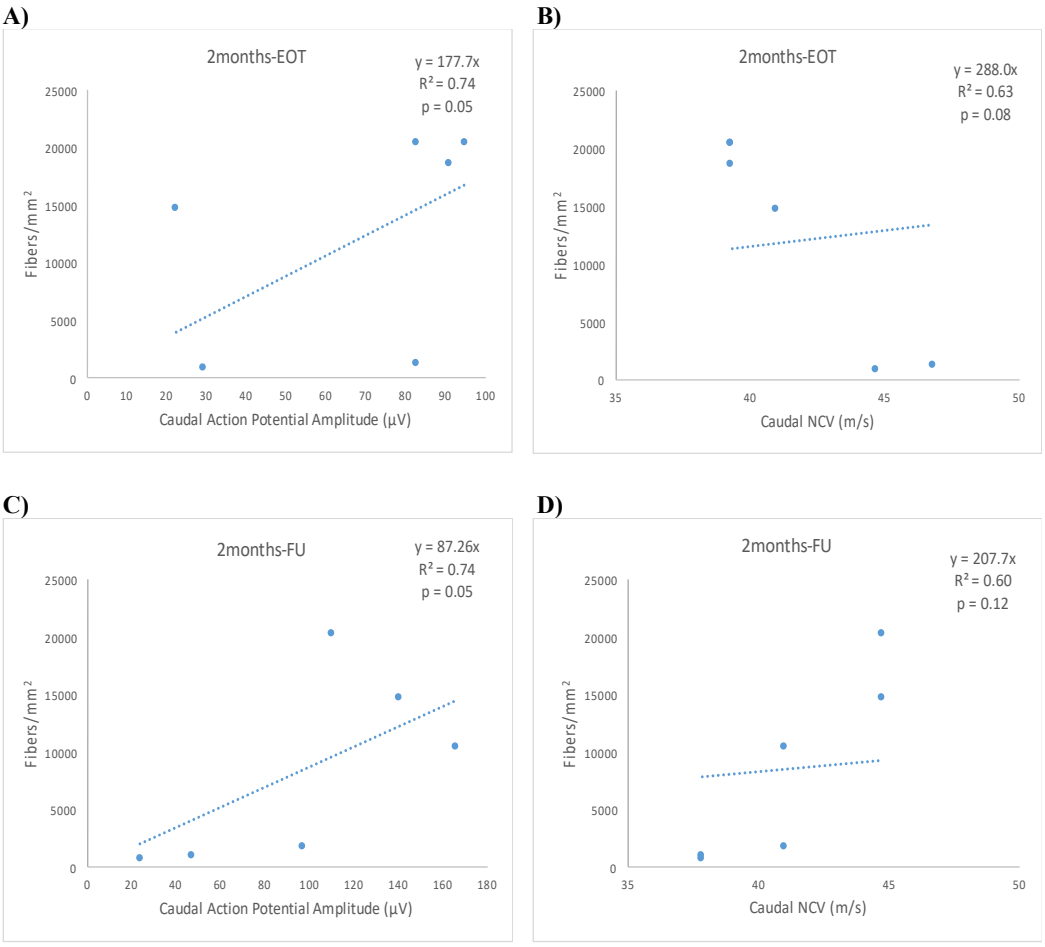

Figure 10. Correlation analysis results of the caudal nerve in young animals.

The graphs show the correlation analysis between nerve fiber density and caudal nerve amplitude (A) and velocity (B) at the end of treatment, and caudal nerve amplitude (C) and velocity (D) at the end of the follow-up period. EOT: end of treatment; FU: end of the follow-up period; NCV: nerve conduction velocity. Strong correlation: $r^2 > 0.65$; $p < 0.05$.

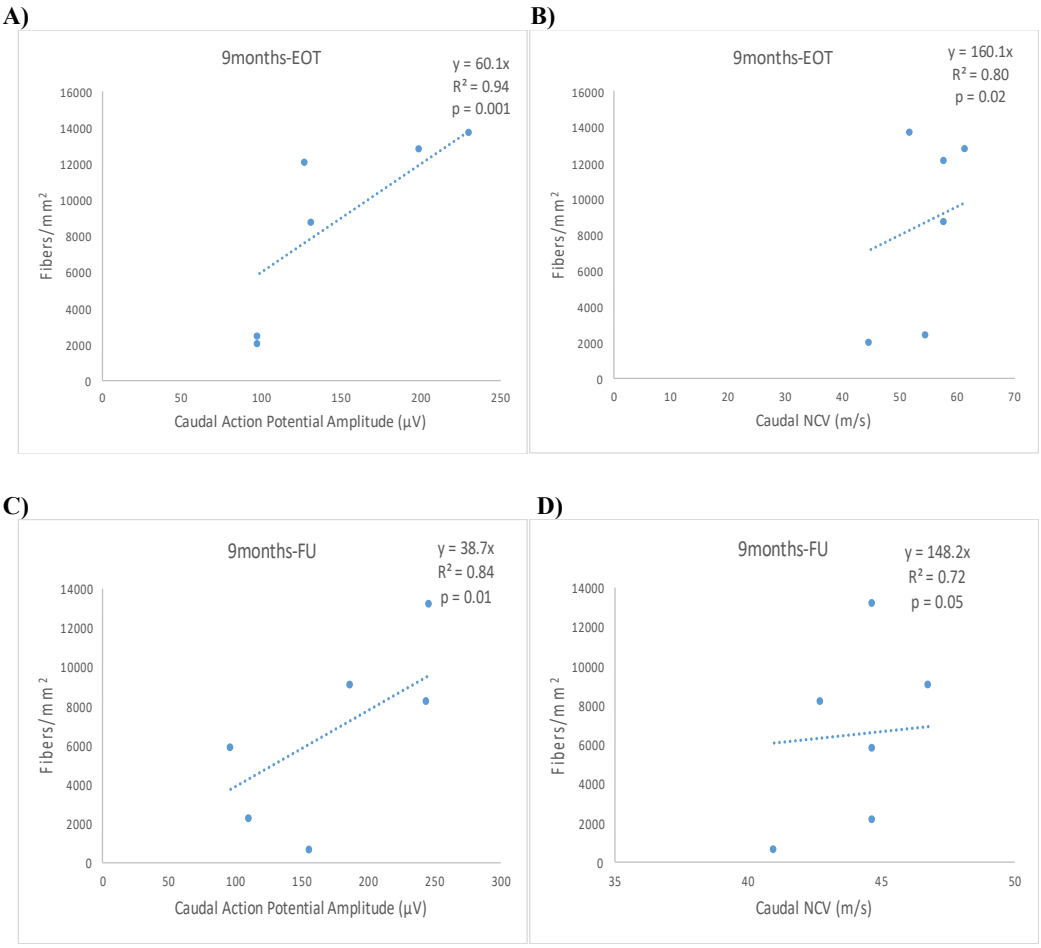

Figure 11. Correlation analysis results of the caudal nerve in adult animals.

The graphs show the correlation analysis between nerve fiber density and caudal nerve amplitude (A) and velocity (B) at the end of treatment, and caudal nerve amplitude (C) and velocity (D) at the end of the follow-up period. EOT: end of treatment; FU: end of the follow-up period; NCV: nerve conduction velocity. Strong correlation: $r^2 > 0.65$; $p < 0.05$.

Only a few alterations were observed in DRGs of young- and adult-treated animals after treatment completion, comprising scattered dark and lamellar inclusions in the cytoplasm of neurons and satellite cells. Some vacuolization was also present in DRG neurons of adult controls, as an effect of aging.

4.6 Plasma metabolomics analysis

One hundred and twenty-eight (n=128) plasma samples were analyzed. After performing FIA-MS/MS and LC-MS/MS, 624 metabolites from 26 compound classes were quantified. Two metabolites presented more than 50% of missing values (3-nitrotyrosine and phenylethylamine), thus they were not included in the analysis. The remaining 622 quantified metabolites were represented by triglycerides (n=242, 38.9%), phosphatidylcholines (n=74, 11.9%), diglycerides (n=41, 6.6%), acylcarnitines (n=40, 6.4%), amino acid related (n= 29, 4.7%), ceramides (n=28, 4.5%), cholesteryl-esters (n=22, 3.5%), amino acids (n=20, 3.2%), hexosylceramides (n=19, 3.1%), sphingomyelins (n=14, 2.3%), bile acids (n=14, 2.3%), lysophosphatidylcholines (n=14, 2.3%), fatty acids (n=12, 1.9%), dihexosylceramides (n=9, 1.4%), dihydroceramides (n=8, 1.3%), biogenic amines (n=8, 1.3%), carboxylic acids (n=7, 1.1%), trihexosylceramides (n=6, 1%), hormones and related (n=4, 0.6%), indoles and derivatives (n=4, 0.6%), nucleobases and related (n=2, 0.3%), monosaccharides (n=1, 0.2%), alkaloids (n=1, 0.2%), amine oxides (n=1, 0.2%), cresols (n=1, 0.2%), vitamins and cofactors (n=1, 0.2%).

Random forest method qualified 3 samples out of 128 as outliers (2.3%), which were spread across the different study groups (2×adult-control group; 1×young-paclitaxel group). Metabolomics data (n=622) were normalized by log-transformation and pareto-scaling.

At baseline, no metabolites with significant FDR (<0.05) were detected with univariate analysis (t-test) between treated-groups and controls. When performing PCA analysis, scree plot showed that the two first Principal Components (PCs) explained 48.1% (2 months) and 42.3 % (9 months) of the variation in the concentration of the selected

metabolites (**Figure 12**). Similarly, supervised models, validated by permutation analysis, had no predictive relevance in both 2-month and 9-month animals (**Figure 13**). We found an overlap between controls and paclitaxel-treated groups (**Figure 14**).

A) **B)**

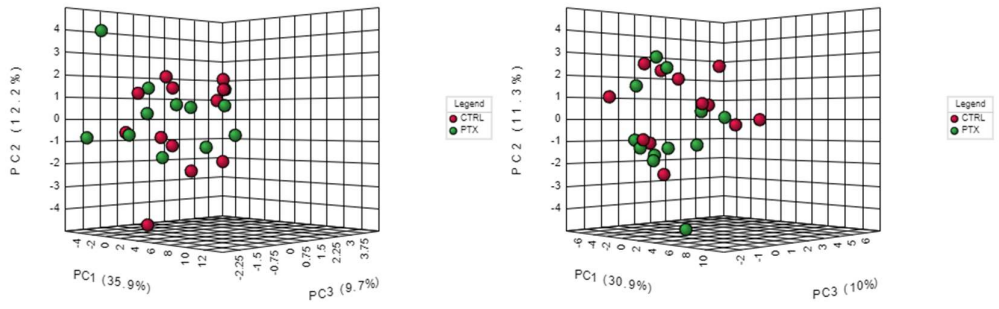

Figure 12. Plasma 3D score plot between the selected Principal Components at baseline.

The explained variances are shown in parentheses for the young (A) and adult (B) groups. CTRL: control group; PC: Principal Component; PTX: paclitaxel-treated group.

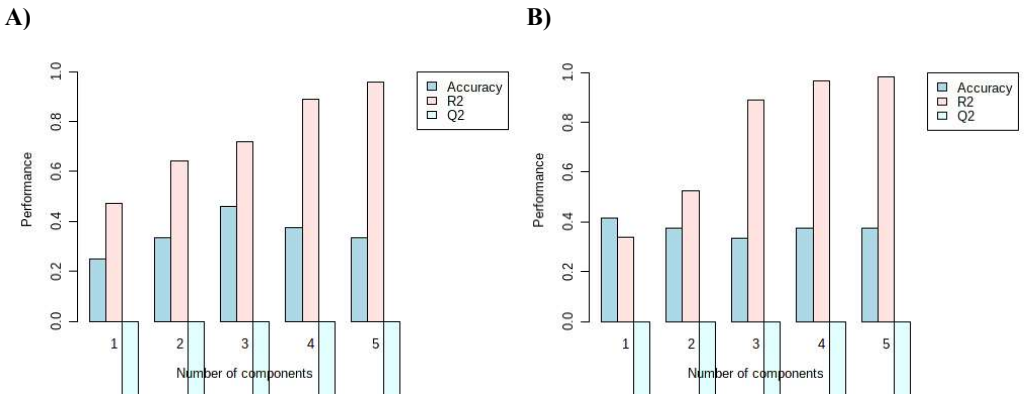

Figure 13. Overview of plasma PLS-DA model at baseline.

PLS-DA classification using different number of components for the young (A) and adult (B) groups. We considered a model robust if R^2 and Q^2 values > 0.5, with Q^2 value close to the R^2 value. Models were rejected if there was complete overlap of Q^2 distributions, $Q^2(cum)< 0$, or low classification rates, $Q^2(cum)<0.05$.

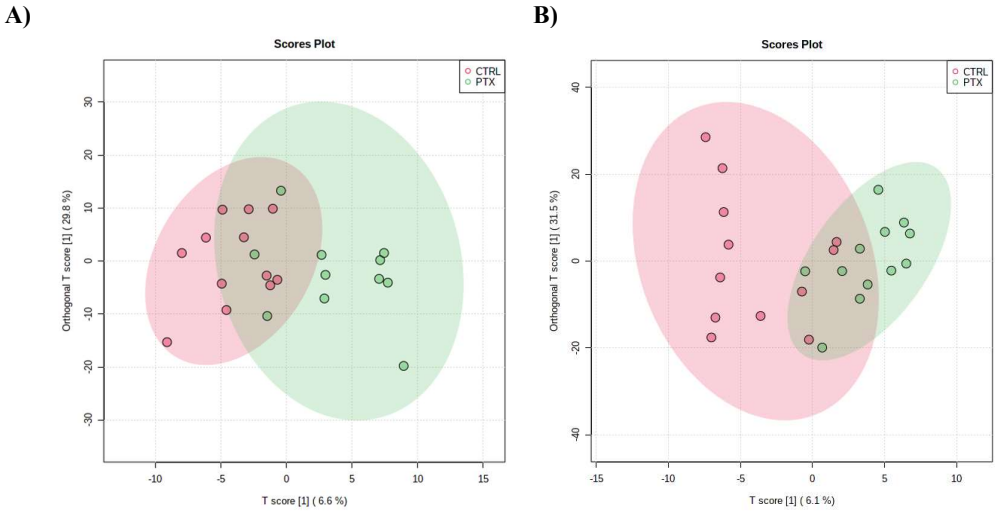

Figure 14. Plasma OPLS-DA score plot of all metabolites at baseline.

The image shows the score plot of all metabolites at baseline in young (A) and adult (B) animals. The explained variances are reported in parentheses along the axis. CTRL: control group; PTX: paclitaxel-treated group.

After treatment completion, the resulting PCA scree plot showed that the two first PCs explained 64.2% (2 months) and 52.6 % (9 months) of the variation of the selected metabolites (**Figure 15**). The supervised models discriminated controls from treated animals with substantial (2-month animals) and moderate (9-month animals) predictive

accuracy (**Figure 16**). Paclitaxel-treated and control groups created separate clusters in the OPLS-DA score plot of the quantitative data (**Figure 17**).

A) **B)**

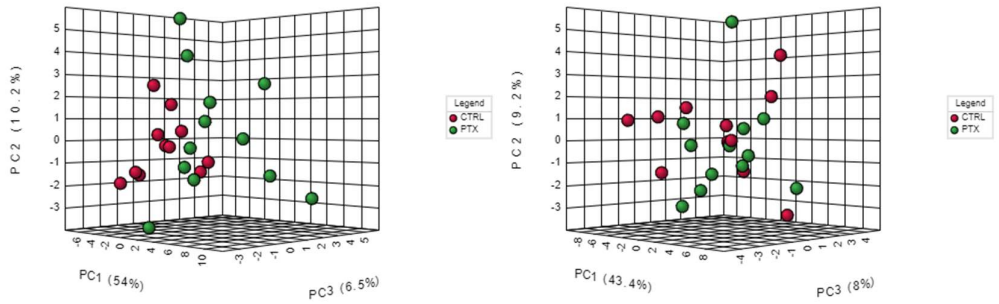

Figure 15. Plasma 3D score plot between the selected Principal Components at the end of treatment.

The explained variances are shown in parentheses for the young (A) and adult (B) groups. CTRL: control group; PC: Principal Component; PTX: paclitaxel-treated group.

A) **B)**

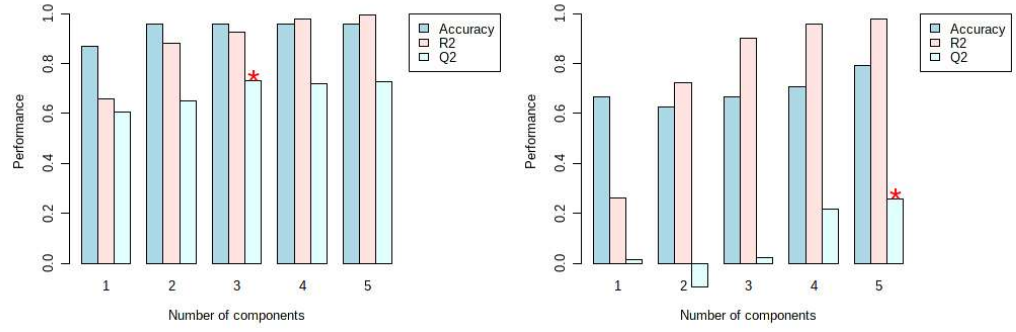

Figure 16. Overview of plasma PLS-DA model at the end of treatment.

PLS-DA classification using different number of components for the young (A) and adult (B) groups. The red star indicates the best classifier. We considered a model robust if R^2 and Q^2 values > 0.5, with Q^2 value close to the R^2 value. Models were rejected if there was complete overlap of Q^2 distributions, $Q^2(cum) < 0$, or low classification rates, $Q^2(cum) < 0.05$.

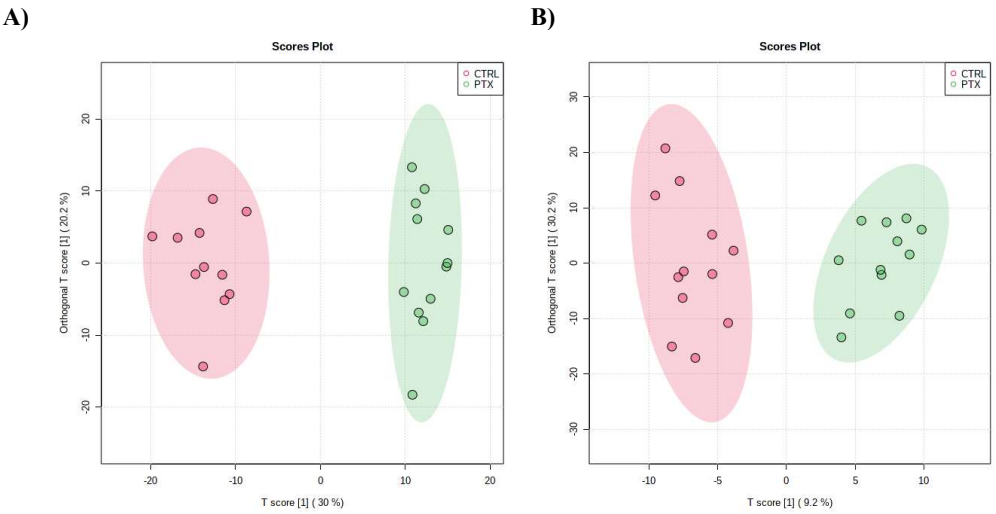

Figure 17. Plasma OPLS-DA score plot of all metabolites at the end of treatment.

The image shows the score plot of all metabolites at the end of treatment in young (A) and adult (B) animals. The explained variances are reported in parentheses along the axis. CTRL: control group; PTX: paclitaxel-treated group.

The contribution score plot identified the relative importance of each compound to differentiating paclitaxel-treated animals from controls at each time-point, with a total of 227 significant metabolites in the young group and 205 significant metabolites in the adult group at the end of treatment (**Appendix 1**). Out of the total 227 discriminative compounds, the major metabolites (VIP values >1) driving these significant differences between young-treated animals and controls were lower levels of triglycerides (n=211, 92.9%), diglycerides (n=8, 3.5%), and C14, C22 and C26 ceramides (**Figure 18**). Similarly, in the adult group, out of the total 205 metabolites, we mainly found that lower levels of triglycerides (n=173, 84.4%), diglycerides (n=8, 3.9%), and C14 and C22 ceramides were discriminative between treated animals and controls, plus lower levels of bile acids (taurodeoxycholic, tauro-b-muricholic acid, taurocholic acid), carnosine, L-kynurenine and serotonin. In addition, higher levels of phosphatidylcholines (n=3, 1.5%), chenodeoxycholic acid glycine conjugate,

chenodeoxycholic acid and cholic acid, spermidine and histamine were able to significantly separate adult-treated animals from controls (**Figure 18**).

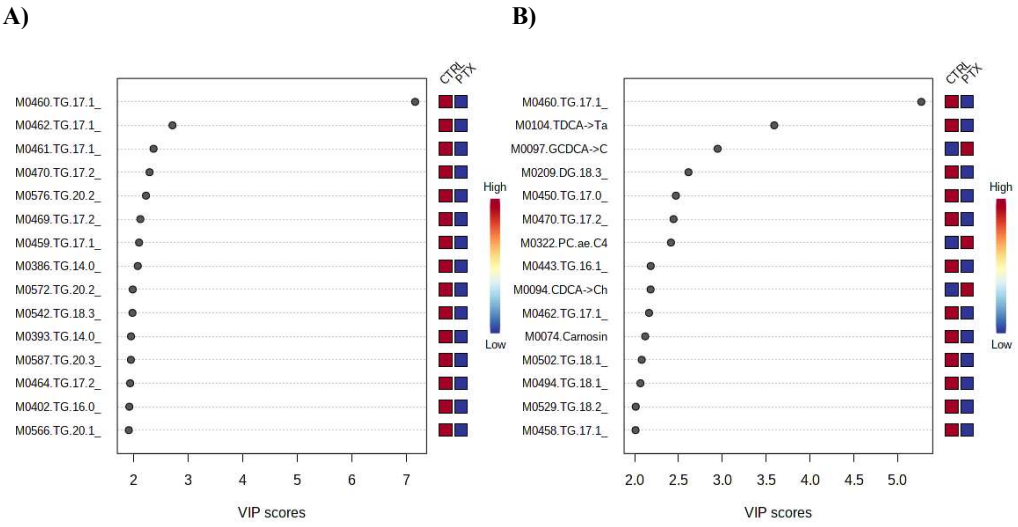

Figure 18. Discriminative metabolites at the end of treatment in plasma.

The colored boxes on the right indicate the relative concentrations of the corresponding metabolite in each group under study for young (A) and adult (B) animals. Variable influence on prediction (VIP) values >1 were considered relevant. CDCA: chenodeoxycholic acid; CTRL: control group; DG: diglyceride; GCDCA: glycochenodeoxycholic acid; PC ae: phosphatidylcholine acyl-alkyl; PTX: paclitaxel-treated group; TDCA: taurodeoxycholic acid; TG: triglyceride.

The metabolites identified as discriminative were the same as those identified by univariate analysis as being significantly different or having a trend toward being different between the two groups. The VIP analysis revealed 171 overlapping significant metabolites between age groups, but different between controls and treated groups; among those not overlapping (n=14), specific of adult animals, we mainly found bile acids (n=3, 21.4%), phosphatidylcholines (n=2, 14.3%), serotonin, spermidine and histamine. Discriminative metabolites showed a high correlation (r^2>0.65; p<0.05) with neurophysiological, behavioral and neuropathological findings (**Figure 19** and **20**).

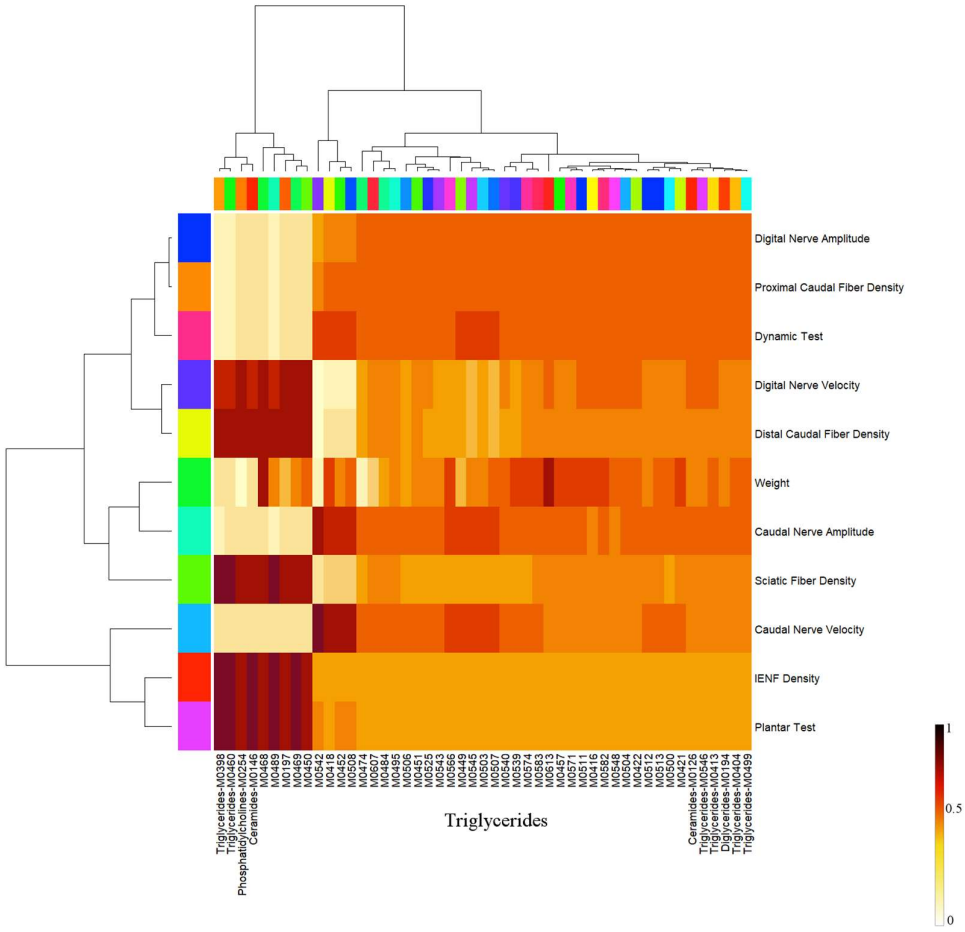

Figure 19. Plasma correlation analysis results at the end of treatment in young animals.

The heat map shows the significant associations (r^2>0.65; p<0.05) from correlation analysis results between metabolite concentrations and neurophysiological, behavioral and neuropathological findings. IENF: intraepidermal nerve fiber.

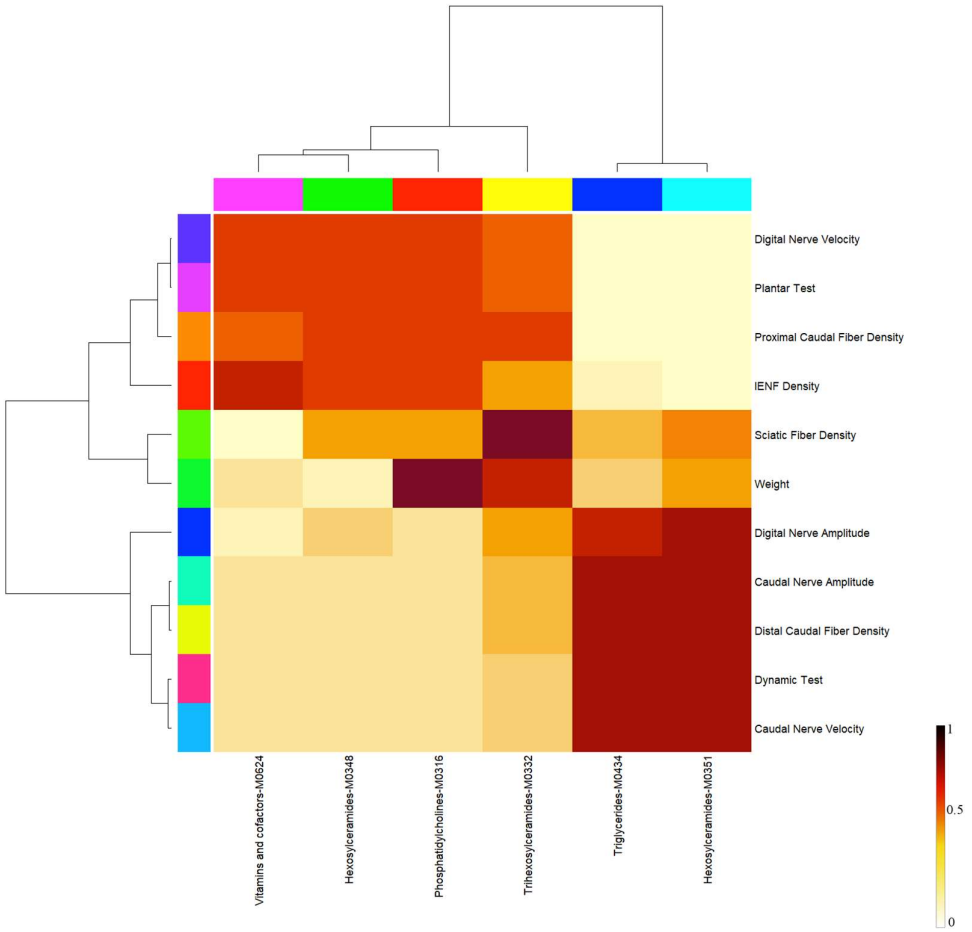

Figure 20. Plasma correlation analysis results at the end of treatment in adult animals.

The heat map shows the significant associations (r^2>0.65; p<0.05) from correlation analysis results between metabolite concentrations and neurophysiological, behavioral and neuropathological findings. IENF: intraepidermal nerve fiber.

At the end of the follow-up period, the PCA scree plot showed that the two first PCs explained 55.3% (2 months) and 53.6 % (9 months) of the variation of the selected metabolites (**Figure 21**). The supervised models showed a separation between control and paclitaxel-treated groups with moderate (2 months) and scarce (9 months) predictive accuracy (**Figure 22** and **23**).

A) **B)**

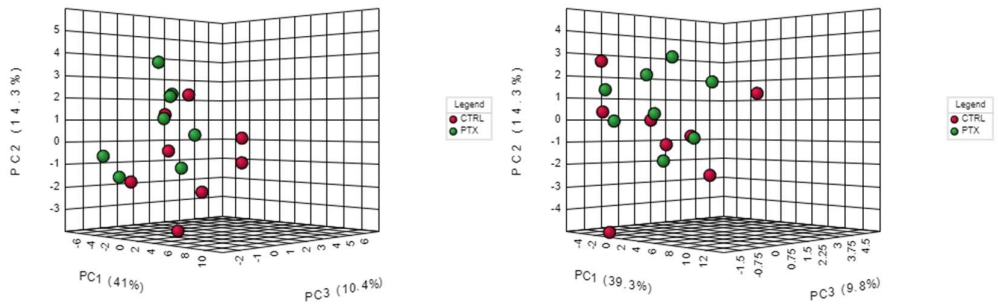

Figure 21. Plasma 3D score plot between the selected Principal Components at the end of the follow-up period.

The explained variances are shown in parentheses for the young (A) and adult (B) groups. CTRL: control group; PC: Principal Component; PTX: paclitaxel-treated group.

A) **B)**

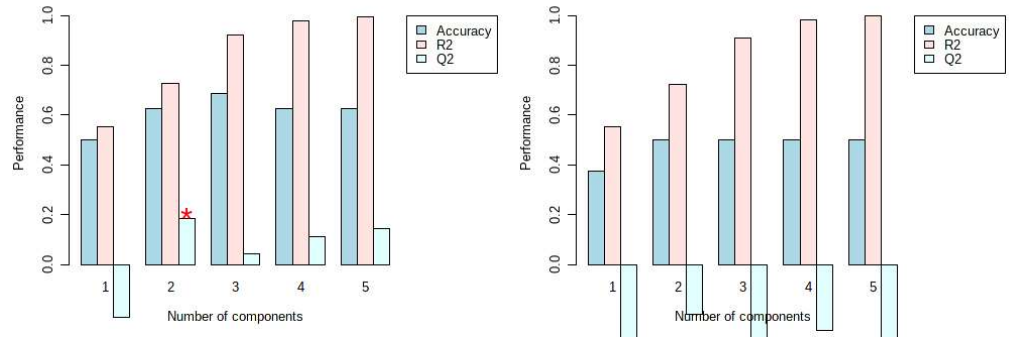

Figure 22. Overview of plasma PLS-DA model at the end of the follow-up period.

PLS-DA classification using different number of components for the young (A) and adult (B) groups. The red star indicates the best classifier. We considered a model robust if R^2 and Q^2 values > 0.5, with Q^2 value close to the R^2 value. Models were rejected if there was complete overlap of Q^2 distributions, $Q^2(cum) < 0$, or low classification rates, $Q^2(cum) < 0.05$.

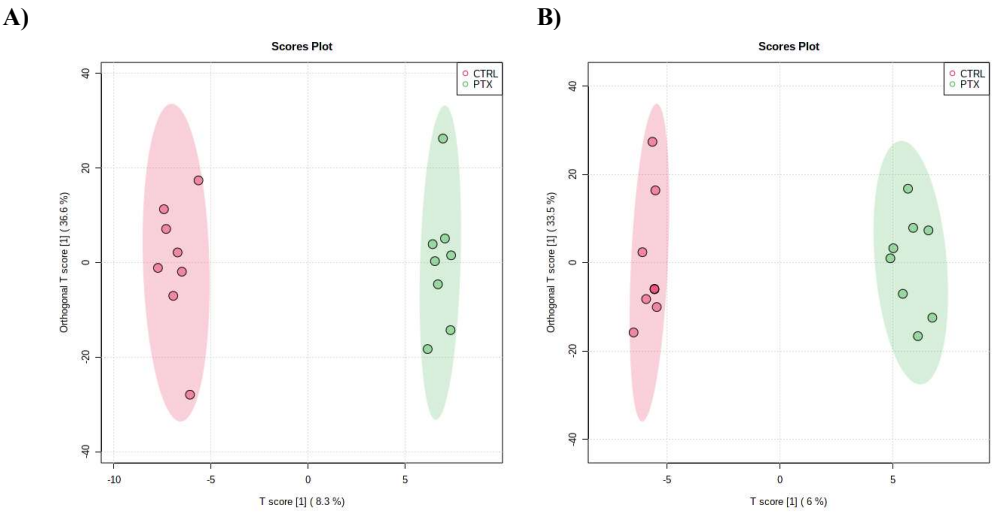

Figure 23. Plasma OPLS-DA score plot of all metabolites at the end of the follow-up period.

The image shows the score plot of all metabolites at the end of the follow-up period in young (A) and adult (B) animals. The explained variances are reported in parentheses along the axis. CTRL: control group; PTX: paclitaxel-treated group.

The relevant metabolites driving the discrimination (VIP values >1) between treated animals and controls were a total of 161 significant metabolites in the young group and 155 significant metabolites in the adult group at the end of the follow-up period (**Appendix 1**). In young animals, out of the total 161 significant compounds, discriminative metabolites were mainly represented by lower levels of triglycerides (n=48, 29.8%), diglycerides (n=28, 17.4%), acylcarnitines (n=14, 8.7%), phosphatidylcholines (n=11, 6.8%), cholesteryl esters (n=11, 6.8%), ceramides (n=9, 5.6%), hexosylceramides (n=5, 3.1%), sphingomyelins (n=4, 2.5%), dihydroceramides (n=4, 2.5%), lysophosphatidylcholines (n=3, 1.9%) and carnosine (**Figure 24**). In the adult group, out of the total 155 significant compounds, we mainly observed a persistence of higher levels of phosphatidylcholines (n=40, 25.8%); while triglycerides were represented in both increased (n=34, 21.9%) and decreased (n=22, 14.2%) categories (**Figure 24**). The metabolites identified in the young group were also the same as those detected by the t-test as being significantly different between the two

experimental groups; while in the adult group, only 1-Behenyl-2-docosahexaenoyl-sn-glycero-3-phosphocholine presented a significant FDR (<0.05) at the t-test. Discriminative metabolites showed a high correlation (r^2>0.65; p<0.05) with neurophysiological, behavioral and neuropathological findings (**Figure 25** and **26**).

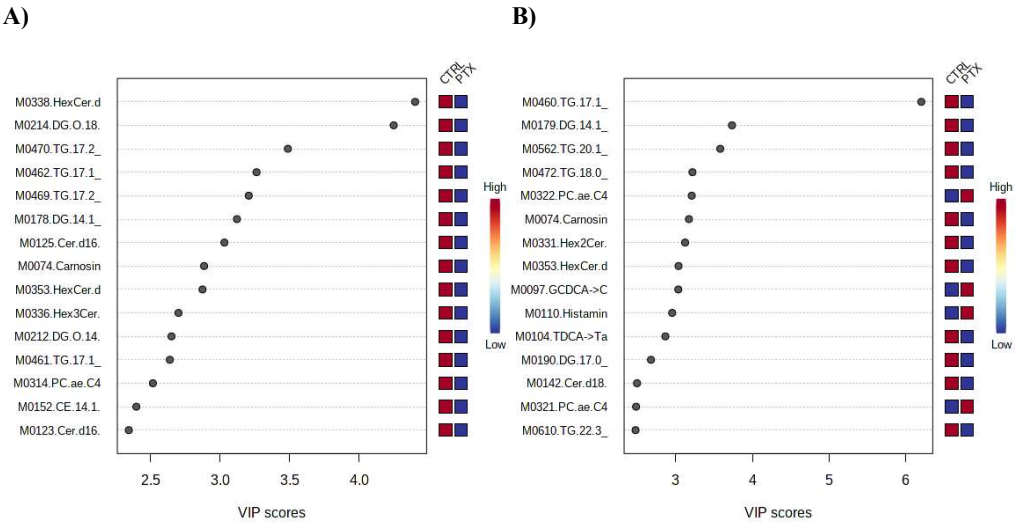

Figure 24. Discriminative metabolites at the end of the follow-up period in plasma.

The colored boxes on the right indicate the relative concentrations of the corresponding metabolite in each group under study for young (A) and adult (B) animals. Variable influence on prediction (VIP) values >1 were considered relevant. CE: cholesteryl-ester; Cer: ceramide; CTRL: control group; DG: diglyceride; GCDCA: glycochenodeoxycholic acid; HexCer: hexosylceramide; Hex2Cer: dihexosylceramide; Hex3Cer: trihexosylceramide; PC ae: phosphatidylcholine acyl-alkyl; PTX: paclitaxel-treated group; TDCA: taurodeoxycholic acid; TG: triglyceride.

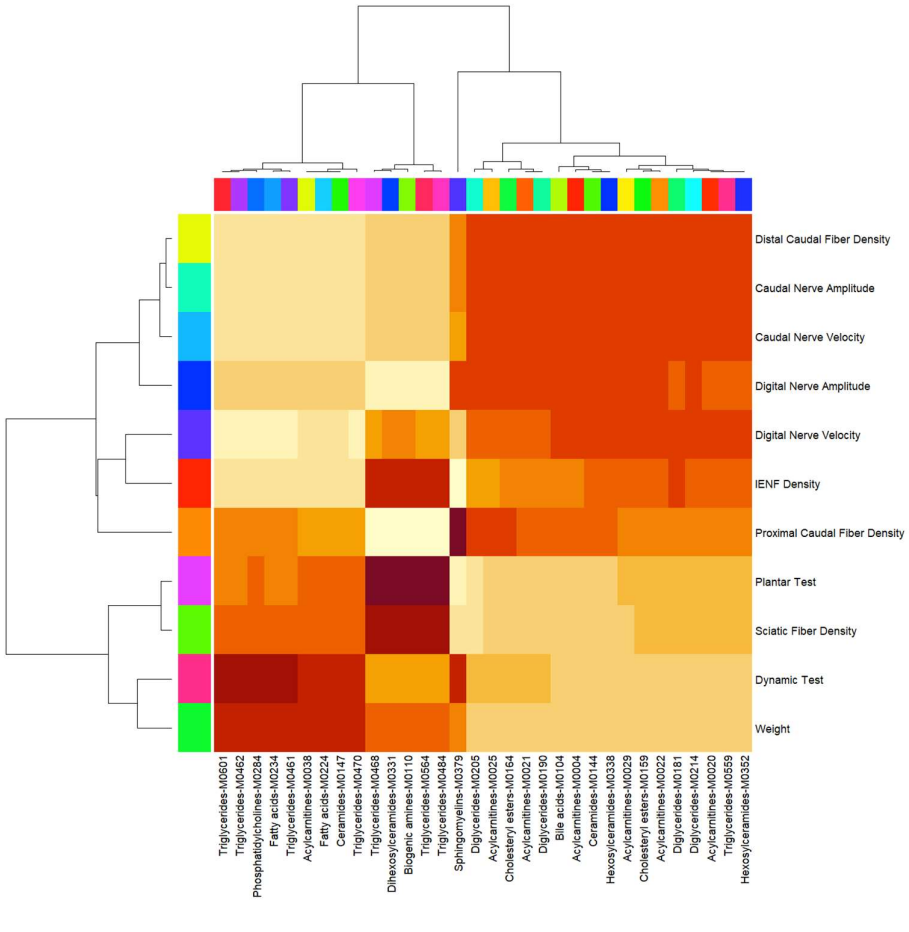

Figure 25. Plasma correlation analysis results at the end of the follow-up period in young animals.

The heat map shows the significant associations (r^2>0.65; p<0.05) from correlation analysis results between metabolite concentrations and neurophysiological, behavioral and neuropathological findings. IENF: intraepidermal nerve fiber.

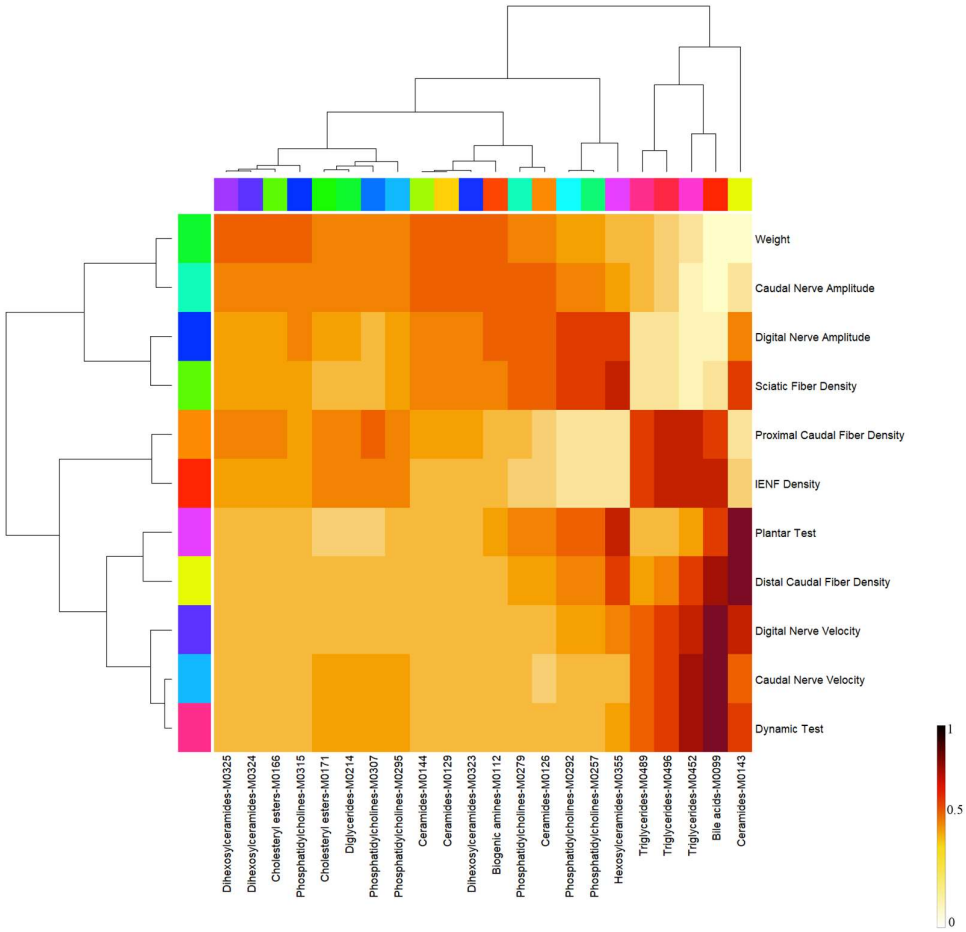

Figure 26. Plasma correlation analysis results at the end of the follow-up period in adult animals.

The heat map shows the significant associations (r^2>0.65; p<0.05) from correlation analysis results between metabolite concentrations and neurophysiological, behavioral and neuropathological findings. IENF: intraepidermal nerve fiber.

4.6.1 Plasma Enrichment analysis

When analyzing trends over time of the different compound classes in young-treated animals and controls, the Enrichment analysis and Over Representation Analysis (ORA) revealed a significant alteration of triacylglycerols and diacylglycerols from baseline to the end of treatment; while diacylglycerols plus fatty acyl carnitines were the most represented compound classes from the last paclitaxel administration until the end of the observational period (**Figure 27**).

A)

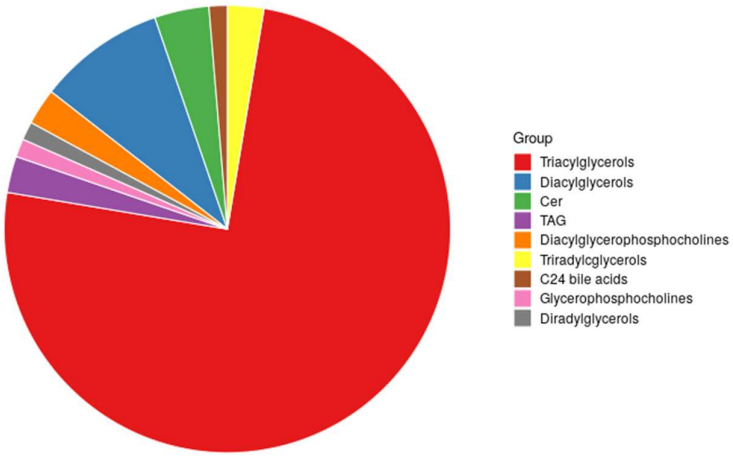

B)

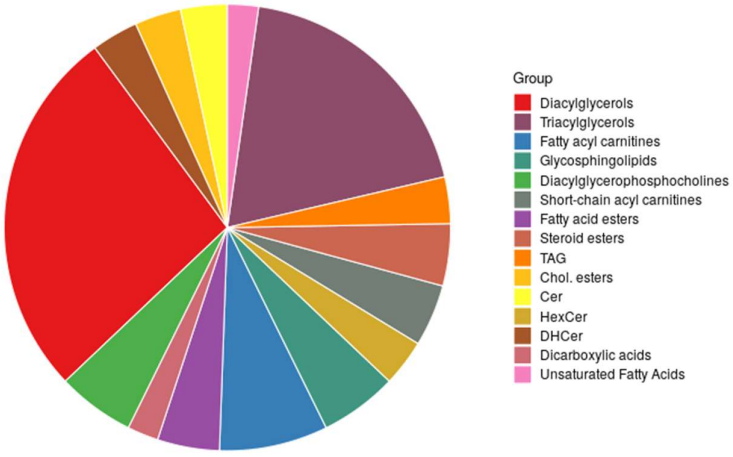

Figure 27. Summary of plasma Enrichment Analysis of young animals.

The pie charts show the most represented metabolite sets influenced by paclitaxel administration (FDR <0.05, impact >0.05) at the end of treatment (A) and at the end of the follow-up period (B). Cer: ceramides; Chol.: cholesteryl; DHCer: dihydroceramides; FDR: False Discovery Rate; HexCer: hexosylceramides; TAG: triacylglycerols.

Similarly, adult animals showed a significantly high representation of triacylglycerols and diacylglycerols, plus glycosphingolipids, taurine conjugates and C24 bile acids

from baseline to the end of treatment. However, differently from young animals, diacylglycerophosphocholines were the most represented compounds at the end of the follow-up period, followed by triacylglycerols and diacylglycerols (**Figure 28**).

A)

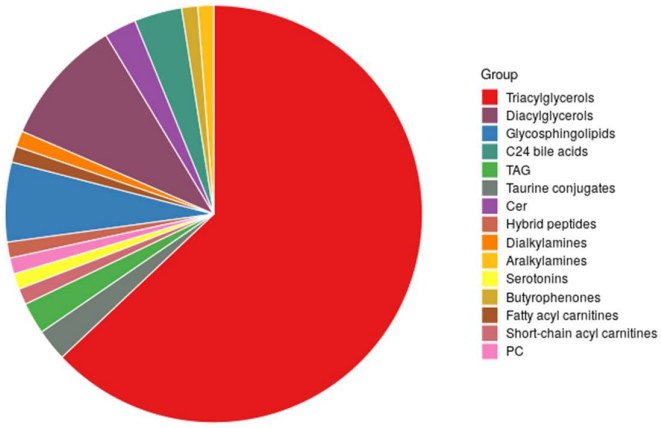

B)

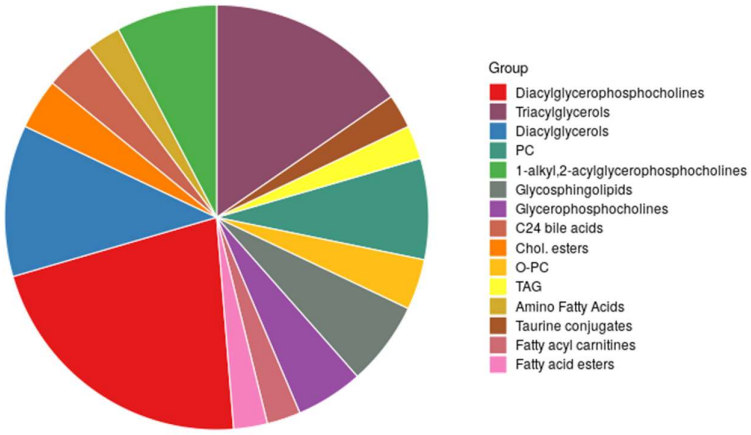

Figure 28. Summary of plasma Enrichment Analysis of adult animals.

The pie charts show the most represented metabolite sets influenced by paclitaxel administration (FDR <0.05, impact > 0.05) at the end of treatment (A) and at the end of the follow-up period (B). Cer: ceramides; FDR: False Discovery Rate; PC: phosphatidylcholines; TAG: triacylglycerols.

4.6.2 Plasma Pathway analysis

Concerning the Pathway analysis, the 2-month and 9-month paclitaxel and age-matched control data (metabolite concentration data, in micromolar) were entered into MetaboAnalyst 5.0, log-transformed, pareto-scaled, normalized, and processed to identify the metabolic pathways affected by paclitaxel administration.

At baseline, no significantly altered pathways were detected. Conversely, at the end of treatment, we identified 10 different pathways significantly affected by paclitaxel administration in 2-month animals: glycine, serine and threonine metabolism; glyoxylate and dicarboxylate metabolism; cysteine and methionine metabolism; citrate cycle, tricarboxylic acid (TCA) cycle; alanine, aspartate and glutamate metabolism; glycerophospholipid metabolism; arginine and proline metabolism; aminoacyl-tRNA biosynthesis; taurine and hypotaurine metabolism; glutathione metabolism (**Table 3**).

The major metabolite (VIP value >1) driving these significant differences was decreased C14 ceramide (glutathione metabolism, arginine and proline metabolism, glyoxylate and dicarboxylate metabolism).

	Total Cmpd	Hits	Raw p	-log10(p)	Holm adjust	FDR	Impact
Glycine, serine and threonine metabolism	34	7	2.67E-06	5.57E+00	1.25E-04	1.25E-04	0.64 *
Glyoxylate and dicarboxylate metabolism	32	5	3.39E-05	4.47E+00	1.56E-03	7.98E-04	0.17 *
Cysteine and methionine metabolism	33	6	4.39E-04	3.36E+00	1.98E-02	4.64E-03	0.40 *
Propanoate metabolism	23	2	4.73E-04	3.32E+00	2.08E-02	4.64E-03	0.00
Butanoate metabolism	15	3	4.94E-04	3.31E+00	2.12E-02	4.64E-03	0.03
Citrate cycle (TCA cycle)	20	2	9.99E-04	3.00E+00	4.19E-02	7.82E-03	0.08 *
Glycerolipid metabolism	16	1	1.42E-03	2.85E+00	5.80E-02	9.50E-03	0.01
Alanine, aspartate and glutamate metabolism	28	7	2.45E-03	2.61E+00	9.78E-02	1.29E-02	0.62 *
Pyrimidine metabolism	39	2	2.47E-03	2.61E+00	9.78E-02	1.29E-02	0.00
Glycerophospholipid metabolism	36	3	5.75E-03	2.24E+00	2.19E-01	2.60E-02	0.14 *
Arginine and proline metabolism	38	9	6.08E-03	2.22E+00	2.25E-01	2.60E-02	0.56 *
Aminoacyl-tRNA biosynthesis	48	20	7.43E-03	2.13E+00	2.68E-01	2.91E-02	0.17 *
Steroid hormone biosynthesis	77	2	9.05E-03	2.04E+00	3.17E-01	3.27E-02	0.01
Pyruvate metabolism	22	1	1.16E-02	1.93E+00	3.95E-01	3.90E-02	0.00
Taurine and hypotaurine metabolism	8	3	1.34E-02	1.87E+00	4.41E-01	4.19E-02	0.43 *
Glutathione metabolism	28	7	1.89E-02	1.72E+00	6.04E-01	5.55E-02	0.13 *
Biotin metabolism	10	1	2.68E-02	1.57E+00	8.31E-01	7.41E-02	0.00
Pantothenate and CoA biosynthesis	19	4	2.97E-02	1.53E+00	8.90E-01	7.75E-02	0.02
Ubiquinone and other terpenoid-quinone biosynthesis	9	1	3.73E-02	1.43E+00	1.00E+00	9.23E-02	0.00
Arginine biosynthesis	14	6	4.35E-02	1.36E+00	1.00E+00	1.02E-01	0.48
Selenocompound metabolism	20	1	5.34E-02	1.27E+00	1.00E+00	1.20E-01	0.00
Porphyrin and chlorophyll metabolism	30	2	6.11E-02	1.21E+00	1.00E+00	1.25E-01	0.00
Glycolysis / Gluconeogenesis	26	2	6.14E-02	1.21E+00	1.00E+00	1.25E-01	0.00
Valine, leucine and isoleucine degradation	40	3	6.82E-02	1.17E+00	1.00E+00	1.34E-01	0.00
Valine, leucine and isoleucine biosynthesis	8	4	7.26E-02	1.14E+00	1.00E+00	1.35E-01	0.00
Phenylalanine, tyrosine and tryptophan biosynthesis	4	2	7.45E-02	1.13E+00	1.00E+00	1.35E-01	1.00
beta-Alanine metabolism	21	7	1.04E-01	9.83E-01	1.00E+00	1.81E-01	0.51
Lysine degradation	25	2	1.31E-01	8.82E-01	1.00E+00	2.20E-01	0.14
Tryptophan metabolism	41	3	1.45E-01	8.38E-01	1.00E+00	2.35E-01	0.34
Purine metabolism	66	3	2.14E-01	6.70E-01	1.00E+00	3.35E-01	0.05
Histidine metabolism	16	7	2.23E-01	6.51E-01	1.00E+00	3.38E-01	0.55
Fatty acid degradation	39	2	3.24E-01	4.90E-01	1.00E+00	4.76E-01	0.00
Thiamine metabolism	7	1	3.45E-01	4.63E-01	1.00E+00	4.78E-01	0.00
Phenylalanine metabolism	12	4	3.46E-01	4.61E-01	1.00E+00	4.78E-01	0.36
Primary bile acid biosynthesis	46	8	3.87E-01	4.12E-01	1.00E+00	5.11E-01	0.14
Steroid biosynthesis	42	1	3.92E-01	4.07E-01	1.00E+00	5.11E-01	0.00
Biosynthesis of unsaturated fatty acids	36	7	4.75E-01	3.23E-01	1.00E+00	6.03E-01	0.00
Sphingolipid metabolism	21	6	5.14E-01	2.89E-01	1.00E+00	6.36E-01	0.49
Tyrosine metabolism	42	3	5.29E-01	2.76E-01	1.00E+00	6.38E-01	0.38
D-Glutamine and D-glutamate metabolism	6	2	6.04E-01	2.19E-01	1.00E+00	6.92E-01	0.50
Nitrogen metabolism	6	2	6.04E-01	2.19E-01	1.00E+00	6.92E-01	0.00
Nicotinate and nicotinamide metabolism	15	1	6.51E-01	1.86E-01	1.00E+00	7.28E-01	0.00
Linoleic acid metabolism	5	2	6.91E-01	1.61E-01	1.00E+00	7.50E-01	1.00
alpha-Linolenic acid metabolism	13	1	7.02E-01	1.54E-01	1.00E+00	7.50E-01	0.00
Arachidonic acid metabolism	36	2	7.81E-01	1.07E-01	1.00E+00	8.16E-01	0.33
Fatty acid biosynthesis	47	1	9.02E-01	4.46E-02	1.00E+00	9.02E-01	0.01
Fatty acid elongation	39	1	9.02E-01	4.46E-02	1.00E+00	9.02E-01	0.00

Table 3. Summary of plasma Pathway Analysis at the end of treatment in young animals.

The star indicates the significant pathways affected by paclitaxel administration (FDR <0.05, impact >0.05, hits ≥ 2). Cmpd: compounds, FDR: False Discovery Rate.

Concerning adult animals, paclitaxel significantly altered the primary bile acid biosynthesis pathway. The metabolites driving this pathway were also the key metabolites identified in the VIP analysis (VIP values >1), namely increased levels of chenodeoxycholic acid glycine conjugate, chenodeoxycholic acid, cholic acid, and decreased levels of taurodeoxycholic acid, tauro-b-muricholic acid, taurocholic acid (**Table 4**).

	Total Cmpd	Hits	Raw p	-log10(p)	Holm adjust	FDR	Impact
Valine, leucine and isoleucine biosynthesis	8	4	1.11E-03	2.96E+00	5.21E-02	3.99E-02	0.00
Biotin metabolism	10	1	2.49E-03	2.60E+00	1.14E-01	3.99E-02	0.00
Primary bile acid biosynthesis	46	7	2.55E-03	2.59E+00	1.15E-01	3.99E-02	0.11 *
Valine, leucine and isoleucine degradation	40	3	4.95E-03	2.31E+00	2.18E-01	5.81E-02	0.00
Aminoacyl-tRNA biosynthesis	48	20	1.14E-02	1.94E+00	4.92E-01	1.08E-01	0.17
Arginine biosynthesis	14	6	1.68E-02	1.78E+00	7.04E-01	1.25E-01	0.48
Taurine and hypotaurine metabolism	8	2	1.86E-02	1.73E+00	7.63E-01	1.25E-01	0.00
Lysine degradation	25	2	2.23E-02	1.65E+00	8.92E-01	1.31E-01	0.14
Histidine metabolism	16	7	4.69E-02	1.33E+00	1.00E+00	2.45E-01	0.55
Porphyrin and chlorophyll metabolism	30	2	6.66E-02	1.18E+00	1.00E+00	2.70E-01	0.00
Glyoxylate and dicarboxylate metabolism	32	5	7.57E-02	1.12E+00	1.00E+00	2.70E-01	0.17
Tryptophan metabolism	41	3	7.76E-02	1.11E+00	1.00E+00	2.70E-01	0.34
Pyrimidine metabolism	39	2	8.16E-02	1.09E+00	1.00E+00	2.70E-01	0.00
Glycine, serine and threonine metabolism	34	7	8.20E-02	1.09E+00	1.00E+00	2.70E-01	0.64
Pantothenate and CoA biosynthesis	19	4	8.81E-02	1.05E+00	1.00E+00	2.70E-01	0.02
Fatty acid biosynthesis	47	1	1.02E-01	9.91E-01	1.00E+00	2.70E-01	0.01
Fatty acid elongation	39	1	1.02E-01	9.91E-01	1.00E+00	2.70E-01	0.00
beta-Alanine metabolism	21	7	1.03E-01	9.86E-01	1.00E+00	2.70E-01	0.51
D-Glutamine and D-glutamate metabolism	6	2	1.15E-01	9.40E-01	1.00E+00	2.70E-01	0.50
Nitrogen metabolism	6	2	1.15E-01	9.40E-01	1.00E+00	2.70E-01	0.00
Propanoate metabolism	23	2	1.29E-01	8.89E-01	1.00E+00	2.89E-01	0.00
Cysteine and methionine metabolism	33	6	1.61E-01	7.94E-01	1.00E+00	3.14E-01	0.40
Biosynthesis of unsaturated fatty acids	36	7	1.64E-01	7.85E-01	1.00E+00	3.14E-01	0.00
Glycerolipid metabolism	16	1	1.74E-01	7.60E-01	1.00E+00	3.14E-01	0.01
Nicotinate and nicotinamide metabolism	15	1	1.77E-01	7.52E-01	1.00E+00	3.14E-01	0.00
Phenylalanine metabolism	12	4	1.80E-01	7.44E-01	1.00E+00	3.14E-01	0.36
Phenylalanine, tyrosine and tryptophan biosynthesis	4	2	1.81E-01	7.43E-01	1.00E+00	3.14E-01	1.00
Linoleic acid metabolism	5	2	2.79E-01	5.55E-01	1.00E+00	4.55E-01	1.00
Glutathione metabolism	28	7	2.99E-01	5.24E-01	1.00E+00	4.55E-01	0.13
Butanoate metabolism	15	3	3.00E-01	5.24E-01	1.00E+00	4.55E-01	0.03
Arginine and proline metabolism	38	9	3.19E-01	4.96E-01	1.00E+00	4.55E-01	0.56
Alanine, aspartate and glutamate metabolism	28	7	3.25E-01	4.88E-01	1.00E+00	4.55E-01	0.62
Arachidonic acid metabolism	36	2	3.29E-01	4.83E-01	1.00E+00	4.55E-01	0.33
Selenocompound metabolism	20	1	3.29E-01	4.83E-01	1.00E+00	4.55E-01	0.00
Citrate cycle (TCA cycle)	20	2	3.53E-01	4.52E-01	1.00E+00	4.75E-01	0.08
alpha-Linolenic acid metabolism	13	1	3.93E-01	4.06E-01	1.00E+00	5.13E-01	0.00
Pyruvate metabolism	22	1	4.30E-01	3.67E-01	1.00E+00	5.36E-01	0.00
Sphingolipid metabolism	21	6	4.34E-01	3.63E-01	1.00E+00	5.36E-01	0.49
Thiamine metabolism	7	1	4.51E-01	3.46E-01	1.00E+00	5.43E-01	0.00
Purine metabolism	66	3	5.39E-01	2.68E-01	1.00E+00	6.29E-01	0.05
Glycerophospholipid metabolism	36	3	5.49E-01	2.61E-01	1.00E+00	6.29E-01	0.14
Fatty acid degradation	39	2	6.48E-01	1.88E-01	1.00E+00	7.25E-01	0.00
Steroid hormone biosynthesis	77	2	6.64E-01	1.78E-01	1.00E+00	7.26E-01	0.01
Glycolysis / Gluconeogenesis	26	2	7.12E-01	1.47E-01	1.00E+00	7.61E-01	0.00
Steroid biosynthesis	42	1	7.79E-01	1.08E-01	1.00E+00	8.14E-01	0.00
Ubiquinone and other terpenoid-quinone biosynthesis	9	1	8.45E-01	7.32E-02	1.00E+00	8.63E-01	0.00
Tyrosine metabolism	42	3	9.79E-01	9.28E-03	1.00E+00	9.79E-01	0.38

Table 4. Summary of plasma Pathway Analysis at the end of treatment in adult animals.

The star indicates the significant pathway affected by paclitaxel administration (FDR <0.05, impact >0.05, hits ≥ 2). Cmpd: compounds, FDR: False Discovery Rate.

At the end of the follow-up period, we found in the 2-month rats a significantly altered sphingolipid metabolism (**Table 5**), with decreased sphingomyelin, N-acylsphingosine, glucosylceramide driving the significant modification (VIP values >1).

	Total Cmpd	Hits	Raw p	-log10(p)	Holm adjust	FDR	Impact
Pyrimidine metabolism	39	2	3.23E-03	2.49E+00	1.52E-01	8.46E-02	0.00
Sphingolipid metabolism	21	6	5.31E-03	2.27E+00	2.44E-01	8.46E-02	0.49 *
Propanoate metabolism	23	2	5.40E-03	2.27E+00	2.44E-01	8.46E-02	0.00
Pantothenate and CoA biosynthesis	19	4	1.76E-02	1.76E+00	7.73E-01	2.06E-01	0.02
Pyruvate metabolism	22	1	3.72E-02	1.43E+00	1.00E+00	3.36E-01	0.00
Histidine metabolism	16	7	4.29E-02	1.37E+00	1.00E+00	3.36E-01	0.55
beta-Alanine metabolism	21	7	7.24E-02	1.14E+00	1.00E+00	4.08E-01	0.51
Tryptophan metabolism	41	3	8.27E-02	1.08E+00	1.00E+00	4.08E-01	0.34
Glycolysis / Gluconeogenesis	26	2	8.27E-02	1.08E+00	1.00E+00	4.08E-01	0.00
Steroid biosynthesis	42	1	8.68E-02	1.06E+00	1.00E+00	4.08E-01	0.00
Thiamine metabolism	7	1	1.15E-01	9.41E-01	1.00E+00	4.60E-01	0.00
Biosynthesis of unsaturated fatty acids	36	7	1.27E-01	8.96E-01	1.00E+00	4.60E-01	0.00
Valine, leucine and isoleucine biosynthesis	8	4	1.27E-01	8.95E-01	1.00E+00	4.60E-01	0.00
Valine, leucine and isoleucine degradation	40	3	1.45E-01	8.37E-01	1.00E+00	4.88E-01	0.00
Ubiquinone and other terpenoid-quinone biosynthesis	9	1	2.17E-01	6.64E-01	1.00E+00	6.30E-01	0.00
Aminoacyl-tRNA biosynthesis	48	20	2.83E-01	5.47E-01	1.00E+00	6.30E-01	0.17
Arachidonic acid metabolism	36	2	2.90E-01	5.37E-01	1.00E+00	6.30E-01	0.33
Phenylalanine metabolism	12	4	2.97E-01	5.27E-01	1.00E+00	6.30E-01	0.36
Citrate cycle (TCA cycle)	20	2	2.98E-01	5.25E-01	1.00E+00	6.30E-01	0.08
Phenylalanine, tyrosine and tryptophan biosynthesis	4	2	2.99E-01	5.24E-01	1.00E+00	6.30E-01	1.00
D-Glutamine and D-glutamate metabolism	6	2	3.00E-01	5.23E-01	1.00E+00	6.30E-01	0.50
Nitrogen metabolism	6	2	3.00E-01	5.23E-01	1.00E+00	6.30E-01	0.00
Glyoxylate and dicarboxylate metabolism	32	5	3.12E-01	5.06E-01	1.00E+00	6.30E-01	0.17
Glycerophospholipid metabolism	36	3	3.26E-01	4.87E-01	1.00E+00	6.30E-01	0.14
Glycine, serine and threonine metabolism	34	7	3.35E-01	4.75E-01	1.00E+00	6.30E-01	0.64
Cysteine and methionine metabolism	33	6	3.59E-01	4.45E-01	1.00E+00	6.48E-01	0.40
Taurine and hypotaurine metabolism	8	3	3.81E-01	4.19E-01	1.00E+00	6.64E-01	0.43
Butanoate metabolism	15	3	4.18E-01	3.78E-01	1.00E+00	7.02E-01	0.03
Porphyrin and chlorophyll metabolism	30	2	4.49E-01	3.48E-01	1.00E+00	7.23E-01	0.00
Nicotinate and nicotinamide metabolism	15	1	4.62E-01	3.36E-01	1.00E+00	7.23E-01	0.00
Arginine biosynthesis	14	6	5.19E-01	2.85E-01	1.00E+00	7.63E-01	0.48
Purine metabolism	66	3	5.19E-01	2.84E-01	1.00E+00	7.63E-01	0.05
Glutathione metabolism	28	7	5.68E-01	2.46E-01	1.00E+00	8.09E-01	0.13
Alanine, aspartate and glutamate metabolism	28	7	5.88E-01	2.31E-01	1.00E+00	8.12E-01	0.62
Lysine degradation	25	2	6.19E-01	2.08E-01	1.00E+00	8.32E-01	0.14
Tyrosine metabolism	42	3	6.73E-01	1.72E-01	1.00E+00	8.54E-01	0.38
alpha-Linolenic acid metabolism	13	1	6.82E-01	1.66E-01	1.00E+00	8.54E-01	0.00
Primary bile acid biosynthesis	46	8	6.91E-01	1.61E-01	1.00E+00	8.54E-01	0.14
Steroid hormone biosynthesis	77	2	7.31E-01	1.36E-01	1.00E+00	8.60E-01	0.01
Arginine and proline metabolism	38	9	7.59E-01	1.20E-01	1.00E+00	8.60E-01	0.56
Linoleic acid metabolism	5	2	7.83E-01	1.06E-01	1.00E+00	8.60E-01	1.00
Fatty acid biosynthesis	47	1	7.87E-01	1.04E-01	1.00E+00	8.60E-01	0.01
Fatty acid elongation	39	1	7.87E-01	1.04E-01	1.00E+00	8.60E-01	0.00
Selenocompound metabolism	20	1	8.56E-01	6.77E-02	1.00E+00	9.08E-01	0.00
Glycerolipid metabolism	16	1	8.76E-01	5.75E-02	1.00E+00	9.08E-01	0.01
Fatty acid degradation	39	2	8.89E-01	5.13E-02	1.00E+00	9.08E-01	0.00
Biotin metabolism	10	1	9.24E-01	3.42E-02	1.00E+00	9.24E-01	0.00

Table 5. Summary of plasma Pathway Analysis at the end of the follow-up period in young animals.

The star indicates the significant pathway affected by paclitaxel administration (FDR <0.05, impact >0.05, hits ≥ 2). Cmpd: compounds, FDR: False Discovery Rate.

By contrast, the 9-month animals presented a significantly altered histidine metabolism (**Table 6**), with carnosine leading the significant alteration (VIP value >1).

	Total Cmpd	Hits	Raw p	-log10(p)	Holm adjust	FDR	Impact
Histidine metabolism	16	7	1.94E-04	3.71E+00	9.10E-03	9.10E-03	0.55 *
beta-Alanine metabolism	21	7	1.10E-02	1.96E+00	5.05E-01	2.58E-01	0.51
Taurine and hypotaurine metabolism	8	3	8.18E-02	1.09E+00	1.00E+00	8.33E-01	0.43
Butanoate metabolism	15	3	1.11E-01	9.55E-01	1.00E+00	8.33E-01	0.03
Primary bile acid biosynthesis	46	8	1.53E-01	8.15E-01	1.00E+00	8.33E-01	0.14
Valine, leucine and isoleucine degradation	40	3	1.99E-01	7.00E-01	1.00E+00	8.33E-01	0.00
Pyrimidine metabolism	39	2	2.19E-01	6.60E-01	1.00E+00	8.33E-01	0.00
Biosynthesis of unsaturated fatty acids	36	7	2.20E-01	6.57E-01	1.00E+00	8.33E-01	0.00
Purine metabolism	66	3	2.27E-01	6.45E-01	1.00E+00	8.33E-01	0.05
Tryptophan metabolism	41	3	2.62E-01	5.82E-01	1.00E+00	8.33E-01	0.34
Ubiquinone and other terpenoid-quinone biosynthesis	9	1	2.76E-01	5.59E-01	1.00E+00	8.33E-01	0.00
Fatty acid biosynthesis	47	1	2.77E-01	5.57E-01	1.00E+00	8.33E-01	0.01
Fatty acid elongation	39	1	2.77E-01	5.57E-01	1.00E+00	8.33E-01	0.00
Arginine and proline metabolism	38	9	2.80E-01	5.53E-01	1.00E+00	8.33E-01	0.56
Valine, leucine and isoleucine biosynthesis	8	4	2.99E-01	5.24E-01	1.00E+00	8.33E-01	0.00
Tyrosine metabolism	42	3	3.27E-01	4.86E-01	1.00E+00	8.33E-01	0.38
Phenylalanine, tyrosine and tryptophan biosynthesis	4	2	3.37E-01	4.72E-01	1.00E+00	8.33E-01	1.00
Alanine, aspartate and glutamate metabolism	28	7	3.52E-01	4.54E-01	1.00E+00	8.33E-01	0.62
Pyruvate metabolism	22	1	3.70E-01	4.32E-01	1.00E+00	8.33E-01	0.00
Propanoate metabolism	23	2	4.10E-01	3.87E-01	1.00E+00	8.33E-01	0.00
Phenylalanine metabolism	12	4	4.14E-01	3.83E-01	1.00E+00	8.33E-01	0.36
Steroid biosynthesis	42	1	4.34E-01	3.63E-01	1.00E+00	8.33E-01	0.00
Cysteine and methionine metabolism	33	6	4.42E-01	3.55E-01	1.00E+00	8.33E-01	0.40
Thiamine metabolism	7	1	4.46E-01	3.51E-01	1.00E+00	8.33E-01	0.00
Linoleic acid metabolism	5	2	4.59E-01	3.38E-01	1.00E+00	8.33E-01	1.00
Selenocompound metabolism	20	1	4.72E-01	3.26E-01	1.00E+00	8.33E-01	0.00
Pantothenate and CoA biosynthesis	19	4	4.79E-01	3.20E-01	1.00E+00	8.33E-01	0.02
Glycolysis / Gluconeogenesis	26	2	5.40E-01	2.67E-01	1.00E+00	8.44E-01	0.00
Arachidonic acid metabolism	36	2	5.41E-01	2.67E-01	1.00E+00	8.44E-01	0.33
Aminoacyl-tRNA biosynthesis	48	20	5.54E-01	2.57E-01	1.00E+00	8.44E-01	0.17
Citrate cycle (TCA cycle)	20	2	5.68E-01	2.45E-01	1.00E+00	8.44E-01	0.08
Glutathione metabolism	28	7	5.75E-01	2.41E-01	1.00E+00	8.44E-01	0.13
Lysine degradation	25	2	5.97E-01	2.24E-01	1.00E+00	8.51E-01	0.14
Glycine, serine and threonine metabolism	34	7	6.66E-01	1.76E-01	1.00E+00	8.97E-01	0.64
Arginine biosynthesis	14	6	7.13E-01	1.47E-01	1.00E+00	8.97E-01	0.48
Glyoxylate and dicarboxylate metabolism	32	5	7.17E-01	1.45E-01	1.00E+00	8.97E-01	0.17
Nicotinate and nicotinamide metabolism	15	1	7.43E-01	1.29E-01	1.00E+00	8.97E-01	0.00
Sphingolipid metabolism	21	6	7.69E-01	1.14E-01	1.00E+00	8.97E-01	0.49
Fatty acid degradation	39	2	7.79E-01	1.08E-01	1.00E+00	8.97E-01	0.00
D-Glutamine and D-glutamate metabolism	6	2	7.83E-01	1.06E-01	1.00E+00	8.97E-01	0.50
Nitrogen metabolism	6	2	7.83E-01	1.06E-01	1.00E+00	8.97E-01	0.00
alpha-Linolenic acid metabolism	13	1	8.12E-01	9.04E-02	1.00E+00	9.09E-01	0.00
Glycerolipid metabolism	16	1	9.06E-01	4.31E-02	1.00E+00	9.68E-01	0.01
Porphyrin and chlorophyll metabolism	30	2	9.20E-01	3.61E-02	1.00E+00	9.68E-01	0.00
Biotin metabolism	10	1	9.27E-01	3.28E-02	1.00E+00	9.68E-01	0.00
Glycerophospholipid metabolism	36	3	9.60E-01	1.80E-02	1.00E+00	9.80E-01	0.14
Steroid hormone biosynthesis	77	2	9.80E-01	8.87E-03	1.00E+00	9.80E-01	0.01

Table 6. Summary of plasma Pathway Analysis at the end of the follow-up period in adult animals.

The star indicates the significant pathway affected by paclitaxel administration (FDR <0.05, impact >0.05, hits ≥ 2). Cmpd: compounds, FDR: False Discovery Rate.

There were no common significant metabolic pathways between the 2-month and 9-month groups. However, glycine, despite not being significant (VIP value <1), was represented in both the 2-month and 9-month animals' significant pathways identified at the end of treatment (aminoacyl-tRNA biosynthesis; glycine, serine and threonine metabolism; primary bile acid biosynthesis).

4.7 Liver metabolomics analysis

Twenty-eight (n=28) liver samples were analyzed. After performing FIA-MS/MS and LC-MS/MS, 624 metabolites from 26 compound classes were quantified. Seven metabolites presented more than 50% of missing values (L-arginine, N-acetylornithine, carnosine, 4-hydroxyproline, methionine sulfoxide, phenylethylamine and 3-nitrotyrosine), thus they were not included in the analysis. The remaining 617 quantified metabolites were represented by triglycerides (n=242, 39.2%), phosphatidylcholines (n=74, 12%), diglycerides (n=41, 6.6%), acylcarnitines (n=40, 6.5%), ceramides (n=28, 4.5%), amino acid related (n= 25, 4.1%), cholesteryl-esters (n=22, 3.6%), amino acids (n=19, 3.1%), hexosylceramides (n=19, 3.1%), sphingomyelins (n=14, 2.3%), bile acids (n=14, 2.3%), lysophosphatidylcholines (n=14, 2.3%), fatty acids (n=12, 1.9%), dihexosylceramides (n=9, 1.5%), dihydroceramides (n=8, 1.3%), biogenic amines (n=8, 1.3%), carboxylic acids (n=7, 1.1%), trihexosylceramides (n=6, 1%), hormones and related (n=4, 0.6%), indoles and derivatives (n=4, 0.6%), nucleobases and related (n=2, 0.3%), monosaccharides (n=1, 0.2%), alkaloids (n=1, 0.2%), amine oxides (n=1, 0.2%), cresols (n=1, 0.2%), vitamins and cofactors (n=1, 0.2%).

Random forest method qualified 3 samples out of 28 as outliers (10.7%), which were spread across the different study groups (1×adult-control group; 1×young-control group; 1×adult-paclitaxel group). Metabolomics data (n=617) were normalized by log-transformation and pareto-scaling.

After treatment completion, the resulting PCA scree plot showed that the two first PCs explained 52.9% (2 months) and 55% (9 months) of the variation of the selected metabolites (**Figure 29**). The supervised models discriminated controls from treated

animals with moderate predictive accuracy (**Figure 30)**. Paclitaxel-treated and control groups formed separate clusters in the OPLS-DA score plot of the quantitative data (**Figure 31**).

A) **B)**

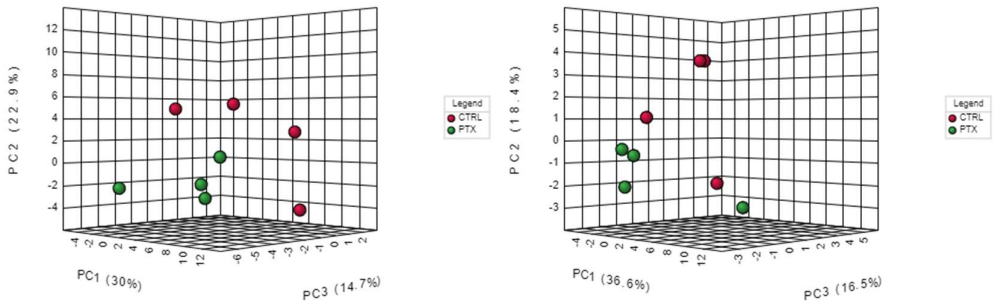

Figure 29. Liver 3D score plot between the selected Principal Components at the end of treatment.

The explained variances are shown in parentheses for the young (A) and adult (B) groups. CTRL: control group; PC: Principal Component; PTX: paclitaxel-treated group.

A) **B)**

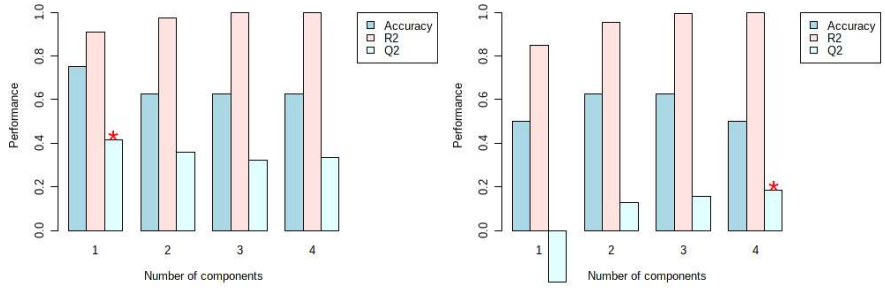

Figure 30. Overview of liver PLS-DA model at the end of treatment.

PLS-DA classification using different number of components for the young (A) and adult (B) groups. The red star indicates the best classifier. We considered a model robust if R^2 and Q^2 values > 0.5, with Q^2 value close to the R^2 value. Models were rejected if there was complete overlap of Q^2 distributions, $Q^2(cum) < 0$, or low classification rates, $Q^2(cum) < 0.05$.

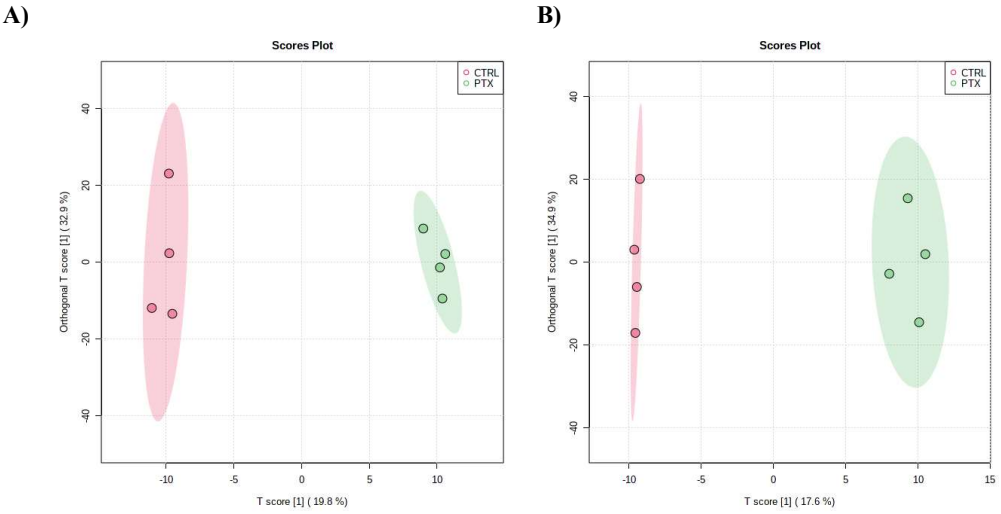

Figure 31. Liver OPLS-DA score plot of all metabolites at the end of treatment.

The image shows the score plot of all metabolites at the end of treatment in young (A) and adult (B) animals. The explained variances are reported in parentheses along the axis. CTRL: control group; PTX: paclitaxel-treated group.

The contribution score plot identified the relative importance of each compound to differentiating young-treated animals from controls and showed a total of 72 significant metabolites in the young group and 172 significant metabolites in the adult group at the end of treatment (**Appendix 1**). In young rats, out of the total 72 compounds, the major metabolites (VIP values >1) driving these significant differences were lower levels of triglycerides (n=39, 54.2%), diglycerides (n=6, 8.3%), ceramides (n=4, 5.6%), dihydroceramides (n=4, 5.6%), and amino acid related (n=4, 5.6%). We also observed higher levels of chenodeoxycholic acid glycine conjugate and cholic acid, and decreased taurine and taurodeoxycholic acid. In adult animals, out of the total 172 compounds, we mainly observed significantly increased levels of triglycerides (n=93, 54.1%), phosphatidylcholines (n=10, 5.8%), diglycerides (n=5, 2.9%), and acylcarnitines (n=4, 2.3%). Discriminative metabolites are presented in **Figure 32**.

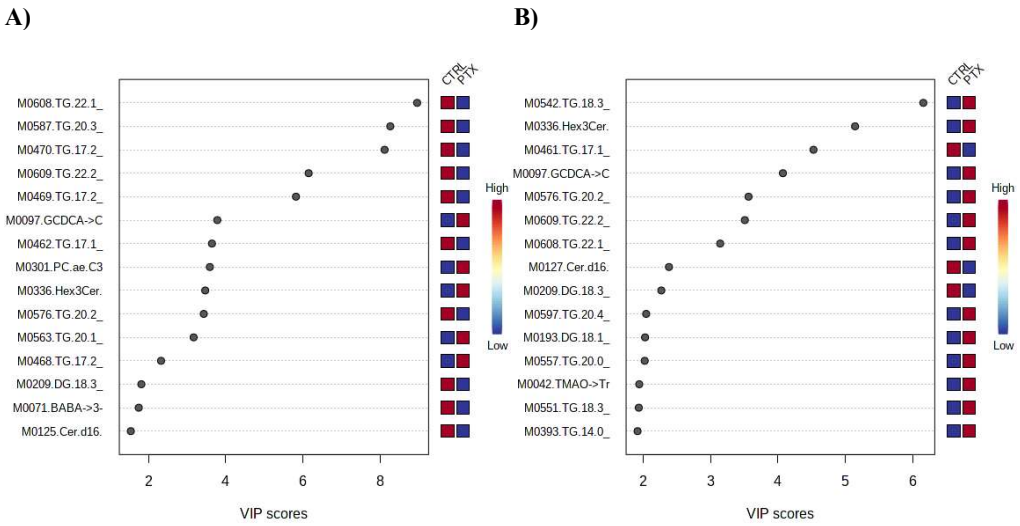

Figure 32. Discriminative metabolites at the end of treatment in the liver.

The colored boxes on the right indicate the relative concentrations of the corresponding metabolite in each group under study for young (A) and adult (B) animals. Variable influence on prediction (VIP) values >1 were considered relevant. BABA: β-aminobutyric acid; Cer: ceramide; CTRL: control group; DG: diglyceride; GCDCA: glycochenodeoxycholic acid; Hex3Cer: trihexosylceramide; PC ae: phosphatidylcholine acyl-alkyl; PTX: paclitaxel-treated group; TG: triglyceride; TMAO: trimethylamine-N-oxide.

The VIP analysis showed 34 overlapping significant metabolites between age groups, but different between controls and treated groups. Among those not overlapping, 38 metabolites were specific of the young group, mainly represented by triglycerides (n=20, 52.6%), amino acid related (n=3, 7.9%), biogenic amines (n=3, 7.9%), dihydroceramides (n=3, 7.9%), ceramides (n=2, 5.3%); while among the 137 specific metabolites of the adult group, we mainly found triglycerides (n=85, 62%), phosphatidylcholines (n=12, 8.8%), diglycerides (n=8, 5.8%), acylcarnitines (n=5, 3.6%), amino acid related (n=4, 2.9%), lysophosphatidylcholines (n=4, 2.9%), biogenic amines (n=3, 2.2%), ceramides (n=3, 2.2%), hexosylceramides (n=3, 2.2%), dihydroceramides (n=2, 1.5%) and bile acids (n=2, 1.5%).

The metabolites identified as discriminative were the same as those identified by univariate analysis as being significantly different or having a trend toward being

different between the two groups. Discriminative metabolites showed a high correlation (r^2>0.65; p<0.05) with neurophysiological, behavioral and neuropathological findings (**Figure 33** and **34**).

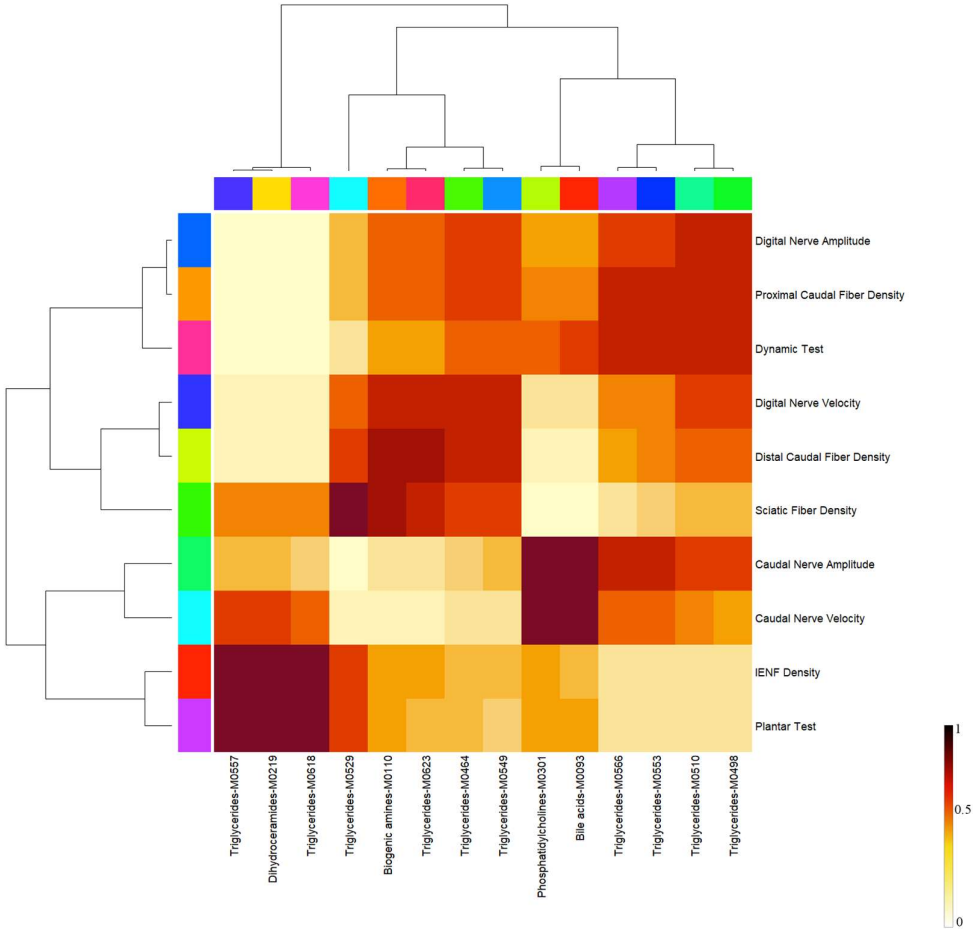

Figure 33. Liver correlation analysis results at the end of treatment in young animals.

The heat map shows the significant associations (r^2>0.65; p<0.05) from correlation analysis results between metabolite concentrations and neurophysiological, behavioral and neuropathological findings. IENF: intraepidermal nerve fiber.

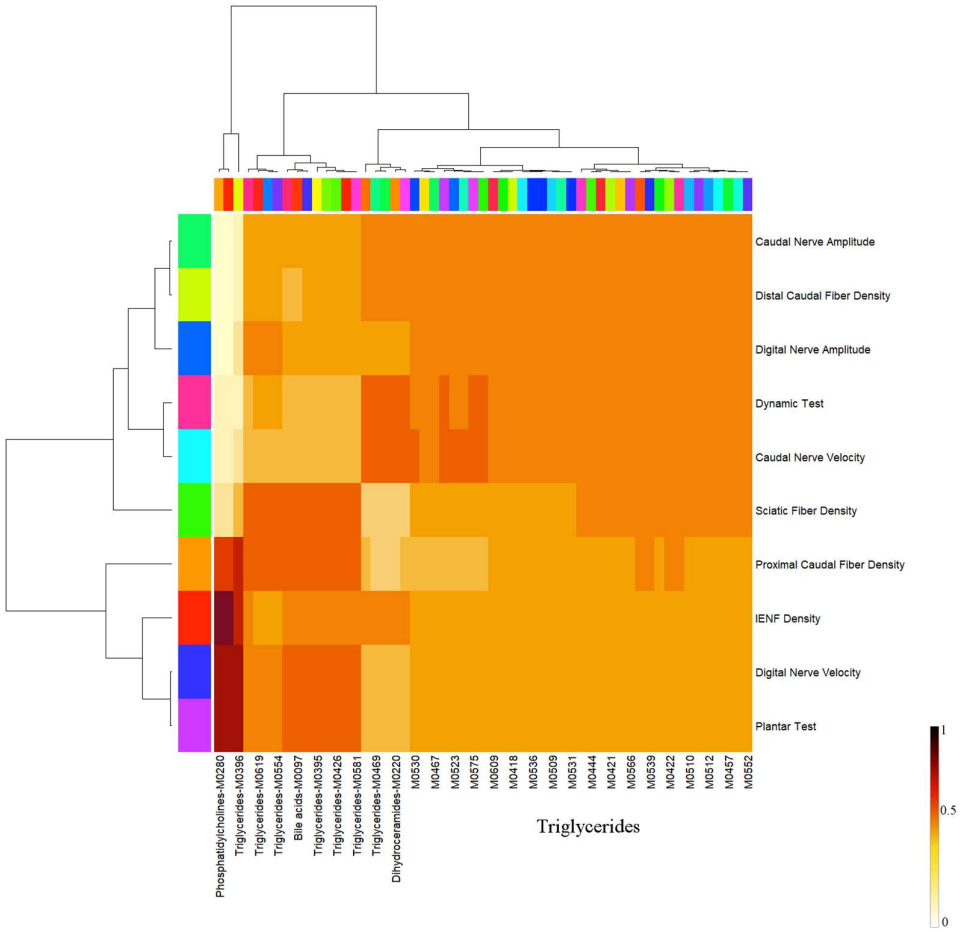

Figure 34. Liver correlation analysis results at the end of treatment in adult animals.

The heat map shows the significant associations (r^2>0.65; p<0.05) from correlation analysis results between metabolite concentrations and neurophysiological, behavioral and neuropathological findings. IENF: intraepidermal nerve fiber.

At the end of the follow-up period, the PCA scree plot showed that the two first PCs explained 61.6% (2 months) and 63.2 % (9 months) of the variation of the selected metabolites (**Figure 35**). The supervised models showed a scarce (2-month animals) and inadequate (9-month animals) predictive accuracy in separating the experimental groups (**Figure 36** and **37**). When testing the ability to discriminate treated animals from controls, no metabolites presented a significant FDR (<0.05).

A) **B)**

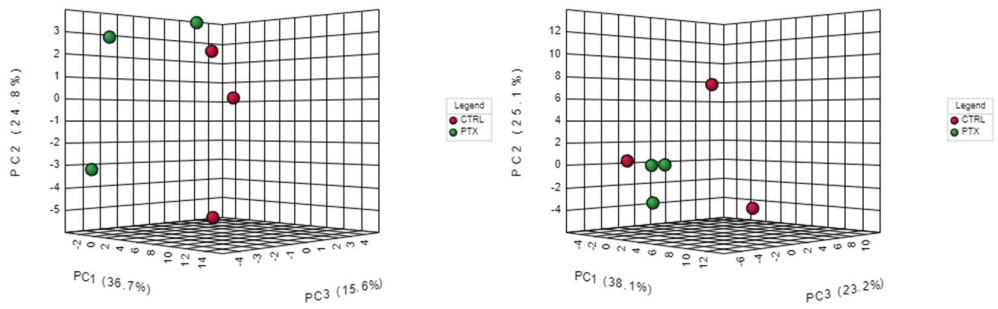

Figure 35. Liver 3D score plot between the selected Principal Components at the end of the follow-up period.

The explained variances are shown in parentheses for the young (A) and adult (B) groups. CTRL: control group; PC: Principal Component; PTX: paclitaxel-treated group.

A) **B)**

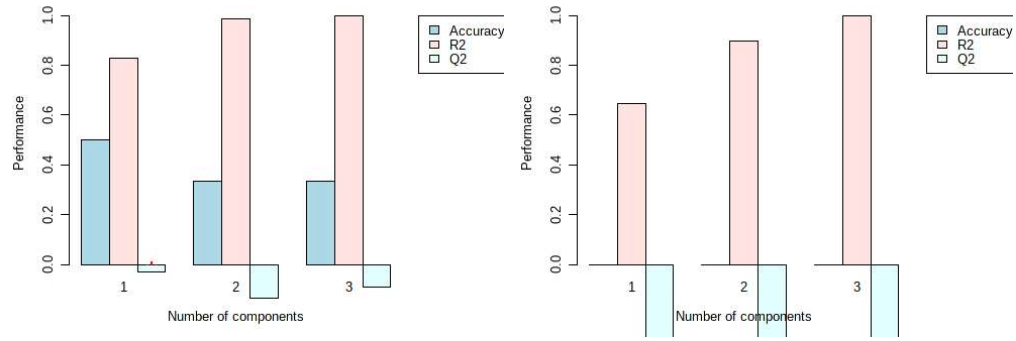

Figure 36. Overview of liver PLS-DA model at the end of the follow-up period.

PLS-DA classification using different number of components for the young (A) and adult (B) groups. We considered a model robust if R^2 and Q^2 values > 0.5, with Q^2 value close to the R^2 value. Models were rejected if there was complete overlap of Q^2 distributions, $Q^2(cum) < 0$, or low classification rates, $Q^2(cum) < 0.05$.

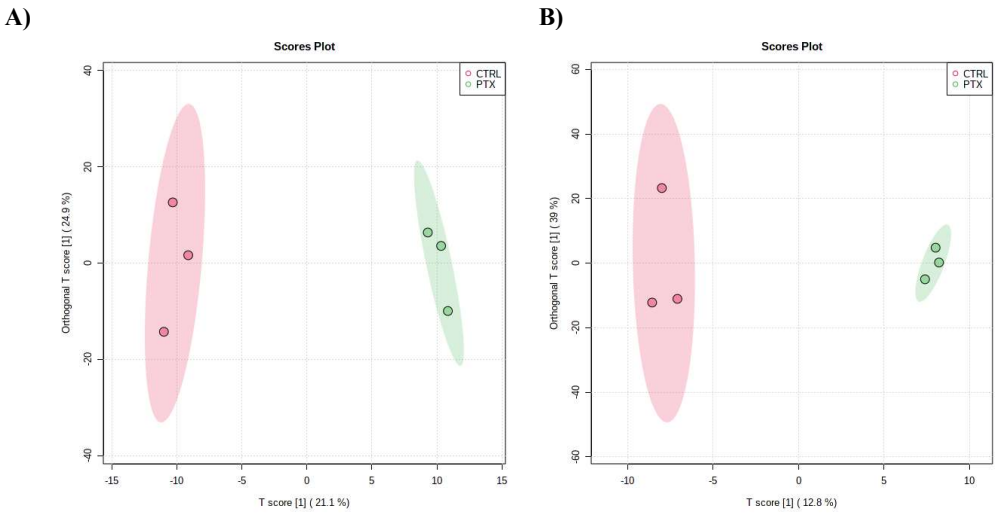

Figure 37. Liver OPLS-DA score plot of all metabolites at the end of the follow-up period.

The image shows the score plot of all metabolites at the end of the follow-up period in young (A) and adult (B) animals. The explained variances are reported in parentheses along the axis. CTRL: control group; PTX: paclitaxel-treated group.

4.7.1 Liver Enrichment analysis

When investigating the most representative liver compound classes over time points, the Enrichment analysis and Over Representation Analysis (ORA) showed in both young and adult animals a significant representation of triacylglycerols and diacylglycerols, as for plasma (**Figure 38** and **39**).

A)

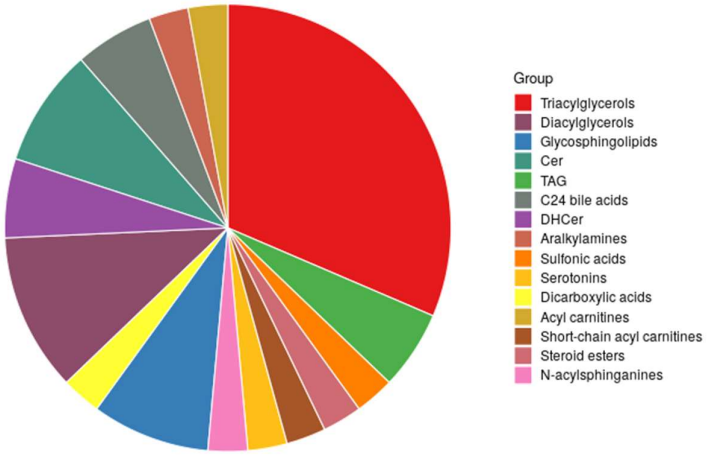

B)

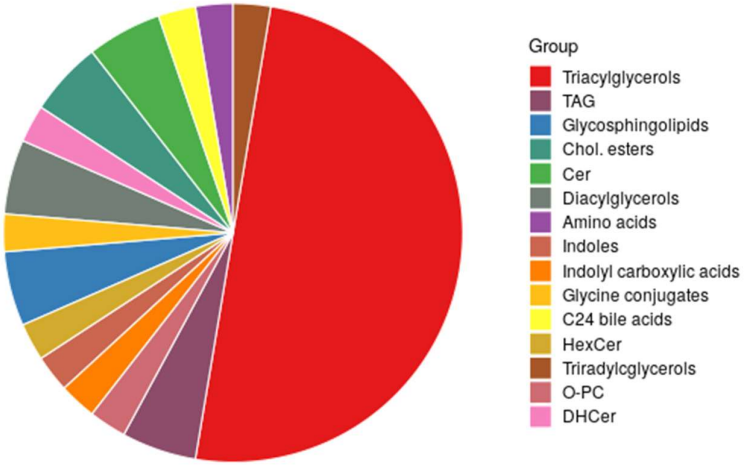

Figure 38. Summary of liver Enrichment Analysis of young animals.

The pie charts show the most represented metabolite sets influenced by paclitaxel administration (FDR <0.05, impact > 0.05) at the end of treatment (A) and at the end of the follow-up period (B). Cer: ceramides; Chol: cholesteryl; DHCer: dihydroceramides; FDR: False Discovery Rate; HexCer: hexosylceramides; PC: phosphatidylcholines; TAG: triacylglycerols.

A)

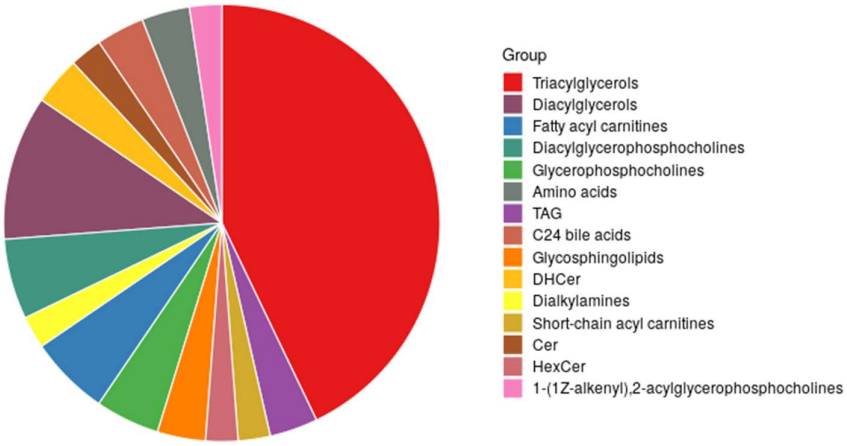

B)

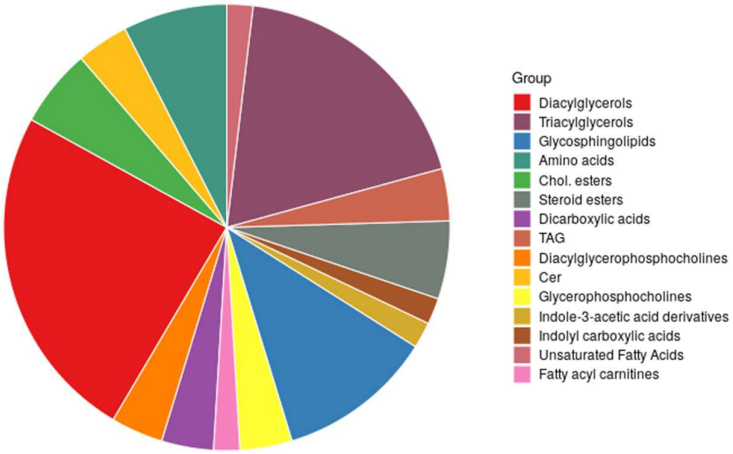

Figure 39. Summary of liver Enrichment Analysis of adult animals.

The pie charts show the most represented metabolite sets influenced by paclitaxel administration (FDR <0.05, impact > 0.05) at the end of treatment (A) and at the end of the follow-up period (B). Cer: ceramides; Chol: cholesteryl; DHCer: dihydroceramides; FDR: False Discovery Rate; HexCer: hexosylceramides; TAG: triacylglycerols.

4.7.2 Liver Pathway analysis

We performed the Pathway analysis in the 2-month and 9-month paclitaxel-treated and age-matched control livers on MetaboAnalyst 5.0. We log-transformed, pareto-scaled, normalized, and processed data (metabolite concentration data, in micromolar) to examine the metabolic pathways in liver affected by paclitaxel administration.

At the end of treatment, we identified one significantly affected pathway by paclitaxel administration only in 9-month animals (citrate cycle, TCA cycle; **Table 7**). The metabolites driving this significant difference (VIP values >1) were decreased levels of succinic acid and cis-aconitic acid. By contrast, at the end of the follow-up period, no pathways satisfied the criteria for significance (FDR <0.05, impact > 0.05, number of hits ≥ 2) in both young and adult animals.

	Total Cmpd	Hits	Raw p	-log10(p)	Holm adjust	FDR	Impact
Citrate cycle (TCA cycle)	20	2	9.59E-04	3.02E+00	4.51E-02	4.51E-02	0.08 *
Glyoxylate and dicarboxylate metabolism	32	4	9.95E-03	2.00E+00	4.58E-01	2.34E-01	0.13
Glutathione metabolism	28	6	3.52E-02	1.45E+00	1.00E+00	3.59E-01	0.12
beta-Alanine metabolism	21	6	3.53E-02	1.45E+00	1.00E+00	3.59E-01	0.46
D-Glutamine and D-glutamate metabolism	6	2	4.84E-02	1.31E+00	1.00E+00	3.59E-01	0.50
Nitrogen metabolism	6	2	4.84E-02	1.31E+00	1.00E+00	3.59E-01	0.00
Arginine and proline metabolism	38	7	5.53E-02	1.26E+00	1.00E+00	3.59E-01	0.39
Butanoate metabolism	15	3	6.24E-02	1.20E+00	1.00E+00	3.59E-01	0.03
Pyruvate metabolism	22	1	7.52E-02	1.12E+00	1.00E+00	3.59E-01	0.00
Cysteine and methionine metabolism	33	5	7.63E-02	1.12E+00	1.00E+00	3.59E-01	0.38
Primary bile acid biosynthesis	46	8	1.11E-01	9.55E-01	1.00E+00	4.73E-01	0.14
Thiamine metabolism	7	1	1.30E-01	8.85E-01	1.00E+00	5.11E-01	0.00
Taurine and hypotaurine metabolism	8	3	1.87E-01	7.28E-01	1.00E+00	6.44E-01	0.43
Porphyrin and chlorophyll metabolism	30	2	2.08E-01	6.81E-01	1.00E+00	6.44E-01	0.00
Propanoate metabolism	23	2	2.20E-01	6.57E-01	1.00E+00	6.44E-01	0.00
alpha-Linolenic acid metabolism	13	1	2.59E-01	5.86E-01	1.00E+00	6.44E-01	0.00
Fatty acid degradation	39	2	2.72E-01	5.66E-01	1.00E+00	6.44E-01	0.00
Arachidonic acid metabolism	36	2	2.98E-01	5.26E-01	1.00E+00	6.44E-01	0.33
Pyrimidine metabolism	39	2	3.24E-01	4.90E-01	1.00E+00	6.44E-01	0.00
Phenylalanine, tyrosine and tryptophan biosynthesis	4	2	3.38E-01	4.72E-01	1.00E+00	6.44E-01	1.00
Pantothenate and CoA biosynthesis	19	4	3.38E-01	4.71E-01	1.00E+00	6.44E-01	0.02
Alanine, aspartate and glutamate metabolism	28	7	3.40E-01	4.68E-01	1.00E+00	6.44E-01	0.62
Selenocompound metabolism	20	1	3.43E-01	4.65E-01	1.00E+00	6.44E-01	0.00
Steroid hormone biosynthesis	77	2	3.68E-01	4.34E-01	1.00E+00	6.44E-01	0.01
Tryptophan metabolism	41	2	3.91E-01	4.08E-01	1.00E+00	6.44E-01	0.25
Glycerophospholipid metabolism	36	3	3.96E-01	4.02E-01	1.00E+00	6.44E-01	0.14
Linoleic acid metabolism	5	2	4.18E-01	3.78E-01	1.00E+00	6.44E-01	1.00
Aminoacyl-tRNA biosynthesis	48	18	4.24E-01	3.72E-01	1.00E+00	6.44E-01	0.00
Biosynthesis of unsaturated fatty acids	36	7	4.25E-01	3.72E-01	1.00E+00	6.44E-01	0.00
Histidine metabolism	16	6	4.33E-01	3.63E-01	1.00E+00	6.44E-01	0.46
Fatty acid elongation	39	1	4.38E-01	3.59E-01	1.00E+00	6.44E-01	0.00
Arginine biosynthesis	14	5	4.38E-01	3.58E-01	1.00E+00	6.44E-01	0.41
Valine, leucine and isoleucine degradation	40	3	4.74E-01	3.25E-01	1.00E+00	6.74E-01	0.00
Glycine, serine and threonine metabolism	34	6	5.27E-01	2.78E-01	1.00E+00	6.80E-01	0.43
Glycolysis / Gluconeogenesis	26	2	5.39E-01	2.68E-01	1.00E+00	6.80E-01	0.00
Purine metabolism	66	3	5.40E-01	2.67E-01	1.00E+00	6.80E-01	0.05
Sphingolipid metabolism	21	5	5.44E-01	2.65E-01	1.00E+00	6.80E-01	0.49
Glycerolipid metabolism	16	1	5.60E-01	2.52E-01	1.00E+00	6.80E-01	0.01
Phenylalanine metabolism	12	3	5.75E-01	2.40E-01	1.00E+00	6.80E-01	0.36
Valine, leucine and isoleucine biosynthesis	8	4	5.79E-01	2.38E-01	1.00E+00	6.80E-01	0.00
Ubiquinone and other terpenoid-quinone biosynthesis	9	1	5.96E-01	2.25E-01	1.00E+00	6.83E-01	0.00
Lysine degradation	25	2	7.18E-01	1.44E-01	1.00E+00	7.86E-01	0.14
Steroid biosynthesis	42	1	7.35E-01	1.34E-01	1.00E+00	7.86E-01	0.00
Biotin metabolism	10	1	7.36E-01	1.33E-01	1.00E+00	7.86E-01	0.00
Fatty acid biosynthesis	47	2	8.04E-01	9.50E-02	1.00E+00	8.39E-01	0.01
Nicotinate and nicotinamide metabolism	15	1	8.39E-01	7.63E-02	1.00E+00	8.57E-01	0.00
Tyrosine metabolism	42	3	9.39E-01	2.74E-02	1.00E+00	9.39E-01	0.38

Table 7. Summary of liver Pathway Analysis at the end of treatment in adult animals.

The star indicates the significant pathway affected by paclitaxel administration (FDR <0.05, impact >0.05, hits ≥ 2). Cmpd: compounds, FDR: False Discovery Rate.

5. Discussion

This neurotoxicity preclinical study suggests that age might be a potential risk factor for more severe peripheral nerve damage after paclitaxel administration, and that the metabolic processes activated in response to neurotoxicity may change according to age.

Our analyses revealed significant peripheral nerve damage induced by paclitaxel administration in both young- and adult-treated animals, with major peripheral nerve impairment in the adult-treated group compared to the young-treated one after treatment completion.

In particular, we observed that paclitaxel administration caused a significant weight loss in adult-treated rats (9 months of age), but not in young-treated animals (2 months of age), denoting a higher chemotherapy-related distress with aging.

The results of our neurophysiological studies further indicated a more extensive caudal and digital nerve impairment in the adult-treated group compared to the young-treated one, which presented only caudal nerve damage. However, we observed a similar persistence in young- and adult-treated animals of caudal nerve neuropathy at the end of the follow-up period, where a coasting effect with myelin damage also emerged.

Neurophysiological observations correlated with the neuropathological findings, which confirmed the significant peripheral nerve damage with a substantial reduction in large myelinated fiber density in treated-animals compared to controls.

We also found a more evident fiber loss in adult rats compared to young animals in both the caudal nerve and the sciatic nerve, in agreement with previous studies describing a substantial decrease in the density of myelinated fibers, particularly in the caudal nerve, with aging (*Verdú et al., 1996; Ceballos et al., 1999; Canta et al., 2016*).

When analyzing behavioral tests, we observed a statistically significant development of mechanical allodynia in young-treated animals, while the mechanical threshold in adult-treated animals was not significantly different from age-matched controls. However, the IENF density analysis revealed a significant loss of small fibers in treated animals, with a more severe involvement of small fibers in adult-treated rats, suggesting a possible increase of withdrawal thresholds in adult dynamic test due to skin denervation or sensitization of nociceptors (*Bruna et al., 2020*).

Indeed, age-related changes in reflexive responses can also contribute to an altered performance in adult behavioral tests (*Ruiz-Medina et al., 2013*). Interestingly, Ruiz-Medina and colleagues reported similar findings in a mice model of PIPN, documenting that the severity of mechanical allodynia related to paclitaxel was higher in young-paclitaxel treated mice than aged paclitaxel-treated animals (*Ruiz-Medina et al., 2013*). The authors ascribed this observation to a paclitaxel-related marked microglial and astrocytic response in the spinal cord of young animals compared to adult mice. Other studies reported age-related differences in nociception and pain behaviors in rodents (*Gagliese and Melzack, 2000*), suggesting a "juvenile window of susceptibility" to painful stimuli (*Lawson and Perry, 1995*).

Concerning IENF density, previous rodent models documented the impact of aging on small fiber damage (*Canta et al., 2016*), as well as a decrease in IENF density after paclitaxel treatment (*Meregalli et al., 2020).* In this regard, our analysis provides evidence for a more severe small fiber impairment when paclitaxel therapy is administered to older animals.

Together, our neurophysiological, behavioral and histopathological results indicate a significant peripheral nerve damage induced by paclitaxel administration in both young- and adult-treated rats, with a more severe chemotherapy-related distress and

peripheral nerve impairment in adult-treated animals considering the concomitant caudal and digital nerve involvement, and the relevant alteration of fiber density. On the other hand, we observed a similar persistence of caudal nerve damage in both ages at the end of the follow-up period, where a coasting effect with myelin sheath injury equally affected young- and adult-treated animals.

In our study, we further investigated the impact of age on the metabolic profile in response to a neurotoxic agent. Specifically, we performed a targeted metabolomics analysis on plasma and liver samples, which showed significant differences in the metabolite profiles between animals developing paclitaxel-related peripheral neuropathy and age-matched controls. Our results also suggest a metabolomics fingerprint of PIPN, with lipids playing a major role in nerve metabolic dysfunction/response to paclitaxel administration (**Figure 40**).

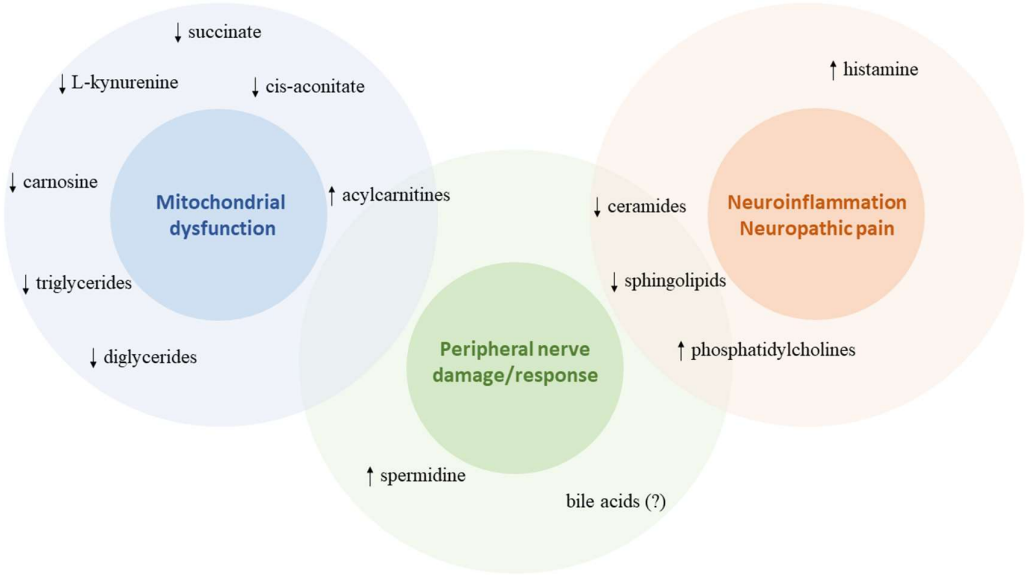

Figure 40. Main metabolic axes affected by paclitaxel administration.

In particular, our multivariate analysis showed that both young- and adult-treated animals presented lower levels of triglycerides and diglycerides compared to controls. These findings point to the major involvement of lipid compounds in support of drug-stress, as an obligate source of energy. Indeed, nerve axons and Schwann cells use a composite pattern of substrates for energy provision, with a preferential use of glucose (*Greene and Winegrad, 1979*).

In cases of fasting or extreme effort, with a limited source of glucose, fatty acid utilization can increase, determining a significant production of ROS from the β-oxidation pathway (*Tracey et al., 2018*). Specifically, during β-oxidation in the mitochondria, electron leakage at various steps in the electron transport chain produces superoxide radicals (*Han et al., 2003; Turrens, 2003; Murphy, 2009; Perevoshchikova et al., 2013*). Besides mitochondria, peroxisomal β-oxidation also contributes to ROS production (*Tracey et al., 2018*). It has also been observed that free fatty acids are able to bind to complexes I and III of electron transport chain, determining an increase in superoxide generation (*Wojtczak and Schönfeld, 1993; Di Paola and Lorusso, 2006*). Accordingly, the preferential use of lipids as the energy source, resulting in the decrease of several lipid classes, in our case supports the hypothesis of a paclitaxel-related metabolic imbalance toward oxidative stress (*Schönfeld and Reiser, 2013*), leading to mitochondrial impairment, and excitotoxicity (*Tracey et al., 2018*).

In support of mitochondrial dysfunction, we also observed altered levels of acylcarnitines at the end of the follow-up period in young-treated animals. Carnitine pool metabolites, including acylcarnitines, have the role of facilitating fatty acid β-oxidation in mitochondria and peroxisomes (*Evans and Fornasini, 2003; Reuter and Evans, 2012*). Elevated serum levels of acylcarnitines can be found as a consequence of incompletely oxidized fatty acids due to an overload of beta oxidation ability and

associated pathways, determining perturbations in mitochondrial fuel utilization, but also as a consequence of oxidative stress (*Noland et al., 2009; McCann et al., 2021*). Another marker supporting the increased oxidative stress and lipid peroxidation observed is certainly the alteration of carnosine levels. In fact, we found decreased levels of carnosine in adult-treated animals at treatment completion and at the end of the follow-up period, in the latter case significantly impacting on the pathway analysis. Of note, this endogenous dipeptide, composed of β-alanine and L-histidine, usually decreases in concentration with age (*Everaert et al., 2011*). Moreover, carnosine was also discriminative in young-treated animals at the end of the follow-up period. Carnosine acts as an antioxidant agent, by scavenging reactive oxygen species and lipid peroxidation through complex chemical composites with zinc and copper ions (*Guney et al., 2006; Hipkiss, 2009*). Previous studies emphasized the possible neuroprotective function of carnosine, due to its antioxidant and anti-inflammatory properties, against neurotoxins (*Kozan et al., 2008; Hipkiss, 2009; Tsai et al., 2010; Cheng et al., 2011*). A recent report supported the ability of carnosine administration to alleviate CIPN in colorectal cancer patients via Nrf2 and nuclear factor-kappa light chain enhancer of B cells (NF-κB) mediated pathways (*Yehia et al., 2019*).

Besides mitochondrial dysfunction, our findings support the hypothesis that paclitaxel-related alterations in the synthesis and/or breakdown of ceramides and sphingolipids may have a major impact on membrane function, neuroinflammatory signaling and pain development, in addition to the myelination deficits.

Specifically, we found lower levels of long chain ceramides in paclitaxel-treated animals compared to controls. In the nervous system, ceramides can be generated from the salvage pathway, via enzymatic hydrolysis of sphingomyelin by sphingomyelinase,

and from *de novo* synthesis by serine palmitoyltransferase and ceramide synthase (*Cruciani-Guglielmacci et al., 2017*).

Plasma pathway analysis further confirmed the role of lower ceramide levels in PIPN development in young animals after treatment completion. In particular, we found that C14 ceramide was involved in three different significant pathways (glutathione metabolism, arginine and proline metabolism, glyoxylate and dicarboxylate metabolism), determining an impactful discrimination between young treated-animals and controls. Long-chain ceramides (C14-C26) are synthetized from sphingosine by ceramide synthase, and influence the physicochemical properties of lipid membranes in a chain length dependent manner (*Grösch et al., 2012*). Long-chain ceramides combine with dihydroceramides to provide the hydrophobic supports for sphingolipids (*Merrill, 2011*). A recent preclinical metabolomics study with mice undergoing docetaxel administration revealed that the majority of dihydroceramide and ceramide species are up-regulated in the DRGs of taxane-treated animals, but not in the spinal cord, where the effect might be indirect (*Becker et al., 2020*). Interestingly, the authors observed reduced levels of ceramides in the sciatic nerve samples of the treated animals, suggesting that taxane metabolic impact on the nervous system is not uniform, possibly due to the different drug permeability.

Our study corroborates other findings supporting the role of sphingolipids in PIPN development. In fact, plasma pathway analysis revealed the alteration of sphingolipid metabolism in young-treated animals at the end of the follow-up period, with decreased sphingomyelin, N-acylsphingosine, glucosylceramide leading an impactful alteration in paclitaxel-treated animals.

Sphingolipids are involved in cell membrane structure and cellular signaling sustenance (*Hannun and Obeid, 2008*). Myelin damage determines the release of its structural

components into the bloodstream, including sphingolipids, which can be measured as potential biomarkers of disease (*Diestel et al., 2003; Safaiyan et al., 2016*). In this regard, the alteration of sphingolipid concentrations may be associated with the impairment of myelin sheath as observed at the end of the follow-up period. Glucosylceramide synthase-derived gangliosides, highly expressed by neurons, also contribute to the formation of membrane microdomains and intracellular signal transduction regulation (*Jennemann et al., 2005; Simons and Gerl, 2010*). Of note, sphingosine can be converted by sphingosine kinases to sphingosine-1-phosphate (S1P), which acts as an active pro-inflammatory sphingolipid through G-protein coupled S1P receptors (*Langeslag and Kress, 2020*). The ceramide/S1P balance, the so-called sphingolipid rheostat, is regulated by the expression of sphingosine kinase. This crucial enzyme modulates the production of these interconvertible sphingolipids in response to stress, and directs cell fate through numerous signaling pathways involving cell proliferation, apoptosis, autophagy and senescence (*Van Brocklyn and Williams, 2012*).

Compelling evidence suggests that ceramides and other sphingolipid derivatives, like S1P, have a relevant role in inflammatory responses and the development of peripheral neuropathic pain (*Hannun and Obeid, 2008; Janes et al., 2014; Stockstill et al., 2018; Langeslag and Kress, 2020*). Previous reports documented the role of S1P in the induction of acute pain and sensitization of primary afferent nociceptors by binding preferentially to S1P1 and S1P3 receptors (S1PR1and S1PR3) in sensory neurons (*Chi and Nicol, 2010; Mair et al., 2011; Camprubí-Robles et al., 2013; Li et al., 2015*). Preclinical models showed that intraplantar sphingolipid injection can cause hyperalgesic responses through the S1PR1, inducing a hypersensitivity to noxious thermal stimulation via TRPV1 channels (*Doyle et al., 2011; Mair et al., 2011*), and by

S1PR3, mainly conveying mechanical pain and itch (*Camprubí-Robles et al., 2013; Hill et al., 2018*). Further evidence indicates the role of endogenous sphingosines in inflammatory astrocyte responses leading to sensory neuron sensitization and neuropathic pain-like behavior (*Chen et al., 2014*).

Our analysis also provides evidence for the presence of specific metabolic responses with aging. In particular, at treatment completion, we found significantly altered levels of phosphatidylcholines, which are mainly engaged in the transfer of choline and fatty acids to tissues in both physiological and pathological states (*Yokota and Hansson, 1995; Murugesan and Fox, 1996*). The derivative lysophosphatidylcholines are reported to be involved in peripheral nerve damage resulting in mechanical allodynia and thermal hyperalgesia (*Wallace et al., 2003; Inoue et al., 2008*). Furthermore, lysophosphatidylcholines can induce nerve demyelination and an increase in pain-related protein levels in DRGs (*Wallace et al., 2003; Bhangoo et al., 2007*). In aged rats, this metabolic alteration persisted at the end of the follow-up period, where diacylglycerophosphocholines were the most represented altered compounds according to Enrichment analysis.

Adult-treated animals also presented increased levels of spermidine and histamine, and lower levels of L-kynurenine and serotonin compared to controls at treatment completion.

A number of reports have documented the effect of polyamines on the nervous system, including brain development (*Slotkin and Bartolome, 1986*), peripheral nerve regeneration (*Gilad et al., 1996*), on neuronal survival and neuritogenesis (*Dornay et al., 1986; Gilad and Gilad, 1988*). The biosynthesis of spermidine is regulated by the enzyme arginase I, responsible for the increase in production of polyamines such as putrescine. It has been demonstrated that in case of nerve damage putrescine is

converted to spermidine to overcome inhibition by myelin-associated inhibitors of regeneration, and to promote axonal regeneration after injury (*Deng et al., 2009*).

In the peripheral nervous system, histamine usually increases in response to tissue damage, and contributes to the generation of pain hypersensitivity through the sensitization of nociceptors determining enhanced firing rates (*Obara et al., 2020*). Intriguingly, it has been suggested a potential role of neuronal histamine H4 receptor in the modulation of painful peripheral neuropathy, by attenuating hyperalgesia, neuroinflammation and oxidative stress in both the spinal cord and sciatic nerve (*Sanna et al., 2017*).

L-kynurenine, a key metabolite of tryptophan metabolism, has various functions including scavenging properties and antioxidant effects (*Tan et al., 2001; Zsizsik and Hardeland, 2002*). Indeed, tryptophan is an endogenous amino acid necessary not only for the kynurenine pathway, but also as a precursor for the synthesis of biologically active molecules, such as serotonin (*Savitz, 2020*). However, only 5% of tryptophan is metabolized to serotonin, while almost 95% undergoes transformations through the kynurenine pathway for the regulation of numerous biological mechanisms, involving neuronal excitability and immunological responses (*Badawy, 2017*). The upregulation of tryptophan-kynurenine metabolism with aging has been previously documented, along with changes in the kynurenine pathway metabolites and enzymes (*Beal et al., 1991; Frick et al., 2004; Guillemin et al., 2005; Reyes Ocampo et al., 2014*). The preferential oxidation of tryptophan along the kynurenine pathway in adult animals might thus explain the observed low levels of serotonin. Of note, some kynurenine derivatives contribute to neurotoxicity, and via glutamate receptors also to pain development (*Dantzer et al., 2008*). Interestingly, inhibition of a key enzyme of the kynurenine pathway, namely indolamine 2,3-dioxygenase-1, can decrease the

hypersensitivity to mechanical and thermal stimuli after ligation of the sciatic nerve in animal models of neuropathy (*Ciapała et al., 2021*). Accordingly, the role of L-kynurenine might be multifaceted and controversial in pain modulation.

Our study additionally reveals the importance of primary bile acid biosynthesis metabolism in plasma of treated older animals compared to age-matched controls. Bile acids play a key function in modulating lipid metabolism, specifically cholesterol. Increased levels of primary bile acids in the blood may indicate a reduction in hepatocellular functionality or alteration of the enterohepatic circulation. On the other hand, a reduction in taurine-conjugated bile acids could indicate a failure to convert cholic acid and chenodeoxycholic acid due to hepatic distress. Intriguingly, recent reports have identified that bile acids are involved in S1PR2 signaling in the heart, lung, liver, and brain (*Yang et al., 2002*). Apparently, S1PR2 signaling via bile acids may have a role in different neurological functions (*McMillin and DeMorrow, 2016*). In fact, in dorsal root ganglion neurons, S1PR1 and S1PR2 seem to be involved in the neurite extension process (*Toman et al., 2004*). In addition, neuropathic models have revealed that selective S1PR2 activation can reduce allodynia and attenuate the associated inflammatory processes in the DRGs of CIPN animals (*Wang et al., 2020*). Other reports have supported the role of tauroursodeoxycholic acid in neuroprotection and mitigation of neuroinflammatory and neuronal death processes (*Rodrigues et al., 2000; Ramalho et al., 2004; Ved et al., 2005; Nunes et al., 2012; Gaspar et al., 2013; Dionísio et al., 2015*). According to some studies, bile acids could also be involved in neurotransmission by interacting with NMDA and gamma-aminobutyric acid receptors (*Schubring et al., 2012*). Indeed, it is becoming increasingly clear that bile acid metabolism is critical in numerous disorders outside of the gastrointestinal tract. The involvement of bile acid signaling in the nervous system is an emerging concept that is

gaining interest, albeit only a few studies have investigated the possible underlying mechanisms (*McMillin and DeMorrow, 2016*). Enrichment analysis confirmed the importance of taurine conjugates and C24 bile acids, the most represented classes in the adult group after treatment completion, pointing to a possible role of these compounds in aged animals developing PIPN.

Our metabolomics analysis also outlined the importance of bile acid metabolism in the liver of young animals, suggesting a more local impact of the hepatic metabolic distress to the external stimulus, which was not evident at a systemic level (plasma) in the young group. In particular, we observed increased levels of chenodeoxycholic acid glycine conjugate and cholic acid, and decreased taurine and taurodeoxycholic acid. Conversely, the liver of adult treated-animals showed an excess of triglycerides and diglycerides, which was coupled with a reduction of acylcarnitines, thus revealing a decrease in mitochondrial fatty acid β-oxidation and possible hepatic steatosis.

Adult liver metabolomics analysis also revealed alterations in Krebs cycle metabolites (also called tricarboxylic acid or TCA cycle), involving low levels of succinic acid and cis-aconitic acid. A recent review outlined the role of metabolites in the TCA cycle in regulating chromatin modifications, DNA methylation, and post-translational modifications of proteins to alter their function (*Martínez-Reyes and Chandel, 2020*). Any alteration in any step of the Krebs cycle due to genetic or environmental factors can lead to higher or lower levels of organic acids. Apparently, changes in succinate can have profound effects on histones and DNA methylation, altering the epigenetic landscape of the cells and gene expression (*Martínez-Reyes and Chandel, 2020*). On the other hand, cis-aconitate and its derivative itaconate seem to activate antioxidant and anti-inflammatory pathways involving Nrf2, as well as limit succinate oxidation

(*Lampropoulou et al., 2016; Cordes et al., 2016; Mills et al., 2018; Bambouskova et al., 2018*).

Collectively, our findings suggest that the mechanisms underlying PIPN are complex and multidimensional, and persist after treatment completion. Numerous neurophysiological and molecular changes determine morphological and functional responses both systemically and in the peripheral nervous system. Among them, we found markers of mitochondrial dysfunction, involving increased β-oxidation of lipid sources and altered organic acids of the Krebs cycle, suggesting an intensification of supplementary metabolic pathways leading to an oxidative stress state. Changes in lipid levels were associated with antioxidant peptide alterations, i.e., decreased carnosine, which was equally reduced in young- and adult-treated animals, and decreased L-kynurenine, only observed in the adult-treated group.

In addition, markers of direct peripheral nerve damage/response also emerged. In this regard, modifications in sphingolipids and ceramides supported relevant changes in the constituents of cell membranes, and increased spermidine suggested axonal regeneration. Sphingolipids, ceramides, phosphatidylcholines and histamine are also responsible for the multifactorial mechanisms underlying the development and maintenance of neuroinflammation and neuropathic pain.

Of note, despite not being discriminative (VIP < 1), glycine was represented in multiple comparisons in both young- and adult-treated animals, suggesting an impaired synaptic transmission, probably involved in pain signaling.

Indeed, our analysis revealed specific metabolic strategies adopted with aging, namely increased levels of spermidine and histamine, and lower levels of kynurenine and serotonin, which were discriminative between treated animals and controls at treatment completion. Likewise, bile acids seem to be involved in the metabolic changes induced

by paclitaxel administration in adult animals, reflecting substantial liver involvement and possible dysregulation of S1PR2 signaling.

The strengths of our targeted metabolomics study applied to a neurotoxic model are several. First, our animal model allowed us to reproduce the development of peripheral neuropathy in the absence of comorbidities potentially confounding the effects of the drug, with an age-matched control design. Indeed, inconsistencies between metabolomics studies in humans may be related to numerous challenges associated with different diets, lighting conditions, sleep/wake status and time of day of sampling, which all have a considerable impact on metabolic profiling (*Davies et al., 2014; Hancox et al., 2021*). By contrast, diet and lighting conditions can be more easily managed in animals, allowing highly-controlled laboratory conditions. Second, the inclusion of adult animals introduced an age variable, thus allowing us to further investigate the association of the toxic effects of paclitaxel with aging. Certainly, the greatest advantage lies in the opportunity to use the Biocrates p500 kit for the metabolomics analysis, providing us with the chance to comprehensively explore the changes on the metabolic profile resulting from paclitaxel administration. This undoubtedly allowed us to closely explore the complex interactions between metabolic pathways underlying the response to neurotoxicity and chemotherapy-induced axonal damage. Our decision to use a targeted rather than an untargeted metabolomics approach was practical, considering the large number of samples collected and the cost/time involved in untargeted compared to targeted methods. By performing targeted metabolomics analysis, we acquired absolute concentrations of the metabolites (compared to relative expression in untargeted analysis), using a fully validated method which is selective and easily reproducible in other facilities (*Siskos et al., 2017*).

We also acknowledge some limitations in our model. First, our experiments involved the evaluation only of male animals to prevent the influence of estrus cycle on metabolomics profiles. Consequently, our results need further validation in samples including also female animals. Second, although the study of animal models of neurotoxicity is validated and widely used, the application of the same approach in the clinical setting is advisable to confirm our findings. Third, at this stage of the study, we only analyzed metabolites extracted from blood and liver samples to get an overview of the main metabolic changes caused by paclitaxel administration. In the future, complementary metabolomics analysis of nerve, DRG and spinal tissue may reveal additional chemotherapy-induced metabolic alterations.

This is the first study providing an extensive and comprehensive overview of the metabolic dysregulations/responses in PIPN according to age.

As well as providing support for the presence of metabolic biomarkers of PIPN, the metabolic changes we observe in our study strongly validate the use of animal models to reproduce a neurotoxicity state. The particular advantage of the animal model is that it can be examined longitudinally to determine changes and progression of the metabolic alterations over time, and to monitor the possible regression of the condition under study.

Clearly, the set of metabolites we have detected as potential biomarkers of CIPN will also need to be measured in paclitaxel-treated cancer patients under supervised conditions, to confirm our findings from the animal model. To date, clinical outcome measures are used for identifying the occurrence and progression of CIPN. Nevertheless, the demand for supportive, reliable and easily accessible biomarkers has never been greater, especially as objective measures in clinical trials for therapeutic evaluations.

In summary, our findings identify for the first time multiple related metabolic axes as promising molecular and therapeutic targets in PIPN, and provide a mechanistic insight into the biomolecular signaling pathways involved in the development of peripheral neuropathy. Our study also shows that age might be a potential risk factor for more severe CIPN, and should be considered in future studies in order to tailor the chemotherapy regimen and dosage on individual susceptibility of older cancer patients.

6. References

- Aaronson NK, Ahmedzai S, Bergman B, Bullinger M, Cull A, Duez NJ, Filiberti A, Flechtner H, Fleishman SB, de Haes JC, et al. The European Organization for Research and Treatment of Cancer QLQ-C30: a quality-of-life instrument for use in international clinical trials in oncology. J Natl Cancer Inst. 1993 Mar 3;85(5):365-76. doi: 10.1093/jnci/85.5.365. PMID: 8433390.
- Abraham JE, Guo Q, Dorling L, Tyrer J, Ingle S, Hardy R, Vallier AL, Hiller L, Burns R, Jones L, Bowden SJ, Dunn JA, Poole CJ, Caldas C, Pharoah PP, Earl HM. Replication of genetic polymorphisms reported to be associated with taxane-related sensory neuropathy in patients with early breast cancer treated with Paclitaxel. Clin Cancer Res. 2014 May 1;20(9):2466-75. doi: 10.1158/1078-0432.CCR-13-3232. Epub 2014 Mar 5. PMID: 24599932.
- Alberti P. Chemotherapy-induced peripheral neurotoxicity - outcome measures: the issue. Expert Opin Drug Metab Toxicol. 2017 Mar;13(3):241-243. doi: 10.1080/17425255.2017.1258400. Epub 2016 Nov 17. PMID: 27819147.
- Arbitrio M, Scionti F, Altomare E, Di Martino MT, Agapito G, Galeano T, Staropoli N, Iuliano E, Grillone F, Fabiani F, Caracciolo D, Cannataro M, Arpino G, Santini D, Tassone P, Tagliaferri P. Polymorphic Variants in NR1I3 and UGT2B7 Predict Taxane Neurotoxicity and Have Prognostic Relevance in Patients With Breast Cancer: A Case-Control Study. Clin Pharmacol Ther. 2019 Aug;106(2):422-431. doi: 10.1002/cpt.1391. Epub 2019 Mar 28. PMID: 30739312.
- Areti A, Yerra VG, Naidu V, Kumar A. Oxidative stress and nerve damage: role in chemotherapy induced peripheral neuropathy. Redox Biol. 2014 Jan

18;2:289-95. doi: 10.1016/j.redox.2014.01.006. PMID: 24494204; PMCID: PMC3909836.

- Argyriou AA, Polychronopoulos P, Koutras A, Iconomou G, Iconomou A, Kalofonos HP, Chroni E. Peripheral neuropathy induced by administration of cisplatin- and paclitaxel-based chemotherapy. Could it be predicted? Support Care Cancer. 2005 Aug;13(8):647-51. doi: 10.1007/s00520-005-0776-9. Epub 2005 Feb 15. PMID: 15711945.
- Argyriou AA, Polychronopoulos P, Koutras A, Iconomou G, Gourzis P, Assimakopoulos K, Kalofonos HP, Chroni E. Is advanced age associated with increased incidence and severity of chemotherapy-induced peripheral neuropathy? Support Care Cancer. 2006 Mar;14(3):223-9. doi: 10.1007/s00520-005-0868-6. Epub 2005 Jul 15. PMID: 16021477.
- Authier N, Balayssac D, Marchand F, Ling B, Zangarelli A, Descoeur J, Coudore F, Bourinet E, Eschalier A. Animal models of chemotherapy-evoked painful peripheral neuropathies. Neurotherapeutics. 2009 Oct;6(4):620-9. doi: 10.1016/j.nurt.2009.07.003. PMID: 19789067; PMCID: PMC5084284.
- Azoulay D, Leibovici A, Sharoni R, Shaoul E, Gross B, Braester A, Goldberg H. Association between Met-BDNF allele and vulnerability to paclitaxel-induced peripheral neuropathy. Breast Cancer Res Treat. 2015 Oct;153(3):703-4. doi: 10.1007/s10549-015-3546-5. Epub 2015 Aug 14. PMID: 26272744.
- Ba X, Wang J, Zhou S, Luo X, Peng Y, Yang S, Hao Y, Jin G. Cinobufacini protects against paclitaxel-induced peripheral neuropathic pain and suppresses TRPV1 up-regulation and spinal astrocyte activation in rats. Biomed Pharmacother. 2018 Dec;108:76-84. doi: 10.1016/j.biopha.2018.09.018. Epub 2018 Sep 12. PMID: 30218861.

- Badawy AA. Kynurenine Pathway of Tryptophan Metabolism: Regulatory and Functional Aspects. Int J Tryptophan Res. 2017 Mar 15;10:1178646917691938. doi: 10.1177/1178646917691938. PMID: 28469468; PMCID: PMC5398323.
- Baldwin RM, Owzar K, Zembutsu H, Chhibber A, Kubo M, Jiang C, Watson D, Eclov RJ, Mefford J, McLeod HL, Friedman PN, Hudis CA, Winer EP, Jorgenson EM, Witte JS, Shulman LN, Nakamura Y, Ratain MJ, Kroetz DL. A genome-wide association study identifies novel loci for paclitaxel-induced sensory peripheral neuropathy in CALGB 40101. Clin Cancer Res. 2012 Sep 15;18(18):5099-109. doi: 10.1158/1078-0432.CCR-12-1590. Epub 2012 Jul 27. PMID: 22843789; PMCID: PMC3445665.
- Ballarini E, Malacrida A, Rodriguez-Menendez V, Pozzi E, Canta A, Chiorazzi A, Monza L, Semperboni S, Meregalli C, Carozzi VA, Hashemi M, Nicolini G, Scuteri A, Housley SN, Cavaletti G, Alberti P. Sodium-Calcium Exchanger 2: A Pivotal Role in Oxaliplatin Induced Peripheral Neurotoxicity and Axonal Damage? Int J Mol Sci. 2022 Sep 2;23(17):10063. doi: 10.3390/ijms231710063. PMID: 36077454; PMCID: PMC9456447.
- Bambouskova M, Gorvel L, Lampropoulou V, Sergushichev A, Loginicheva E, Johnson K, Korenfeld D, Mathyer ME, Kim H, Huang LH, Duncan D, Bregman H, Keskin A, Santeford A, Apte RS, Sehgal R, Johnson B, Amarasinghe GK, Soares MP, Satoh T, Akira S, Hai T, de Guzman Strong C, Auclair K, Roddy TP, Biller SA, Jovanovic M, Klechevsky E, Stewart KM, Randolph GJ, Artyomov MN. Electrophilic properties of itaconate and derivatives regulate the IκBζ-ATF3 inflammatory axis. Nature. 2018 Apr;556(7702):501-504. doi: 10.1038/s41586-018-0052-z. Epub 2018 Apr 18. PMID: 29670287; PMCID: PMC6037913.

- Beal MF, Ferrante RJ, Swartz KJ, Kowall NW. Chronic quinolinic acid lesions in rats closely resemble Huntington's disease. J Neurosci. 1991 Jun;11(6):1649-59. doi: 10.1523/JNEUROSCI.11-06-01649.1991. PMID: 1710657; PMCID: PMC6575424.
- Becker KA, Uerschels AK, Goins L, Doolen S, McQuerry KJ, Bielawski J, Sure U, Bieberich E, Taylor BK, Gulbins E, Spassieva SD. Role of 1-Deoxysphingolipids in docetaxel neurotoxicity. J Neurochem. 2020 Sep;154(6):662-672. doi: 10.1111/jnc.14985. Epub 2020 Mar 13. PMID: 32058598; PMCID: PMC7426245.
- Beissner F, Brandau A, Henke C, Felden L, Baumgärtner U, Treede RD, Oertel BG, Lötsch J. Quick discrimination of A(delta) and C fiber mediated pain based on three verbal descriptors. PLoS One. 2010 Sep 23;5(9):e12944. doi: 10.1371/journal.pone.0012944. PMID: 20886070; PMCID: PMC2944851.
- Bhangoo S, Ren D, Miller RJ, Henry KJ, Lineswala J, Hamdouchi C, Li B, Monahan PE, Chan DM, Ripsch MS, White FA. Delayed functional expression of neuronal chemokine receptors following focal nerve demyelination in the rat: a mechanism for the development of chronic sensitization of peripheral nociceptors. Mol Pain. 2007 Dec 12;3:38. doi: 10.1186/1744-8069-3-38. PMID: 18076762; PMCID: PMC2228278.
- Blasco H, Błaszczyński J, Billaut JC, Nadal-Desbarats L, Pradat PF, Devos D, Moreau C, Andres CR, Emond P, Corcia P, Słowiński R. Comparative analysis of targeted metabolomics: dominance-based rough set approach versus orthogonal partial least square-discriminant analysis. J Biomed Inform. 2015 Feb;53:291-9. doi: 10.1016/j.jbi.2014.12.001. Epub 2014 Dec 11. PMID: 25499899.

- Boehmerle W, Huehnchen P, Peruzzaro S, Balkaya M, Endres M. Electrophysiological, behavioral and histological characterization of paclitaxel, cisplatin, vincristine and bortezomib-induced neuropathy in C57Bl/6 mice. Sci Rep. 2014 Sep 18;4:6370. doi: 10.1038/srep06370. PMID: 25231679; PMCID: PMC5377307.
- Bonomo R, Cavaletti G, Skene DJ. Metabolomics markers in Neurology: current knowledge and future perspectives for therapeutic targeting. Expert Rev Neurother. 2020 Jul;20(7):725-738. doi: 10.1080/14737175.2020.1782746. Epub 2020 Jun 27. PMID: 32538242.
- Bonomo R, Cavaletti G. Clinical and biochemical markers in CIPN: A reappraisal. Rev Neurol (Paris). 2021 Oct;177(8):890-907. doi: 10.1016/j.neurol.2020.11.001. Epub 2021 Feb 26. PMID: 33648782.
- Boora GK, Kanwar R, Kulkarni AA, Abyzov A, Sloan J, Ruddy KJ, Banck MS, Loprinzi CL, Beutler AS. Testing of candidate single nucleotide variants associated with paclitaxel neuropathy in the trial NCCTG N08C1 (Alliance). Cancer Med. 2016 Apr;5(4):631-9. doi: 10.1002/cam4.625. Epub 2016 Jan 14. PMID: 26763541; PMCID: PMC4831281.
- Boyette-Davis JA, Cata JP, Driver LC, Novy DM, Bruel BM, Mooring DL, Wendelschafer-Crabb G, Kennedy WR, Dougherty PM. Persistent chemoneuropathy in patients receiving the plant alkaloids paclitaxel and vincristine. Cancer Chemother Pharmacol. 2013 Mar;71(3):619-26. doi: 10.1007/s00280-012-2047-z. Epub 2012 Dec 11. PMID: 23228992; PMCID: PMC3581748.

- Boyle FM, Wheeler HR, Shenfield GM. Amelioration of experimental cisplatin and paclitaxel neuropathy with glutamate. J Neurooncol. 1999 Jan;41(2):107-16. doi: 10.1023/a:1006124917643. PMID: 10222430.
- Boyle FM, Beatson C, Monk R, Grant SL, Kurek JB. The experimental neuroprotectant leukaemia inhibitory factor (LIF) does not compromise antitumour activity of paclitaxel, cisplatin and carboplatin. Cancer Chemother Pharmacol. 2001 Dec;48(6):429-34. doi: 10.1007/s00280-001-0382-6. PMID: 11800022.
- Branham MT, Nadin SB, Vargas-Roig LM, Ciocca DR. DNA damage induced by paclitaxel and DNA repair capability of peripheral blood lymphocytes as evaluated by the alkaline comet assay. Mutat Res. 2004 May 9;560(1):11-7. doi: 10.1016/j.mrgentox.2004.01.013. PMID: 15099819.
- Brewer AL, Shirachi DY, Quock RM, Craft RM. Effect of hyperbaric oxygen on chemotherapy-induced neuropathy in male and female rats. Behav Pharmacol. 2020 Feb;31(1):61-72. doi: 10.1097/FBP.0000000000000497. PMID: 31503072.
- Bruna J, Alberti P, Calls-Cobos A, Caillaud M, Damaj MI, Navarro X. Methods for in vivo studies in rodents of chemotherapy induced peripheral neuropathy. Exp Neurol. 2020 Mar;325:113154. doi: 10.1016/j.expneurol.2019.113154. Epub 2019 Dec 15. PMID: 31837318; PMCID: PMC7105293.
- Bulls HW, Hoogland AI, Kennedy B, James BW, Arboleda BL, Apte S, Chon HS, Small BJ, Gonzalez BD, Jim HSL. A longitudinal examination of associations between age and chemotherapy-induced peripheral neuropathy in patients with gynecologic cancer. Gynecol Oncol. 2019 Feb;152(2):310-315.

doi: 10.1016/j.ygyno.2018.12.002. Epub 2018 Dec 14. PMID: 30558975; PMCID: PMC6380347.

- Burgos E, Gómez-Nicola D, Pascual D, Martín MI, Nieto-Sampedro M, Goicoechea C. Cannabinoid agonist WIN 55,212-2 prevents the development of paclitaxel-induced peripheral neuropathy in rats. Possible involvement of spinal glial cells. Eur J Pharmacol. 2012 May 5;682(1-3):62-72. doi: 10.1016/j.ejphar.2012.02.008. Epub 2012 Feb 21. PMID: 22374260.
- Camprubí-Robles M, Mair N, Andratsch M, Benetti C, Beroukas D, Rukwied R, Langeslag M, Proia RL, Schmelz M, Ferrer Montiel AV, Haberberger RV, Kress M. Sphingosine-1-phosphate-induced nociceptor excitation and ongoing pain behavior in mice and humans is largely mediated by S1P3 receptor. J Neurosci. 2013 Feb 6;33(6):2582-92. doi: 10.1523/JNEUROSCI.4479-12.2013. PMID: 23392686; PMCID: PMC6619173.
- Canta A, Chiorazzi A, Carozzi VA, Meregalli C, Oggioni N, Bossi M, Rodriguez-Menendez V, Avezza F, Crippa L, Lombardi R, de Vito G, Piazza V, Cavaletti G, Marmiroli P. Age-related changes in the function and structure of the peripheral sensory pathway in mice. Neurobiol Aging. 2016 Sep;45:136-148. doi: 10.1016/j.neurobiolaging.2016.05.014. Epub 2016 May 20. PMID: 27459934.
- Carozzi VA, Canta A, Chiorazzi A. Chemotherapy-induced peripheral neuropathy: What do we know about mechanisms? Neurosci Lett. 2015a Jun 2;596:90-107. doi: 10.1016/j.neulet.2014.10.014. Epub 2014 Oct 22. Erratum in: Neurosci Lett. 2015 Jun 2;596():108. PMID: 25459280.
- Carozzi VA, Chiorazzi A, Canta A, Meregalli C, Oggioni N, Cavaletti G, Marmiroli P. Chemotherapy-induced peripheral neurotoxicity in immune-

deficient mice: new useful ready-to-use animal models. Exp Neurol. 2015b Feb;264:92-102. doi: 10.1016/j.expneurol.2014.11.002. Epub 2014 Nov 18. PMID: 25450467.

- Casals-Díaz L, Vivó M, Navarro X. Nociceptive responses and spinal plastic changes of afferent C-fibers in three neuropathic pain models induced by sciatic nerve injury in the rat. Exp Neurol. 2009 May;217(1):84-95. doi: 10.1016/j.expneurol.2009.01.014. Epub 2009 Feb 3. PMID: 19416675.
- Cashman CR, Höke A. Mechanisms of distal axonal degeneration in peripheral neuropathies. Neurosci Lett. 2015 Jun 2;596:33-50. doi: 10.1016/j.neulet.2015.01.048. Epub 2015 Jan 21. PMID: 25617478; PMCID: PMC4428955.
- Cavaletti G, Bogliun G, Marzorati L, Zincone A, Piatti M, Colombo N, Franchi D, La Presa MT, Lissoni A, Buda A, Fei F, Cundari S, Zanna C. Early predictors of peripheral neurotoxicity in cisplatin and paclitaxel combination chemotherapy. Ann Oncol. 2004 Sep;15(9):1439-42. doi: 10.1093/annonc/mdh348. PMID: 15319252.
- Cavaletti G, Gilardini A, Canta A, Rigamonti L, Rodriguez-Menendez V, Ceresa C, Marmiroli P, Bossi M, Oggioni N, D'Incalci M, De Coster R. Bortezomib-induced peripheral neurotoxicity: a neurophysiological and pathological study in the rat. Exp Neurol. 2007 Mar;204(1):317-25. doi: 10.1016/j.expneurol.2006.11.010. Epub 2007 Jan 9. PMID: 17214983.
- Ceballos D, Cuadras J, Verdú E, Navarro X. Morphometric and ultrastructural changes with ageing in mouse peripheral nerve. J Anat. 1999 Nov;195 (Pt 4)(Pt 4):563-76. doi: 10.1046/j.1469-7580.1999.19540563.x. PMID: 10634695; PMCID: PMC1468027.

- Chaplan SR, Bach FW, Pogrel JW, Chung JM, Yaksh TL. Quantitative assessment of tactile allodynia in the rat paw. J Neurosci Methods. 1994 Jul;53(1):55-63. doi: 10.1016/0165-0270(94)90144-9. PMID: 7990513.
- Chase DM, Huang H, Foss CD, Wenzel LB, Monk BJ, Burger RA. Neurotoxicity in ovarian cancer patients on Gynecologic Oncology Group (GOG) protocol 218: characteristics associated with toxicity and the effect of substitution with docetaxel: an NRG Oncology/Gynecologic Oncology Group study. Gynecol Oncol. 2015 Feb;136(2):323-7. doi: 10.1016/j.ygyno.2014.12.021. Epub 2014 Dec 18. PMID: 25529832; PMCID: PMC4520309.
- Chen CS, Smith EML, Stringer KA, Henry NL, Hertz DL. Co-occurrence and metabolic biomarkers of sensory and motor subtypes of peripheral neuropathy from paclitaxel. Breast Cancer Res Treat. 2022 Aug;194(3):551-560. doi: 10.1007/s10549-022-06652-x. Epub 2022 Jun 28. PMID: 35760975; PMCID: PMC9310087.
- Chen Y, Chen SR, Chen H, Zhang J, Pan HL. Increased α2δ-1-NMDA receptor coupling potentiates glutamatergic input to spinal dorsal horn neurons in chemotherapy-induced neuropathic pain. J Neurochem. 2019 Jan;148(2):252-274. doi: 10.1111/jnc.14627. Epub 2018 Dec 21. PMID: 30431158; PMCID: PMC6340760.
- Chen YJ, Hill S, Huang H, Taraboletti A, Cho K, Gallo R, Manchester M, Shriver LP, Patti GJ. Inflammation triggers production of dimethylsphingosine from oligodendrocytes. Neuroscience. 2014 Oct 24;279:113-21. doi: 10.1016/j.neuroscience.2014.08.011. Epub 2014 Aug 21. PMID: 25151189.

- Cheng J, Wang F, Yu DF, Wu PF, Chen JG. The cytotoxic mechanism of malondialdehyde and protective effect of carnosine via protein cross-linking/mitochondrial dysfunction/reactive oxygen species/MAPK pathway in neurons. Eur J Pharmacol. 2011 Jan 10;650(1):184-94. doi: 10.1016/j.ejphar.2010.09.033. Epub 2010 Sep 21. PMID: 20868662.
- Chi XX, Nicol GD. The sphingosine 1-phosphate receptor, $S1PR_1$, plays a prominent but not exclusive role in enhancing the excitability of sensory neurons. J Neurophysiol. 2010 Nov;104(5):2741-8. doi: 10.1152/jn.00709.2010. Epub 2010 Sep 15. PMID: 20844107; PMCID: PMC2997035.
- Ciapała K, Mika J, Rojewska E. The Kynurenine Pathway as a Potential Target for Neuropathic Pain Therapy Design: From Basic Research to Clinical Perspectives. Int J Mol Sci. 2021 Oct 13;22(20):11055. doi: 10.3390/ijms222011055. PMID: 34681715; PMCID: PMC8537209.
- Cordes T, Wallace M, Michelucci A, Divakaruni AS, Sapcariu SC, Sousa C, Koseki H, Cabrales P, Murphy AN, Hiller K, Metallo CM. Immunoresponsive Gene 1 and Itaconate Inhibit Succinate Dehydrogenase to Modulate Intracellular Succinate Levels. J Biol Chem. 2016 Jul 1;291(27):14274-14284. doi: 10.1074/jbc.M115.685792. Epub 2016 May 9. PMID: 27189937; PMCID: PMC4933182.
- Cornblath DR, Chaudhry V, Carter K, Lee D, Seysedadr M, Miernicki M, Joh T. Total neuropathy score: validation and reliability study. Neurology. 1999 Nov 10;53(8):1660-4. doi: 10.1212/wnl.53.8.1660. PMID: 10563609.
- Cresteil T, Monsarrat B, Alvinerie P, Tréluyer JM, Vieira I, Wright M. Taxol metabolism by human liver microsomes: identification of cytochrome P450

isozymes involved in its biotransformation. Cancer Res. 1994 Jan 15;54(2):386-92. PMID: 7903909.

- Cruccu G, Sommer C, Anand P, Attal N, Baron R, Garcia-Larrea L, Haanpaa M, Jensen TS, Serra J, Treede RD. EFNS guidelines on neuropathic pain assessment: revised 2009. Eur J Neurol. 2010 Aug;17(8):1010-8. doi: 10.1111/j.1468-1331.2010.02969.x. Epub 2010 Mar 8. PMID: 20298428.
- Cruciani-Guglielmacci C, López M, Campana M, le Stunff H. Brain Ceramide Metabolism in the Control of Energy Balance. Front Physiol. 2017 Oct 12;8:787. doi: 10.3389/fphys.2017.00787. PMID: 29075199; PMCID: PMC5643460.
- da Costa Junior LC, de Castro CL, Freitas-Alves DR, Vianna-Jorge R, Santos PCJL. ABCB1 and ERCC1 gene polymorphisms are associated with nephro- and hepatotoxicity to carboplatin/paclitaxel-based chemotherapy in patients with gynecologic cancers. Eur J Clin Pharmacol. 2020 Oct;76(10):1401-1408. doi: 10.1007/s00228-020-02934-9. Epub 2020 Jun 20. PMID: 32564116.
- Dantzer R, O'Connor JC, Freund GG, Johnson RW, Kelley KW. From inflammation to sickness and depression: when the immune system subjugates the brain. Nat Rev Neurosci. 2008 Jan;9(1):46-56. doi: 10.1038/nrn2297. PMID: 18073775; PMCID: PMC2919277.
- Dauvilliers Y, Barateau L, Middleton B, van der Veen DR, Skene DJ. Metabolomics Signature of Patients With Narcolepsy. Neurology. 2022 Feb 1;98(5):e493-e505. doi: 10.1212/WNL.0000000000013128. Epub 2021 Nov 29. PMID: 34845055.
- Davies SK, Ang JE, Revell VL, Holmes B, Mann A, Robertson FP, Cui N, Middleton B, Ackermann K, Kayser M, Thumser AE, Raynaud FI, Skene DJ.

Effect of sleep deprivation on the human metabolome. Proc Natl Acad Sci U S A. 2014 Jul 22;111(29):10761-6. doi: 10.1073/pnas.1402663111. Epub 2014 Jul 7. PMID: 25002497; PMCID: PMC4115565.

- De Iuliis F, Taglieri L, Salerno G, Lanza R, Scarpa S. Taxane induced neuropathy in patients affected by breast cancer: Literature review. Crit Rev Oncol Hematol. 2015 Oct;96(1):34-45. doi: 10.1016/j.critrevonc.2015.04.011. Epub 2015 May 11. PMID: 26004917.
- De Santis S, Pace A, Bove L, Cognetti F, Properzi F, Fiore M, Triaca V, Savarese A, Simone MD, Jandolo B, Manzione L, Aloe L. Patients treated with antitumor drugs displaying neurological deficits are characterized by a low circulating level of nerve growth factor. Clin Cancer Res. 2000 Jan;6(1):90-5. PMID: 10656436.
- Deng K, He H, Qiu J, Lorber B, Bryson JB, Filbin MT. Increased synthesis of spermidine as a result of upregulation of arginase I promotes axonal regeneration in culture and in vivo. J Neurosci. 2009;29(30):9545-9552. doi:10.1523/JNEUROSCI.1175-09.2009
- Di Paola M, Lorusso M. Interaction of free fatty acids with mitochondria: coupling, uncoupling and permeability transition. Biochim Biophys Acta. 2006 Sep-Oct;1757(9-10):1330-7. doi: 10.1016/j.bbabio.2006.03.024. Epub 2006 Apr 7. PMID: 16697347.
- Diestel A, Aktas O, Hackel D, Hake I, Meier S, Raine CS, Nitsch R, Zipp F, Ullrich O. Activation of microglial poly(ADP-ribose)-polymerase-1 by cholesterol breakdown products during neuroinflammation: a link between demyelination and neuronal damage. J Exp Med. 2003 Dec 1;198(11):1729-40. doi: 10.1084/jem.20030975. PMID: 14657223; PMCID: PMC2194134.

- Dionísio PA, Amaral JD, Ribeiro MF, Lo AC, D'Hooge R, Rodrigues CM. Amyloid-β pathology is attenuated by tauroursodeoxycholic acid treatment in APP/PS1 mice after disease onset. Neurobiol Aging. 2015 Jan;36(1):228-40. doi: 10.1016/j.neurobiolaging.2014.08.034. Epub 2014 Sep 28. PMID: 25443293.
- Dornay M, Gilad VH, Shiler I, Gilad GM. Early polyamine treatment accelerates regeneration of rat sympathetic neurons. Exp Neurol. 1986 Jun;92(3):665-74. doi: 10.1016/0014-4886(86)90307-9. PMID: 3709740.
- Doyle T, Chen Z, Obeid LM, Salvemini D. Sphingosine-1-phosphate acting via the $S1P_1$ receptor is a downstream signaling pathway in ceramide-induced hyperalgesia. Neurosci Lett. 2011 Jul 15;499(1):4-8. doi: 10.1016/j.neulet.2011.05.018. Epub 2011 May 13. PMID: 21605625; PMCID: PMC3119782.
- Doyle T, Chen Z, Muscoli C, Bryant L, Esposito E, Cuzzocrea S, Dagostino C, Ryerse J, Rausaria S, Kamadulski A, Neumann WL, Salvemini D. Targeting the overproduction of peroxynitrite for the prevention and reversal of paclitaxel-induced neuropathic pain. J Neurosci. 2012 May 2;32(18):6149-60. doi: 10.1523/JNEUROSCI.6343-11.2012. PMID: 22553021; PMCID: PMC3752044.
- Duggett NA, Griffiths LA, McKenna OE, de Santis V, Yongsanguanchai N, Mokori EB, Flatters SJ. Oxidative stress in the development, maintenance and resolution of paclitaxel-induced painful neuropathy. Neuroscience. 2016 Oct 1;333:13-26. doi: 10.1016/j.neuroscience.2016.06.050. Epub 2016 Jul 5. PMID: 27393249; PMCID: PMC4996646.

- Evans AM, Fornasini G. Pharmacokinetics of L-carnitine. Clin Pharmacokinet. 2003;42(11):941-67. doi: 10.2165/00003088-200342110-00002. PMID: 12908852.
- Everaert I, Mooyaart A, Baguet A, Zutinic A, Baelde H, Achten E, Taes Y, De Heer E, Derave W. Vegetarianism, female gender and increasing age, but not CNDP1 genotype, are associated with reduced muscle carnosine levels in humans. Amino Acids. 2011 Apr;40(4):1221-9. doi: 10.1007/s00726-010-0749-2. Epub 2010 Sep 24. PMID: 20865290.
- Falah M, Rayan M, Rayan A. A Novel Paclitaxel Conjugate with Higher Efficiency and Lower Toxicity: A New Drug Candidate for Cancer Treatment. Int J Mol Sci. 2019 Oct 8;20(19):4965. doi: 10.3390/ijms20194965. PMID: 31597361; PMCID: PMC6801939.
- Fernandes R, Mazzarello S, Majeed H, Smith S, Shorr R, Hutton B, Ibrahim MF, Jacobs C, Ong M, Clemons M. Treatment of taxane acute pain syndrome (TAPS) in cancer patients receiving taxane-based chemotherapy-a systematic review. Support Care Cancer. 2016a Apr;24(4):1583-94. doi: 10.1007/s00520-015-2941-0. Epub 2015 Sep 19. PMID: 26386706.
- Fernandes R, Mazzarello S, Hutton B, Shorr R, Majeed H, Ibrahim MF, Jacobs C, Ong M, Clemons M. Taxane acute pain syndrome (TAPS) in patients receiving taxane-based chemotherapy for breast cancer-a systematic review. Support Care Cancer. 2016b Aug;24(8):3633-50. doi: 10.1007/s00520-016-3256-5. Epub 2016 May 5. PMID: 27146496.
- Flatters SJL, Bennett GJ. Studies of peripheral sensory nerves in paclitaxel-induced painful peripheral neuropathy: evidence for mitochondrial dysfunction.

Pain. 2006 Jun;122(3):245-257. doi: 10.1016/j.pain.2006.01.037. Epub 2006 Mar 13. PMID: 16530964; PMCID: PMC1805481.

- Flatters SJL, Dougherty PM, Colvin LA. Clinical and preclinical perspectives on Chemotherapy-Induced Peripheral Neuropathy (CIPN): a narrative review. Br J Anaesth. 2017 Oct 1;119(4):737-749. doi: 10.1093/bja/aex229. PMID: 29121279.
- Freilich RJ, Balmaceda C, Seidman AD, Rubin M, DeAngelis LM. Motor neuropathy due to docetaxel and paclitaxel. Neurology. 1996 Jul;47(1):115-8. doi: 10.1212/wnl.47.1.115. PMID: 8710063.
- Frick B, Schroecksnadel K, Neurauter G, Leblhuber F, Fuchs D. Increasing production of homocysteine and neopterin and degradation of tryptophan with older age. Clin Biochem. 2004 Aug;37(8):684-7. doi: 10.1016/j.clinbiochem.2004.02.007. PMID: 15302611.
- Gagliese L, Melzack R. Age differences in nociception and pain behaviours in the rat. Neurosci Biobehav Rev. 2000 Dec;24(8):843-54. doi: 10.1016/s0149-7634(00)00041-5. PMID: 11118609.
- Garcia-Perez E, Schönberger T, Sumalla M, Stierstorfer B, Solà R, Doods H, Serra J, Gorodetskaya N. Behavioural, morphological and electrophysiological assessment of the effects of type 2 diabetes mellitus on large and small nerve fibres in Zucker diabetic fatty, Zucker lean and Wistar rats. Eur J Pain. 2018 Sep;22(8):1457-1472. doi: 10.1002/ejp.1235. Epub 2018 May 17. PMID: 29676840.
- Garell PC, McGillis SL, Greenspan JD. Mechanical response properties of nociceptors innervating feline hairy skin. J Neurophysiol. 1996 Mar;75(3):1177-89. doi: 10.1152/jn.1996.75.3.1177. PMID: 8867127.

- Gaspar JM, Martins A, Cruz R, Rodrigues CM, Ambrósio AF, Santiago AR. Tauroursodeoxycholic acid protects retinal neural cells from cell death induced by prolonged exposure to elevated glucose. Neuroscience. 2013 Dec 3;253:380-8. doi: 10.1016/j.neuroscience.2013.08.053. Epub 2013 Sep 5. PMID: 24012838.
- Gilad GM, Gilad VH. Early polyamine treatment enhances survival of sympathetic neurons after postnatal axonal injury or immunosympathectomy. Brain Res. 1988 Feb 1;466(2):175-81. doi: 10.1016/0165-3806(88)90042-9. PMID: 3359309.
- Gilad VH, Tetzlaff WG, Rabey JM, Gilad GM. Accelerated recovery following polyamines and aminoguanidine treatment after facial nerve injury in rats. Brain Res. 1996 Jun 10;724(1):141-4. doi: 10.1016/0006-8993(96)00287-9. PMID: 8816269.
- Gradishar WJ, Tjulandin S, Davidson N, Shaw H, Desai N, Bhar P, Hawkins M, O'Shaughnessy J. Phase III trial of nanoparticle albumin-bound paclitaxel compared with polyethylated castor oil-based paclitaxel in women with breast cancer. J Clin Oncol. 2005 Nov 1;23(31):7794-803. doi: 10.1200/JCO.2005.04.937. Epub 2005 Sep 19. PMID: 16172456.
- Greene DA, Winegrad AI. In vitro studies of the substrates for energy production and the effects of insulin on glucose utilization in the neural components of peripheral nerve. Diabetes. 1979 Oct;28(10):878-87. doi: 10.2337/diab.28.10.878. PMID: 478182.
- Grisold W, Cavaletti G, Windebank AJ. Peripheral neuropathies from chemotherapeutics and targeted agents: diagnosis, treatment, and prevention.

Neuro Oncol. 2012 Sep;14 Suppl 4(Suppl 4):iv45-54. doi: 10.1093/neuonc/nos203. PMID: 23095830; PMCID: PMC3480245.

- Grösch S, Schiffmann S, Geisslinger G. Chain length-specific properties of ceramides. Prog Lipid Res. 2012 Jan;51(1):50-62. doi: 10.1016/j.plipres.2011.11.001. Epub 2011 Nov 25. PMID: 22133871.
- Guillemin GJ, Brew BJ, Noonan CE, Takikawa O, Cullen KM. Indoleamine 2,3 dioxygenase and quinolinic acid immunoreactivity in Alzheimer's disease hippocampus. Neuropathol Appl Neurobiol. 2005 Aug;31(4):395-404. doi: 10.1111/j.1365-2990.2005.00655.x. PMID: 16008823.
- Guney Y, Turkcu UO, Hicsonmez A, Andrieu MN, Guney HZ, Bilgihan A, Kurtman C. Carnosine may reduce lung injury caused by radiation therapy. Med Hypotheses. 2006;66(5):957-9. doi: 10.1016/j.mehy.2005.11.023. Epub 2006 Jan 10. PMID: 16406688.
- Ha JW, You MJ, Park HS, Kim JW, Kwon MS. Differential effect of LPS and paclitaxel on microglial functional phenotypes and circulating cytokines: the possible role of CX3CR1 and IL-4/10 in blocking persistent inflammation. Arch Pharm Res. 2019 Apr;42(4):359-368. doi: 10.1007/s12272-019-01137-w. Epub 2019 Mar 9. PMID: 30852731.
- Haanpää M, Attal N, Backonja M, Baron R, Bennett M, Bouhassira D, Cruccu G, Hansson P, Haythornthwaite JA, Iannetti GD, Jensen TS, Kauppila T, Nurmikko TJ, Rice ASC, Rowbotham M, Serra J, Sommer C, Smith BH, Treede RD. NeuPSIG guidelines on neuropathic pain assessment. Pain. 2011 Jan;152(1):14-27. doi: 10.1016/j.pain.2010.07.031. Epub 2010 Sep 19. PMID: 20851519.

- Hama A, Takamatsu H. Chemotherapy-Induced Peripheral Neuropathic Pain and Rodent Models. CNS Neurol Disord Drug Targets. 2016;15(1):7-19. doi: 10.2174/1871527315666151110125325. PMID: 26553161.
- Han D, Antunes F, Canali R, Rettori D, Cadenas E. Voltage-dependent anion channels control the release of the superoxide anion from mitochondria to cytosol. J Biol Chem. 2003 Feb 21;278(8):5557-63. doi: 10.1074/jbc.M210269200. Epub 2002 Dec 12. PMID: 12482755.
- Hancox TPM, Skene DJ, Dallmann R, Dunn WB. Tick-Tock Consider the Clock: The Influence of Circadian and External Cycles on Time of Day Variation in the Human Metabolome-A Review. Metabolites. 2021 May 19;11(5):328. doi: 10.3390/metabo11050328. PMID: 34069741; PMCID: PMC8161100.
- Hannun YA, Obeid LM. Principles of bioactive lipid signalling: lessons from sphingolipids. Nat Rev Mol Cell Biol. 2008 Feb;9(2):139-50. doi: 10.1038/nrm2329. PMID: 18216770.
- Hara T, Chiba T, Abe K, Makabe A, Ikeno S, Kawakami K, Utsunomiya I, Hama T, Taguchi K. Effect of paclitaxel on transient receptor potential vanilloid 1 in rat dorsal root ganglion. Pain. 2013 Jun;154(6):882-9. doi: 10.1016/j.pain.2013.02.023. Epub 2013 Mar 4. PMID: 23602343.
- Hargreaves K, Dubner R, Brown F, Flores C, Joris J. A new and sensitive method for measuring thermal nociception in cutaneous hyperalgesia. Pain. 1988 Jan;32(1):77-88. doi: 10.1016/0304-3959(88)90026-7. PMID: 3340425.
- He F, Liu J, Shen X, Wang Z, Li Q, Li G. Adverse Event Profile for Nanoparticle Albumin-Bound Paclitaxel Compared With Solvent-Based Taxanes in Solid-Organ Tumors: A Systematic Review and Meta-Analysis of

Randomized Clinical Trials. Ann Pharmacother. 2022 Aug;56(8):898-909. doi: 10.1177/10600280211058385. Epub 2021 Dec 28. PMID: 34963337; PMCID: PMC9237853.

- Hershman DL, Till C, Wright JD, Awad D, Ramsey SD, Barlow WE, Minasian LM, Unger J. Comorbidities and Risk of Chemotherapy-Induced Peripheral Neuropathy Among Participants 65 Years or Older in Southwest Oncology Group Clinical Trials. J Clin Oncol. 2016 Sep 1;34(25):3014-22. doi: 10.1200/JCO.2015.66.2346. Epub 2016 Jun 20. PMID: 27325863; PMCID: PMC5012713.
- Hershman DL, Unger JM, Crew KD, Till C, Greenlee H, Minasian LM, Moinpour CM, Lew DL, Fehrenbacher L, Wade JL 3rd, Wong SF, Fisch MJ, Lynn Henry N, Albain KS. Two-Year Trends of Taxane-Induced Neuropathy in Women Enrolled in a Randomized Trial of Acetyl-L-Carnitine (SWOG S0715). J Natl Cancer Inst. 2018 Jun 1;110(6):669-676. doi: 10.1093/jnci/djx259. PMID: 29361042; PMCID: PMC6005110.
- Hill RZ, Hoffman BU, Morita T, Campos SM, Lumpkin EA, Brem RB, Bautista DM. The signaling lipid sphingosine 1-phosphate regulates mechanical pain. Elife. 2018 Mar 21;7:e33285. doi: 10.7554/eLife.33285. PMID: 29561262; PMCID: PMC5896955.
- Hipkiss AR. Carnosine and its possible roles in nutrition and health. Adv Food Nutr Res. 2009;57:87-154. doi: 10.1016/S1043-4526(09)57003-9. PMID: 19595386.
- Hirota J, Shimizu S. Routes of Administration, in: Hedrich H (Ed), The Laboratory Mouse (2nd Edition). Elsevier Ltd, London, 2012;709–725.

- Hirth J, Watkins PB, Strawderman M, Schott A, Bruno R, Baker LH. The effect of an individual's cytochrome CYP3A4 activity on docetaxel clearance. Clin Cancer Res. 2000 Apr;6(4):1255-8. PMID: 10778948.
- Hopkins HL, Duggett NA, Flatters SJL. Chemotherapy-induced painful neuropathy: pain-like behaviours in rodent models and their response to commonly used analgesics. Curr Opin Support Palliat Care. 2016 Jun;10(2):119-128. doi: 10.1097/SPC.0000000000000204. PMID: 27054288; PMCID: PMC4982532.
- Housley SN, Nardelli P, Carrasco DI, Rotterman TM, Pfahl E, Matyunina LV, McDonald JF, Cope TC. Cancer Exacerbates Chemotherapy-Induced Sensory Neuropathy. Cancer Res. 2020 Jul 1;80(13):2940-2955. doi: 10.1158/0008-5472.CAN-19-2331. Epub 2020 Apr 28. PMID: 32345673; PMCID: PMC7340531.
- Huizing MT, Misser VH, Pieters RC, ten Bokkel Huinink WW, Veenhof CH, Vermorken JB, Pinedo HM, Beijnen JH. Taxanes: a new class of antitumor agents. Cancer Invest. 1995;13(4):381-404. doi: 10.3109/07357909509031919. PMID: 7627725.
- Hwang BY, Kim ES, Kim CH, Kwon JY, Kim HK. Gender differences in paclitaxel-induced neuropathic pain behavior and analgesic response in rats. Korean J Anesthesiol. 2012 Jan;62(1):66-72. doi: 10.4097/kjae.2012.62.1.66. Epub 2012 Jan 25. PMID: 22323957; PMCID: PMC3272532.
- Inoue M, Xie W, Matsushita Y, Chun J, Aoki J, Ueda H. Lysophosphatidylcholine induces neuropathic pain through an action of autotaxin to generate lysophosphatidic acid. Neuroscience. 2008 Mar

18;152(2):296-8. doi: 10.1016/j.neuroscience.2007.12.041. Epub 2008 Jan 9. PMID: 18280050.

- Janes K, Little JW, Li C, Bryant L, Chen C, Chen Z, Kamocki K, Doyle T, Snider A, Esposito E, Cuzzocrea S, Bieberich E, Obeid L, Petrache I, Nicol G, Neumann WL, Salvemini D. The development and maintenance of paclitaxel-induced neuropathic pain require activation of the sphingosine 1-phosphate receptor subtype 1. J Biol Chem. 2014 Jul 25;289(30):21082-97. doi: 10.1074/jbc.M114.569574. PMID: 24876379; PMCID: PMC4110312.
- Jennemann R, Sandhoff R, Wang S, Kiss E, Gretz N, Zuliani C, Martin-Villalba A, Jäger R, Schorle H, Kenzelmann M, Bonrouhi M, Wiegandt H, Gröne HJ. Cell-specific deletion of glucosylceramide synthase in brain leads to severe neural defects after birth. Proc Natl Acad Sci U S A. 2005 Aug 30;102(35):12459-64. doi: 10.1073/pnas.0500893102. Epub 2005 Aug 18. PMID: 16109770; PMCID: PMC1194904.
- Kaley TJ, Deangelis LM. Therapy of chemotherapy-induced peripheral neuropathy. Br J Haematol. 2009 Apr;145(1):3-14. doi: 10.1111/j.1365-2141.2008.07558.x. Epub 2009 Jan 16. PMID: 19170681.
- Kim E, Hwang SH, Kim HK, Abdi S, Kim HK. Losartan, an Angiotensin II Type 1 Receptor Antagonist, Alleviates Mechanical Hyperalgesia in a Rat Model of Chemotherapy-Induced Neuropathic Pain by Inhibiting Inflammatory Cytokines in the Dorsal Root Ganglia. Mol Neurobiol. 2019 Nov;56(11):7408-7419. doi: 10.1007/s12035-019-1616-0. Epub 2019 Apr 29. PMID: 31037647.
- Kleckner IR, Jusko TA, Culakova E, Chung K, Kleckner AS, Asare M, Inglis JE, Loh KP, Peppone LJ, Miller J, Melnik M, Kasbari S, Ossip D, Mustian KM. Longitudinal study of inflammatory, behavioral, clinical, and psychosocial risk

factors for chemotherapy-induced peripheral neuropathy. Breast Cancer Res Treat. 2021 Sep;189(2):521-532. doi: 10.1007/s10549-021-06304-6. Epub 2021 Jun 30. PMID: 34191201; PMCID: PMC8668235.

- Kovalchuk O, Filkowski J, Meservy J, Ilnytskyy Y, Tryndyak VP, Chekhun VF, Pogribny IP. Involvement of microRNA-451 in resistance of the MCF-7 breast cancer cells to chemotherapeutic drug doxorubicin. Mol Cancer Ther. 2008 Jul;7(7):2152-9. doi: 10.1158/1535-7163.MCT-08-0021. PMID: 18645025.
- Kozan R, Sefil F, Bağirici F. Anticonvulsant effect of carnosine on penicillin-induced epileptiform activity in rats. Brain Res. 2008 Nov 6;1239:249-55. doi: 10.1016/j.brainres.2008.08.019. Epub 2008 Aug 16. PMID: 18773880.
- Kramer R, Bielawski J, Kistner-Griffin E, Othman A, Alecu I, Ernst D, Kornhauser D, Hornemann T, Spassieva S. Neurotoxic 1-deoxysphingolipids and paclitaxel-induced peripheral neuropathy. FASEB J. 2015 Nov;29(11):4461-72. doi: 10.1096/fj.15-272567. Epub 2015 Jul 21. PMID: 26198449; PMCID: PMC4608911.
- Kuhle J, Gaiottino J, Leppert D, Petzold A, Bestwick JP, Malaspina A, Lu CH, Dobson R, Disanto G, Norgren N, Nissim A, Kappos L, Hurlbert J, Yong VW, Giovannoni G, Casha S. Serum neurofilament light chain is a biomarker of human spinal cord injury severity and outcome. J Neurol Neurosurg Psychiatry. 2015 Mar;86(3):273-9. doi: 10.1136/jnnp-2013-307454. Epub 2014 Jun 16. PMID: 24935984.
- Lampropoulou V, Sergushichev A, Bambouskova M, Nair S, Vincent EE, Loginicheva E, Cervantes-Barragan L, Ma X, Huang SC, Griss T, Weinheimer CJ, Khader S, Randolph GJ, Pearce EJ, Jones RG, Diwan A, Diamond MS, Artyomov MN. Itaconate Links Inhibition of Succinate Dehydrogenase with

Macrophage Metabolic Remodeling and Regulation of Inflammation. Cell Metab. 2016 Jul 12;24(1):158-66. doi: 10.1016/j.cmet.2016.06.004. Epub 2016 Jun 30. PMID: 27374498; PMCID: PMC5108454.

- Landerholm ÅH, Hansson PT. The perception threshold counterpart to dynamic and static mechanical allodynia assessed using von Frey filaments in peripheral neuropathic pain patients. Scand J Pain. 2011 Jan 1;2(1):9-16. doi: 10.1016/j.sjpain.2010.08.001. PMID: 29913720.
- Langeslag M, Kress M. The ceramide-S1P pathway as a druggable target to alleviate peripheral neuropathic pain. Expert Opin Ther Targets. 2020 Sep;24(9):869-884. doi: 10.1080/14728222.2020.1787989. Epub 2020 Jul 9. PMID: 32589067.
- Lauria G, Lombardi R, Borgna M, Penza P, Bianchi R, Savino C, Canta A, Nicolini G, Marmiroli P, Cavaletti G. Intraepidermal nerve fiber density in rat foot pad: neuropathologic-neurophysiologic correlation. J Peripher Nerv Syst. 2005 Jun;10(2):202-8. doi: 10.1111/j.1085-9489.2005.0010210.x. PMID: 15958131.
- Lauria G, Bakkers M, Schmitz C, Lombardi R, Penza P, Devigili G, Smith AG, Hsieh ST, Mellgren SI, Umapathi T, Ziegler D, Faber CG, Merkies IS. Intraepidermal nerve fiber density at the distal leg: a worldwide normative reference study. J Peripher Nerv Syst. 2010 Sep;15(3):202-7. doi: 10.1111/j.1529-8027.2010.00271.x. PMID: 21040142.
- Lawson LJ, Perry VH. The unique characteristics of inflammatory responses in mouse brain are acquired during postnatal development. Eur J Neurosci. 1995 Jul 1;7(7):1584-95. doi: 10.1111/j.1460-9568.1995.tb01154.x. PMID: 7551185.

- Leandro-García LJ, Inglada-Pérez L, Pita G, Hjerpe E, Leskelä S, Jara C, Mielgo X, González-Neira A, Robledo M, Avall-Lundqvist E, Gréen H, Rodríguez-Antona C. Genome-wide association study identifies ephrin type A receptors implicated in paclitaxel induced peripheral sensory neuropathy. J Med Genet. 2013 Sep;50(9):599-605. doi: 10.1136/jmedgenet-2012-101466. Epub 2013 Jun 17. PMID: 23776197.
- Lee JJ, Swain SM. Peripheral neuropathy induced by microtubule-stabilizing agents. J Clin Oncol. 2006 Apr 1;24(10):1633-42. doi: 10.1200/JCO.2005.04.0543. PMID: 16575015.
- Lewis RE, Kunz AL, Bell RE. Error of intraperitoneal injections in rats. Lab Anim Care. 1966 Dec;16(6):505-9. PMID: 4291449.
- Li C, Li JN, Kays J, Guerrero M, Nicol GD. Sphingosine 1-phosphate enhances the excitability of rat sensory neurons through activation of sphingosine 1-phosphate receptors 1 and/or 3. J Neuroinflammation. 2015 Apr 12;12:70. doi: 10.1186/s12974-015-0286-8. PMID: 25880547; PMCID: PMC4397880.
- Li L, Li J, Zuo Y, Dang D, Frost JA, Yang Q. Activation of KCNQ Channels Prevents Paclitaxel-Induced Peripheral Neuropathy and Associated Neuropathic Pain. J Pain. 2019 May;20(5):528-539. doi: 10.1016/j.jpain.2018.11.001. Epub 2018 Nov 22. PMID: 30471428; PMCID: PMC7337983.
- Li Y, Tatsui CE, Rhines LD, North RY, Harrison DS, Cassidy RM, Johansson CA, Kosturakis AK, Edwards DD, Zhang H, Dougherty PM. Dorsal root ganglion neurons become hyperexcitable and increase expression of voltage-gated T-type calcium channels (Cav3.2) in paclitaxel-induced peripheral

neuropathy. Pain. 2017 Mar;158(3):417-429. doi: 10.1097/j.pain.0000000000000774. PMID: 27902567; PMCID: PMC5303135.

- Li Y, North RY, Rhines LD, Tatsui CE, Rao G, Edwards DD, Cassidy RM, Harrison DS, Johansson CA, Zhang H, Dougherty PM. DRG Voltage-Gated Sodium Channel 1.7 Is Upregulated in Paclitaxel-Induced Neuropathy in Rats and in Humans with Neuropathic Pain. J Neurosci. 2018 Jan 31;38(5):1124-1136. doi: 10.1523/JNEUROSCI.0899-17.2017. Epub 2017 Dec 18. PMID: 29255002; PMCID: PMC5792474.
- Loprinzi CL, Lacchetti C, Bleeker J, Cavaletti G, Chauhan C, Hertz DL, Kelley MR, Lavino A, Lustberg MB, Paice JA, Schneider BP, Lavoie Smith EM, Smith ML, Smith TJ, Wagner-Johnston N, Hershman DL. Prevention and Management of Chemotherapy-Induced Peripheral Neuropathy in Survivors of Adult Cancers: ASCO Guideline Update. J Clin Oncol. 2020 Oct 1;38(28):3325-3348. doi: 10.1200/JCO.20.01399. Epub 2020 Jul 14. PMID: 32663120.
- Mair N, Benetti C, Andratsch M, Leitner MG, Constantin CE, Camprubí-Robles M, Quarta S, Biasio W, Kuner R, Gibbins IL, Kress M, Haberberger RV. Genetic evidence for involvement of neuronally expressed $S1P_1$ receptor in nociceptor sensitization and inflammatory pain. PLoS One. 2011 Feb 17;6(2):e17268. doi: 10.1371/journal.pone.0017268. PMID: 21359147; PMCID: PMC3040773.
- Makker PG, Duffy SS, Lees JG, Perera CJ, Tonkin RS, Butovsky O, Park SB, Goldstein D, Moalem-Taylor G. Characterisation of Immune and Neuroinflammatory Changes Associated with Chemotherapy-Induced

Peripheral Neuropathy. PLoS One. 2017 Jan 26;12(1):e0170814. doi: 10.1371/journal.pone.0170814. PMID: 28125674; PMCID: PMC5268425.

- Marmiroli P, Nicolini G, Miloso M, Scuteri A, Cavaletti G. The fundamental role of morphology in experimental neurotoxicology: the example of chemotherapy-induced peripheral neurotoxicity. Ital J Anat Embryol. 2012;117(2):75-97. PMID: 23420996.
- Martínez-Reyes I, Chandel NS. Mitochondrial TCA cycle metabolites control physiology and disease. Nat Commun. 2020 Jan 3;11(1):102. doi: 10.1038/s41467-019-13668-3. PMID: 31900386; PMCID: PMC6941980.
- Materazzi S, Fusi C, Benemei S, Pedretti P, Patacchini R, Nilius B, Prenen J, Creminon C, Geppetti P, Nassini R. TRPA1 and TRPV4 mediate paclitaxel-induced peripheral neuropathy in mice via a glutathione-sensitive mechanism. Pflugers Arch. 2012 Apr;463(4):561-9. doi: 10.1007/s00424-011-1071-x. Epub 2012 Jan 19. PMID: 22258694.
- Mauri D, Kamposioras K, Tsali L, Bristianou M, Valachis A, Karathanasi I, Georgiou C, Polyzos NP. Overall survival benefit for weekly vs. three-weekly taxanes regimens in advanced breast cancer: A meta-analysis. Cancer Treat Rev. 2010 Feb;36(1):69-74. doi: 10.1016/j.ctrv.2009.10.006. Epub 2009 Nov 27. PMID: 19945225.
- McCann MR, George De la Rosa MV, Rosania GR, Stringer KA. L-Carnitine and Acylcarnitines: Mitochondrial Biomarkers for Precision Medicine. Metabolites. 2021;11(1):51. Published 2021 Jan 14. doi:10.3390/metabo11010051

- McMillin M, DeMorrow S. Effects of bile acids on neurological function and disease. FASEB J. 2016 Nov;30(11):3658-3668. doi: 10.1096/fj.201600275R. Epub 2016 Jul 28. PMID: 27468758; PMCID: PMC5067249.
- Meregalli C, Fumagalli G, Alberti P, Canta A, Carozzi VA, Chiorazzi A, Monza L, Pozzi E, Sandelius Å, Blennow K, Zetterberg H, Marmiroli P, Cavaletti G. Neurofilament light chain as disease biomarker in a rodent model of chemotherapy induced peripheral neuropathy. Exp Neurol. 2018 Sep;307:129-132. doi: 10.1016/j.expneurol.2018.06.005. Epub 2018 Jun 13. PMID: 29908147.
- Meregalli C, Fumagalli G, Alberti P, Canta A, Chiorazzi A, Monza L, Pozzi E, Carozzi VA, Blennow K, Zetterberg H, Cavaletti G, Marmiroli P. Neurofilament light chain: a specific serum biomarker of axonal damage severity in rat models of Chemotherapy-Induced Peripheral Neurotoxicity. Arch Toxicol. 2020 Jul;94(7):2517-2522. doi: 10.1007/s00204-020-02755-w. Epub 2020 Apr 24. PMID: 32333051.
- Meregalli C, Bonomo R, Cavaletti G, Carozzi VA. Blood molecular biomarkers for chemotherapy-induced peripheral neuropathy: From preclinical models to clinical practice. Neurosci Lett. 2021 Apr 1;749:135739. doi: 10.1016/j.neulet.2021.135739. Epub 2021 Feb 15. PMID: 33600907.
- Merrill AH Jr. Sphingolipid and glycosphingolipid metabolic pathways in the era of sphingolipidomics. Chem Rev. 2011 Oct 12;111(10):6387-422. doi: 10.1021/cr2002917. Epub 2011 Sep 26. PMID: 21942574; PMCID: PMC3191729.
- Mielke S, Sparreboom A, Steinberg SM, Gelderblom H, Unger C, Behringer D, Mross K. Association of Paclitaxel pharmacokinetics with the development of

peripheral neuropathy in patients with advanced cancer. Clin Cancer Res. 2005 Jul 1;11(13):4843-50. doi: 10.1158/1078-0432.CCR-05-0298. PMID: 16000582.

- Mikuła-Pietrasik J, Witucka A, Pakuła M, Uruski P, Begier-Krasińska B, Niklas A, Tykarski A, Książek K. Comprehensive review on how platinum- and taxane-based chemotherapy of ovarian cancer affects biology of normal cells. Cell Mol Life Sci. 2019 Feb;76(4):681-697. doi: 10.1007/s00018-018-2954-1. Epub 2018 Oct 31. PMID: 30382284; PMCID: PMC6514066.
- Mills EL, Ryan DG, Prag HA, Dikovskaya D, Menon D, Zaslona Z, Jedrychowski MP, Costa ASH, Higgins M, Hams E, Szpyt J, Runtsch MC, King MS, McGouran JF, Fischer R, Kessler BM, McGettrick AF, Hughes MM, Carroll RG, Booty LM, Knatko EV, Meakin PJ, Ashford MLJ, Modis LK, Brunori G, Sévin DC, Fallon PG, Caldwell ST, Kunji ERS, Chouchani ET, Frezza C, Dinkova-Kostova AT, Hartley RC, Murphy MP, O'Neill LA. Itaconate is an anti-inflammatory metabolite that activates Nrf2 via alkylation of KEAP1. Nature. 2018 Apr 5;556(7699):113-117. doi: 10.1038/nature25986. Epub 2018 Mar 28. PMID: 29590092; PMCID: PMC6047741.
- Molassiotis A, Cheng HL, Lopez V, Au JSK, Chan A, Bandla A, Leung KT, Li YC, Wong KH, Suen LKP, Chan CW, Yorke J, Farrell C, Sundar R. Are we mis-estimating chemotherapy-induced peripheral neuropathy? Analysis of assessment methodologies from a prospective, multinational, longitudinal cohort study of patients receiving neurotoxic chemotherapy. BMC Cancer. 2019 Feb 8;19(1):132. doi: 10.1186/s12885-019-5302-4. PMID: 30736741; PMCID: PMC6368751.

- Monza L, Fumagalli G, Chiorazzi A, Alberti P. Addressing the Need of a Translational Approach in Peripheral Neuropathy Research: Morphology Meets Function. Brain Sci. 2021 Jan 22;11(2):139. doi: 10.3390/brainsci11020139. PMID: 33499072; PMCID: PMC7911498.
- Moulder SL, Holmes FA, Tolcher AW, Thall P, Broglio K, Valero V, Buzdar AU, Arbuck SG, Seidman A, Hortobagyi GN. A randomized phase 2 trial comparing 3-hour versus 96-hour infusion schedules of paclitaxel for the treatment of metastatic breast cancer. Cancer. 2010 Feb 15;116(4):814-21. doi: 10.1002/cncr.24870. PMID: 20052721; PMCID: PMC3806193.
- Murphy MP. How mitochondria produce reactive oxygen species. Biochem J. 2009 Jan 1;417(1):1-13. doi: 10.1042/BJ20081386. PMID: 19061483; PMCID: PMC2605959.
- Murugesan G, Fox PL. Role of lysophosphatidylcholine in the inhibition of endothelial cell motility by oxidized low density lipoprotein. J Clin Invest. 1996 Jun 15;97(12):2736-44. doi: 10.1172/JCI118728. PMID: 8675684; PMCID: PMC507366.
- Nair AB, Jacob S. A simple practice guide for dose conversion between animals and human. J Basic Clin Pharm. 2016 Mar;7(2):27-31. doi: 10.4103/0976-0105.177703. PMID: 27057123; PMCID: PMC4804402.
- Naji-Esfahani H, Vaseghi G, Safaeian L, Pilehvarian AA, Abed A, Rafieian-Kopaei M. Gender differences in a mouse model of chemotherapy-induced neuropathic pain. Lab Anim. 2016 Feb;50(1):15-20. doi: 10.1177/0023677215575863. Epub 2015 Mar 2. PMID: 25732574.
- Nakahashi Y, Kamiya Y, Funakoshi K, Miyazaki T, Uchimoto K, Tojo K, Ogawa K, Fukuoka T, Goto T. Role of nerve growth factor-tyrosine kinase

receptor A signaling in paclitaxel-induced peripheral neuropathy in rats. Biochem Biophys Res Commun. 2014 Feb 14;444(3):415-9. doi: 10.1016/j.bbrc.2014.01.082. Epub 2014 Jan 27. PMID: 24480438.

- Nicholson JK, Lindon JC. Systems biology: Metabonomics. Nature. 2008 Oct 23;455(7216):1054-6. doi: 10.1038/4551054a. PMID: 18948945.
- Noda-Narita S, Shimomura A, Tanabe Y, Kawauchi J, Matsuzaki J, Takizawa S, Aoki Y, Shimizu C, Tamura K, Ochiya T. Peripheral neuropathy from paclitaxel: risk prediction by serum microRNAs. BMJ Support Palliat Care. 2020 Jan 14:bmjspcare-2019-001900. doi: 10.1136/bmjspcare-2019-001900. Epub ahead of print. PMID: 31937590.
- Noland RC, Koves TR, Seiler SE, Lum H, Lust RM, Ilkayeva O, Stevens RD, Hegardt FG, Muoio DM. Carnitine insufficiency caused by aging and overnutrition compromises mitochondrial performance and metabolic control. J Biol Chem. 2009 Aug 21;284(34):22840-52. doi: 10.1074/jbc.M109.032888. Epub 2009 Jun 24. PMID: 19553674; PMCID: PM
- Nunes AF, Amaral JD, Lo AC, Fonseca MB, Viana RJ, Callaerts-Vegh Z, D'Hooge R, Rodrigues CM. TUDCA, a bile acid, attenuates amyloid precursor protein processing and amyloid-β deposition in APP/PS1 mice. Mol Neurobiol. 2012 Jun;45(3):440-54. doi: 10.1007/s12035-012-8256-y. Epub 2012 Mar 23. PMID: 22438081.
- Obara I, Telezhkin V, Alrashdi I, Chazot PL. Histamine, histamine receptors, and neuropathic pain relief. Br J Pharmacol. 2020;177(3):580-599. doi:10.1111/bph.14696
- Okubo K, Takahashi T, Sekiguchi F, Kanaoka D, Matsunami M, Ohkubo T, Yamazaki J, Fukushima N, Yoshida S, Kawabata A. Inhibition of T-type

calcium channels and hydrogen sulfide-forming enzyme reverses paclitaxel-evoked neuropathic hyperalgesia in rats. Neuroscience. 2011 Aug 11;188:148-56. doi: 10.1016/j.neuroscience.2011.05.004. Epub 2011 May 11. PMID: 21596106.

- Openshaw H, Beamon K, Synold TW, Longmate J, Slatkin NE, Doroshow JH, Forman S, Margolin K, Morgan R, Shibata S, Somlo G. Neurophysiological study of peripheral neuropathy after high-dose Paclitaxel: lack of neuroprotective effect of amifostine. Clin Cancer Res. 2004 Jan 15;10(2):461-7. doi: 10.1158/1078-0432.ccr-0772-03. PMID: 14760066.
- Pace A, Bove L, Aloe A, Nardi M, Pietrangeli A, Calabresi F, Innocenti P, Jandolo B. Paclitaxel neurotoxicity: clinical and neurophysiological study of 23 patients. Ital J Neurol Sci. 1997 Apr;18(2):73-9. doi: 10.1007/BF01999566. PMID: 9239526.
- Pang Z, Zhou G, Ewald J, Chang L, Hacariz O, Basu N, Xia J. Using MetaboAnalyst 5.0 for LC-HRMS spectra processing, multi-omics integration and covariate adjustment of global metabolomics data. Nat Protoc. 2022 Jun 17. doi: 10.1038/s41596-022-00710-w. Epub ahead of print. PMID: 35715522.
- Park SB, Alberti P, Kolb NA, Gewandter JS, Schenone A, Argyriou AA. Overview and critical revision of clinical assessment tools in chemotherapy-induced peripheral neurotoxicity. J Peripher Nerv Syst. 2019;24 Suppl 2:S13-S25. doi:10.1111/jns.12333
- Peng Q, Mechanic J, Shoieb A, Pardo ID, Schaevitz L, Fenyk-Melody J, Vitsky A, Boucher M, Somps C, Cook JC, Liu CN. Circulating microRNA and automated motion analysis as novel methods of assessing chemotherapy-induced peripheral neuropathy in mice. PLoS One. 2019 Jan

24;14(1):e0210995. doi: 10.1371/journal.pone.0210995. PMID: 30677061; PMCID: PMC6345499.

- Penson RT, Oliva E, Skates SJ, Glyptis T, Fuller AF Jr, Goodman A, Seiden MV. Expression of multidrug resistance-1 protein inversely correlates with paclitaxel response and survival in ovarian cancer patients: a study in serial samples. Gynecol Oncol. 2004 Apr;93(1):98-106. doi: 10.1016/j.ygyno.2003.11.053. PMID: 15047220.
- Perevoshchikova IV, Quinlan CL, Orr AL, Gerencser AA, Brand MD. Sites of superoxide and hydrogen peroxide production during fatty acid oxidation in rat skeletal muscle mitochondria. Free Radic Biol Med. 2013 Aug;61:298-309. doi: 10.1016/j.freeradbiomed.2013.04.006. Epub 2013 Apr 11. PMID: 23583329; PMCID: PMC3871980.
- Persohn E, Canta A, Schoepfer S, Traebert M, Mueller L, Gilardini A, Galbiati S, Nicolini G, Scuteri A, Lanzani F, Giussani G, Cavaletti G. Morphological and morphometric analysis of paclitaxel and docetaxel-induced peripheral neuropathy in rats. Eur J Cancer. 2005 Jul; 41(10): 1460-6.
- Pevida M, Lastra A, Hidalgo A, Baamonde A, Menéndez L. Spinal CCL2 and microglial activation are involved in paclitaxel-evoked cold hyperalgesia. Brain Res Bull. 2013 Jun;95:21-7. doi: 10.1016/j.brainresbull.2013.03.005. Epub 2013 Apr 2. PMID: 23562605.
- Pizzamiglio C, Ripellino P, Prandi P, Clemente N, Saggia C, Rossi V, Strigaro G, Luigi Foglio Bonda P, Comi C, Cantello R. Nerve conduction, circulating osteopontin and taxane-induced neuropathy in breast cancer patients. Neurophysiol Clin. 2020 Feb;50(1):47-54. doi: 10.1016/j.neucli.2019.12.001. Epub 2020 Jan 9. PMID: 31928832.

- Radaelli E, Santagostino SF, Sellers RS, Brayton CF. Immune Relevant and Immune Deficient Mice: Options and Opportunities in Translational Research. ILAR J. 2018 Dec 31;59(3):211-246. doi: 10.1093/ilar/ily026. PMID: 31197363; PMCID: PMC7114723.
- Ramalho RM, Ribeiro PS, Solá S, Castro RE, Steer CJ, Rodrigues CM. Inhibition of the E2F-1/p53/Bax pathway by tauroursodeoxycholic acid in amyloid beta-peptide-induced apoptosis of PC12 cells. J Neurochem. 2004 Aug;90(3):567-75. doi: 10.1111/j.1471-4159.2004.02517.x. PMID: 15255934.
- Reuter SE, Evans AM. Carnitine and acylcarnitines: pharmacokinetic, pharmacological and clinical aspects. Clin Pharmacokinet. 2012 Sep 1;51(9):553-72. doi: 10.1007/BF03261931. PMID: 22804748.
- Reyes Ocampo J, Lugo Huitrón R, González-Esquivel D, Ugalde-Muñiz P, Jiménez-Anguiano A, Pineda B, Pedraza-Chaverri J, Ríos C, Pérez de la Cruz V. Kynurenines with neuroactive and redox properties: relevance to aging and brain diseases. Oxid Med Cell Longev. 2014;2014:646909. doi: 10.1155/2014/646909. Epub 2014 Feb 17. PMID: 24693337; PMCID: PMC3945746.
- Rodrigues CM, Solá S, Silva R, Brites D. Bilirubin and amyloid-beta peptide induce cytochrome c release through mitochondrial membrane permeabilization. Mol Med. 2000 Nov;6(11):936-46. PMID: 11147571; PMCID: PMC1949925.
- Rui L. Energy metabolism in the liver. Compr Physiol. 2014 Jan;4(1):177-97. doi: 10.1002/cphy.c130024. PMID: 24692138; PMCID: PMC4050641.
- Ruiz-Medina J, Baulies A, Bura SA, Valverde O. Paclitaxel-induced neuropathic pain is age dependent and devolves on glial response. Eur J Pain.

2013 Jan;17(1):75-85. doi: 10.1002/j.1532-2149.2012.00172.x. Epub 2012 May 24. PMID: 22623135.

- Römisch-Margl W, Prehn C, Bogumil R, Röhring C, Suhre K, Adamski J. Procedure for tissue sample preparation and metabolite extraction for high-throughput targeted metabolomics. Metabolomics. 2012 8: 133–142. doi:10.1007/s11306-011-0293-4.
- Safaiyan S, Kannaiyan N, Snaidero N, Brioschi S, Biber K, Yona S, Edinger AL, Jung S, Rossner MJ, Simons M. Age-related myelin degradation burdens the clearance function of microglia during aging. Nat Neurosci. 2016 Aug;19(8):995-8. doi: 10.1038/nn.4325. Epub 2016 Jun 13. PMID: 27294511; PMCID: PMC7116794.
- Sanna MD, Lucarini L, Durante M, Ghelardini C, Masini E, Galeotti N. Histamine H4 receptor agonist-induced relief from painful peripheral neuropathy is mediated by inhibition of spinal neuroinflammation and oxidative stress. Br J Pharmacol. 2017 Jan;174(1):28-40. doi: 10.1111/bph.13644. Epub 2016 Nov 18. PMID: 27714773; PMCID: PMC5341487.
- Savitz J. The kynurenine pathway: a finger in every pie. Mol Psychiatry. 2020 Jan;25(1):131-147. doi: 10.1038/s41380-019-0414-4. Epub 2019 Apr 12. PMID: 30980044; PMCID: PMC6790159.
- Schaumburg HH, Spencer PS. Toxic neuropathies. Neurology. 1979 Apr;29(4):429-31. doi: 10.1212/wnl.29.4.429. PMID: 220559.
- Schneider BP, Li L, Radovich M, Shen F, Miller KD, Flockhart DA, Jiang G, Vance G, Gardner L, Vatta M, Bai S, Lai D, Koller D, Zhao F, O'Neill A, Smith ML, Railey E, White C, Partridge A, Sparano J, Davidson NE, Foroud T, Sledge GW Jr. Genome-Wide Association Studies for Taxane-Induced Peripheral

Neuropathy in ECOG-5103 and ECOG-1199. Clin Cancer Res. 2015 Nov 15;21(22):5082-5091. doi: 10.1158/1078-0432.CCR-15-0586. Epub 2015 Jul 2. PMID: 26138065; PMCID: PMC4717479.

- Schubring SR, Fleischer W, Lin JS, Haas HL, Sergeeva OA. The bile steroid chenodeoxycholate is a potent antagonist at NMDA and GABA(A) receptors. Neurosci Lett. 2012 Jan 11;506(2):322-6. doi: 10.1016/j.neulet.2011.11.036. Epub 2011 Dec 2. PMID: 22155097.
- Schönfeld P, Reiser G. Why does brain metabolism not favor burning of fatty acids to provide energy? Reflections on disadvantages of the use of free fatty acids as fuel for brain. J Cereb Blood Flow Metab. 2013 Oct;33(10):1493-9. doi: 10.1038/jcbfm.2013.128. Epub 2013 Aug 7. PMID: 23921897; PMCID: PMC3790936.
- Seidman AD, Berry D, Cirrincione C, Harris L, Muss H, Marcom PK, Gipson G, Burstein H, Lake D, Shapiro CL, Ungaro P, Norton L, Winer E, Hudis C. Randomized phase III trial of weekly compared with every-3-weeks paclitaxel for metastatic breast cancer, with trastuzumab for all HER-2 overexpressors and random assignment to trastuzumab or not in HER-2 nonoverexpressors: final results of Cancer and Leukemia Group B protocol 9840. J Clin Oncol. 2008 Apr 1;26(10):1642-9. doi: 10.1200/JCO.2007.11.6699. PMID: 18375893.
- Shan Z, Cai S, Yu J, Zhang Z, Vallecillo TGM, Serafini MJ, Thomas AM, Pham NYN, Bellampalli SS, Moutal A, Zhou Y, Xu GB, Xu YM, Luo S, Patek M, Streicher JM, Gunatilaka AAL, Khanna R. Reversal of Peripheral Neuropathic Pain by the Small-Molecule Natural Product Physalin F via Block of CaV2.3 (R-Type) and CaV2.2 (N-Type) Voltage-Gated Calcium Channels. ACS Chem

Neurosci. 2019 Jun 19;10(6):2939-2955. doi: 10.1021/acschemneuro.9b00166. Epub 2019 Apr 18. PMID: 30946560.

- Simons K, Gerl MJ. Revitalizing membrane rafts: new tools and insights. Nat Rev Mol Cell Biol. 2010 Oct;11(10):688-99. doi: 10.1038/nrm2977. PMID: 20861879.
- Siskos AP, Jain P, Römisch-Margl W, Bennett M, Achaintre D, Asad Y, Marney L, Richardson L, Koulman A, Griffin JL, Raynaud F, Scalbert A, Adamski J, Prehn C, Keun HC. Interlaboratory Reproducibility of a Targeted Metabolomics Platform for Analysis of Human Serum and Plasma. Anal Chem. 2017 Jan 3;89(1):656-665. doi: 10.1021/acs.analchem.6b02930. Epub 2016 Dec 13. PMID: 27959516; PMCID: PMC6317696.
- Skene DJ, Middleton B, Fraser CK, Pennings JL, Kuchel TR, Rudiger SR, Bawden CS, Morton AJ. Metabolic profiling of presymptomatic Huntington's disease sheep reveals novel biomarkers. Sci Rep. 2017 Feb 22;7:43030. doi: 10.1038/srep43030. PMID: 28223686; PMCID: PMC5320451.
- Slotkin TA, Bartolome J. Role of ornithine decarboxylase and the polyamines in nervous system development: a review. Brain Res Bull. 1986 Sep;17(3):307-20. doi: 10.1016/0361-9230(86)90236-4. PMID: 3094839.
- Sparano JA, Wang M, Martino S, Jones V, Perez EA, Saphner T, Wolff AC, Sledge GW Jr, Wood WC, Davidson NE. Weekly paclitaxel in the adjuvant treatment of breast cancer. N Engl J Med. 2008 Apr 17;358(16):1663-71. doi: 10.1056/NEJMoa0707056. Erratum in: N Engl J Med. 2008 Jul 3;359(1):106. Erratum in: N Engl J Med. 2009 Apr 16;360(16):1685. PMID: 18420499; PMCID: PMC2743943.

- Stockstill K, Doyle TM, Yan X, Chen Z, Janes K, Little JW, Braden K, Lauro F, Giancotti LA, Harada CM, Yadav R, Xiao WH, Lionberger JM, Neumann WL, Bennett GJ, Weng HR, Spiegel S, Salvemini D. Dysregulation of sphingolipid metabolism contributes to bortezomib-induced neuropathic pain. J Exp Med. 2018 May 7;215(5):1301-1313. doi: 10.1084/jem.20170584. Epub 2018 Apr 27. PMID: 29703731; PMCID: PMC5940258.
- Sun Y, Kim JH, Vangipuram K, Hayes DF, Smith EML, Yeomans L, Henry NL, Stringer KA, Hertz DL. Pharmacometabolomics reveals a role for histidine, phenylalanine, and threonine in the development of paclitaxel-induced peripheral neuropathy. Breast Cancer Res Treat. 2018 Oct;171(3):657-666. doi: 10.1007/s10549-018-4862-3. Epub 2018 Jun 26. PMID: 29946863; PMCID: PMC6119501.
- Tan DX, Manchester LC, Burkhardt S, Sainz RM, Mayo JC, Kohen R, Shohami E, Huo YS, Hardeland R, Reiter RJ. N1-acetyl-N2-formyl-5-methoxykynuramine, a biogenic amine and melatonin metabolite, functions as a potent antioxidant. FASEB J. 2001 Oct;15(12):2294-6. doi: 10.1096/fj.01-0309fje. Epub 2001 Aug 17. PMID: 11511530.
- Tanabe Y, Hashimoto K, Shimizu C, Hirakawa A, Harano K, Yunokawa M, Yonemori K, Katsumata N, Tamura K, Ando M, Kinoshita T, Fujiwara Y. Paclitaxel-induced peripheral neuropathy in patients receiving adjuvant chemotherapy for breast cancer. Int J Clin Oncol. 2013 Feb;18(1):132-8. doi: 10.1007/s10147-011-0352-x. Epub 2011 Nov 22. PMID: 22105895.
- Thomas PK, Fraher JP, O'Leary D, Moran MA, Cole M, King RH. Relative growth and maturation of axon size and myelin thickness in the tibial nerve of

the rat. 2. Effect of streptozotocin-induced diabetes. Acta Neuropathol. 1990;79(4):375-86. doi: 10.1007/BF00308713. PMID: 2140232.

- Toman RE, Payne SG, Watterson KR, Maceyka M, Lee NH, Milstien S, Bigbee JW, Spiegel S. Differential transactivation of sphingosine-1-phosphate receptors modulates NGF-induced neurite extension. J Cell Biol. 2004 Aug 2;166(3):381-92. doi: 10.1083/jcb.200402016. PMID: 15289497; PMCID: PMC2172260.
- Tracey TJ, Steyn FJ, Wolvetang EJ, Ngo ST. Neuronal Lipid Metabolism: Multiple Pathways Driving Functional Outcomes in Health and Disease. Front Mol Neurosci. 2018 Jan 23;11:10. doi: 10.3389/fnmol.2018.00010. PMID: 29410613; PMCID: PMC5787076.
- Treede RD, Rolke R, Andrews K, Magerl W. Pain elicited by blunt pressure: neurobiological basis and clinical relevance. Pain. 2002 Aug;98(3):235-240. doi: 10.1016/S0304-3959(02)00203-8. PMID: 12127024.
- Trotti A, Colevas AD, Setser A, Rusch V, Jaques D, Budach V, Langer C, Murphy B, Cumberlin R, Coleman CN, Rubin P. CTCAE v3.0: development of a comprehensive grading system for the adverse effects of cancer treatment. Semin Radiat Oncol. 2003 Jul;13(3):176-81. doi: 10.1016/S1053-4296(03)00031-6. PMID: 12903007.
- Tsai SJ, Kuo WW, Liu WH, Yin MC. Antioxidative and anti-inflammatory protection from carnosine in the striatum of MPTP-treated mice. J Agric Food Chem. 2010 Nov 10;58(21):11510-6. doi: 10.1021/jf103258p. Epub 2010 Oct 6. PMID: 20925384.

- Turrens JF. Mitochondrial formation of reactive oxygen species. J Physiol. 2003 Oct 15;552(Pt 2):335-44. doi: 10.1113/jphysiol.2003.049478. PMID: 14561818; PMCID: PMC2343396.
- Van Brocklyn JR, Williams JB. The control of the balance between ceramide and sphingosine-1-phosphate by sphingosine kinase: oxidative stress and the seesaw of cell survival and death. Comp Biochem Physiol B Biochem Mol Biol. 2012 Sep;163(1):26-36. doi: 10.1016/j.cbpb.2012.05.006. Epub 2012 May 18. PMID: 22613819.
- Ved R, Saha S, Westlund B, Perier C, Burnam L, Sluder A, Hoener M, Rodrigues CM, Alfonso A, Steer C, Liu L, Przedborski S, Wolozin B. Similar patterns of mitochondrial vulnerability and rescue induced by genetic modification of alpha-synuclein, parkin, and DJ-1 in Caenorhabditis elegans. J Biol Chem. 2005 Dec 30;280(52):42655-42668. doi: 10.1074/jbc.M505910200. Epub 2005 Oct 19. PMID: 16239214; PMCID: PMC3910375.
- Velasco R, Bruna J. Taxane-Induced Peripheral Neurotoxicity. Toxics. 2015 Apr 28;3(2):152-169. doi: 10.3390/toxics3020152. PMID: 29056655; PMCID: PMC5634686.
- Velasco R, Navarro X, Gil-Gil M, Herrando-Grabulosa M, Calls A, Bruna J. Neuropathic Pain and Nerve Growth Factor in Chemotherapy-Induced Peripheral Neuropathy: Prospective Clinical-Pathological Study. J Pain Symptom Manage. 2017 Dec;54(6):815-825. doi: 10.1016/j.jpainsymman.2017.04.021. Epub 2017 Aug 8. PMID: 28797868.
- Verdú E, Butí M, Navarro X. Functional changes of the peripheral nervous system with aging in the mouse. Neurobiol Aging. 1996 Jan-Feb;17(1):73-7. doi: 10.1016/0197-4580(95)02010-1. PMID: 8786806.

- Verdú E, Ceballos D, Vilches JJ, Navarro X. Influence of aging on peripheral nerve function and regeneration. J Peripher Nerv Syst. 2000 Dec;5(4):191-208. doi: 10.1046/j.1529-8027.2000.00026.x. PMID: 11151980.
- Wallace VC, Cottrell DF, Brophy PJ, Fleetwood-Walker SM. Focal lysolecithin-induced demyelination of peripheral afferents results in neuropathic pain behavior that is attenuated by cannabinoids. J Neurosci. 2003 Apr 15;23(8):3221-33. doi: 10.1523/JNEUROSCI.23-08-03221.2003. PMID: 12716929; PMCID: PMC6742302.
- Wang W, Xiang P, Chew WS, Torta F, Bandla A, Lopez V, Seow WL, Lam BWS, Chang JK, Wong P, Chayaburakul K, Ong WY, Wenk MR, Sundar R, Herr DR. Activation of sphingosine 1-phosphate receptor 2 attenuates chemotherapy-induced neuropathy. J Biol Chem. 2020 Jan 24;295(4):1143-1152. doi: 10.1074/jbc.RA119.011699. Epub 2019 Dec 27. PMID: 31882542; PMCID: PMC6983853.
- Wang-Fischer Y, Garyantes T. Improving the Reliability and Utility of Streptozotocin-Induced Rat Diabetic Model. J Diabetes Res. 2018 Sep 23;2018:8054073. doi: 10.1155/2018/8054073. PMID: 30345315; PMCID: PMC6174751.
- Ward SJ, Ramirez MD, Neelakantan H, Walker EA. Cannabidiol prevents the development of cold and mechanical allodynia in paclitaxel-treated female C57Bl6 mice. Anesth Analg. 2011 Oct;113(4):947-50. doi: 10.1213/ANE.0b013e3182283486. Epub 2011 Jul 7. PMID: 21737705; PMCID: PMC3249239.
- Willson ML, Burke L, Ferguson T, Ghersi D, Nowak AK, Wilcken N. Taxanes for adjuvant treatment of early breast cancer. Cochrane Database Syst Rev. 2019

Sep 2;9(9):CD004421. doi: 10.1002/14651858.CD004421.pub3. PMID: 31476253; PMCID: PMC6718224.

- Wojtczak L, Schönfeld P. Effect of fatty acids on energy coupling processes in mitochondria. Biochim Biophys Acta. 1993 Nov 2;1183(1):41-57. doi: 10.1016/0005-2728(93)90004-y. PMID: 8399375.
- Wolf SL, Barton DL, Qin R, Wos EJ, Sloan JA, Liu H, Aaronson NK, Satele DV, Mattar BI, Green NB, Loprinzi CL. The relationship between numbness, tingling, and shooting/burning pain in patients with chemotherapy-induced peripheral neuropathy (CIPN) as measured by the EORTC QLQ-CIPN20 instrument, N06CA. Support Care Cancer. 2012 Mar;20(3):625-32. doi: 10.1007/s00520-011-1141-9. Epub 2011 Apr 12. PMID: 21479990; PMCID: PMC3329939.
- Wong ML, Cooper BA, Paul SM, Abrams G, Topp K, Kober KM, Chesney MA, Mazor M, Schumacher MA, Conley YP, Levine JD, Miaskowski C. Age-related differences in patient-reported and objective measures of chemotherapy-induced peripheral neuropathy among cancer survivors. Support Care Cancer. 2019 Oct;27(10):3905-3912. doi: 10.1007/s00520-019-04695-3. Epub 2019 Feb 15. PMID: 30770977; PMCID: PMC6697247.
- Wu FZ, Xu WJ, Deng B, Liu SD, Deng C, Wu MY, Gao Y, Jia LQ. Wen-Luo-Tong Decoction Attenuates Paclitaxel-Induced Peripheral Neuropathy by Regulating Linoleic Acid and Glycerophospholipid Metabolism Pathways. Front Pharmacol. 2018 Aug 28;9:956. doi: 10.3389/fphar.2018.00956. PMID: 30233366; PMCID: PMC6127630.
- Wu J, Hocevar M, Bie B, Foss JF, Naguib M. Cannabinoid Type 2 Receptor System Modulates Paclitaxel-Induced Microglial Dysregulation and Central

Sensitization in Rats. J Pain. 2019 May;20(5):501-514. doi: 10.1016/j.jpain.2018.10.007. Epub 2018 Nov 8. PMID: 30414958.

- Xu J, Zhang L, Xie M, Li Y, Huang P, Saunders TL, Fox DA, Rosenquist R, Lin F. Role of Complement in a Rat Model of Paclitaxel-Induced Peripheral Neuropathy. J Immunol. 2018 Jun 15;200(12):4094-4101. doi: 10.4049/jimmunol.1701716. Epub 2018 Apr 25. PMID: 29695418; PMCID: PMC5988965.
- Yang AH, Ishii I, Chun J. In vivo roles of lysophospholipid receptors revealed by gene targeting studies in mice. Biochim Biophys Acta. 2002 May 23;1582(1-3):197-203. doi: 10.1016/s1388-1981(02)00172-5. PMID: 12069829.
- Yehia R, Saleh S, El Abhar H, Saad AS, Schaalan M. L-Carnosine protects against Oxaliplatin-induced peripheral neuropathy in colorectal cancer patients: A perspective on targeting Nrf-2 and NF-κB pathways. Toxicol Appl Pharmacol. 2019 Feb 15;365:41-50. doi: 10.1016/j.taap.2018.12.015. Epub 2018 Dec 25. PMID: 30592963.
- Yokota T, Hansson GK. Immunological mechanisms in atherosclerosis. J Intern Med. 1995 Dec;238(6):479-89. doi: 10.1111/j.1365-2796.1995.tb01229.x. PMID: 9422033.
- Zajączkowska R, Kocot-Kępska M, Leppert W, Wrzosek A, Mika J, Wordliczek J. Mechanisms of Chemotherapy-Induced Peripheral Neuropathy. Int J Mol Sci. 2019 Mar 22;20(6):1451. doi: 10.3390/ijms20061451. PMID: 30909387; PMCID: PMC6471666.
- Zaks-Zilberman M, Zaks TZ, Vogel SN. Induction of proinflammatory and chemokine genes by lipopolysaccharide and paclitaxel (Taxol) in murine and

human breast cancer cell lines. Cytokine. 2001 Aug 7;15(3):156-65. doi: 10.1006/cyto.2001.0935. PMID: 11554785.

- Zhao X, Liu L, Wang Y, Wang G, Zhao Y, Zhang Y. Electroacupuncture enhances antioxidative signal pathway and attenuates neuropathic pain induced by chemotherapeutic paclitaxel. Physiol Res. 2019 Jun 30;68(3):501-510. doi: 10.33549/physiolres.934084. Epub 2019 Mar 22. PMID: 30904013.
- Zsizsik BK, Hardeland R. Formation of kynurenic and xanthurenic acids from kynurenine and 3-hydroxykynurenine in the dinoflagellate Lingulodinium polyedrum: role of a novel, oxidative pathway. Comp Biochem Physiol C Toxicol Pharmacol. 2002 Nov;133(3):383-92. doi: 10.1016/s1532-0456(02)00126-6. PMID: 12379423.

7. Appendix

PLASMA						LIVER			
Young CTRL vs PTX - EOT		Young CTRL vs PTX - FU		Adult CTRL vs PTX - EOT		Young CTRL vs PTX - EOT		Adult CTRL vs PTX - EOT	
MetIDQ Short name	VIP (>1)	MetIDQ Short name	VIP (>1)	MetIDQ Short name	VIP (>1)	MetIDQ Short name	VIP (>1)	MetIDQ Short name	VIP (>1)
TG(17:1_38:5)	7.515	HexCer(d16:1/22:0)	4.402	TG(17:1_38:5)	5.270	TG(22:1_32:5)	8.960	TG(18:3_30:0)	6.162
TG(17:1_38:7)	3.120	DG-O(18:2_18:2)	4.248	TDCA	3.592	TG(20:3_36:5)	8.264	Hex3Cer(d18:1_20:0)	5.147
TG(20:3_36:5)	2.197	TG(17:2_38:7)	3.488	GCDCA	2.947	TG(17:2_38:7)	8.117	TG(17:1_38:6)	4.530
TG(14:0_34:3)	2.148	TG(17:1_38:7)	3.263	DG(18:3_20:2)	2.614	TG(22:2_32:4)	6.150	GCDCA	4.076
TG(20:2_32:1)	2.078	TG(17:2_38:6)	3.207	TG(17:0_34:3)	2.470	TG(17:2_38:6)	5.822	TG(20:2_34:4)	3.565
TG(22:3_30:2)	2.072	DG(14:1_18:1)	3.122	TG(17:2_38:7)	2.444	GCDCA	3.785	TG(22:2_32:4)	3.510
Cer(d16:1/23:0)	2.029	Cer(d16:1/22:0)	3.032	PC ae C44:6	2.414	TG(17:1_38:7)	3.646	TG(22:1_32:5)	3.144
TG(17:1_34:3)	2.025	Carnosine	2.886	TG(16:1_36:5)	2.183	PC ae C38:1	3.592	Cer(d16:1/24:0)	2.383
TG(18:2_28:0)	1.978	HexCer(d18:2/20:0)	2.875	CDCA	2.182	Hex3Cer(d18:1_20:0)	3.472	DG(18:3_20:2)	2.269
TG(16:0_32:3)	1.959	Hex3Cer(d18:1_20:0)	2.702	TG(17:1_38:7)	2.164	TG(20:2_34:4)	3.434	TG(20:4_35:3)	2.045
TG(20:1_32:3)	1.935	DG-O(14:0_18:2)	2.652	Carnosine	2.120	TG(20:1_32:0)	3.172	DG(18:1_18:1)	2.028
TG(18:2_30:1)	1.895	TG(17:1_38:6)	2.640	TG(18:1_34:4)	2.080	TG(17:2_38:5)	2.328	TG(20:0_32:3)	2.023
TG(18:3_30:0)	1.882	PC ae C42:1	2.518	TG(18:1_32:3)	2.066	DG(18:3_20:2)	1.818	TMAO	1.942
TG(16:1_38:3)	1.878	CE(14:1)	2.400	TG(18:2_34:4)	2.013	BABA	1.751	TG(18:3_36:1)	1.935
TG(17:2_34:3)	1.867	Cer(d16:1/18:0)	2.345	TG(17:1_36:4)	2.010	Cer(d16:1/22:0)	1.545	TG(14:0_38:4)	1.916
TG(22:1_32:5)	1.847	DG(22:1_22:2)	2.294	TG(22:1_32:5)	2.002	TG(20:4_35:3)	1.494	TG(20:2_32:1)	1.886
TG(16:1_36:1)	1.844	HexCer(d18:2/18:0)	2.282	TG(16:1_38:3)	1.969	TG(20:0_32:4)	1.483	Cystine	1.883
TG(17:2_36:4)	1.831	C14:2	2.244	TG(20:1_34:3)	1.964	TG(20:2_36:5)	1.470	TG(20:0_32:4)	1.883
TG(16:1_34:3)	1.813	TG(20:2_36:5)	2.203	TG(20:1_32:2)	1.954	TG(17:1_36:5)	1.415	TG(17:2_36:4)	1.819
TG(16:1_32:2)	1.811	TG(17:2_38:5)	2.178	TG(14:0_38:5)	1.921	C7-DC	1.358	TG(18:1_38:7)	1.801
TG(20:4_30:0)	1.804	DG(17:0_17:1)	2.174	TG(14:0_36:4)	1.919	Hex3Cer(d18:1/16:0)	1.357	Asn	1.798
TG(17:2_38:6)	1.799	TG(18:0_30:1)	2.144	TG(20:3_32:1)	1.916	TDCA	1.338	TG(20:2_36:5)	1.792
TG(20:3_34:0)	1.792	DG(18:1_20:3)	2.130	TG(18:3_32:1)	1.913	TG(18:3_36:4)	1.335	FA(20:3)	1.787
TG(18:1_30:1)	1.791	PC ae C42:0	2.127	TG(16:0_34:4)	1.893	TG(17:2_34:3)	1.330	TG(17:2_36:3)	1.760
TG(16:1_38:4)	1.782	SM C20:2	2.122	TG(16:1_34:3)	1.888	Histamine	1.327	TG(18:0_36:5)	1.746

Appendix 1. VIP (Variable Influence on Prediction) for the Top 25 Metabolites (Scores >1).

The higher the VIP value is, the more the metabolite drives the difference between the group comparisons. Asn: asparagine; BABA: β-aminobutyric acid; C7-DC: pimelylcarnitine; CDCA: chenodeoxycholic acid; CE: cholesterol-ester; Cer: ceramide; CTRL: control group; DG: diglyceride; EOT: end of treatment; FA: fatty acids; FU: end of the follow-up period; GCDCA: glycochenodeoxycholic acid; HexCer: hexosylceramide; Hex3Cer: globoside Gb3/trihexosylceramide; ID: identifier; PC: phosphatidylcholine; PC ae: phosphatidylcholine acyl-alkyl; PTX: paclitaxel-treated group; SM: sphingomyelin; TDCA: taurodeoxycholic acid; TG: triglyceride; TMAO: trimethylamine-N-oxide; VIP: variable influence on prediction.